UNITED IMAGING

RSNA 2022 Edition

Issue Highlights

Editorial Board

Editors/Reviewers

Contributors

Disclaimer

The articles contained in this magazine are provided solely by the authors, and the author(s) of each article appearing in this magazine is/are solely responsible for the content thereof as well as personal data, which is used anonymously or complied with applicable data privacy laws or regulations. United Imaging Healthcare makes no representation or warranties, expressly or impliedly, with respect to the accuracy, timeliness, reliability, legitimacy, applicability, fitness, originality, or completeness of the contents of this magazine. United Imaging Healthcare assumes no legal responsibility or liability for any error, omission, or illegality with respect to the material contained within.

All articles contained in this magazine only represent the opinions and views of the authors and do not implicitly or explicitly represent any official positions or policies, or medical opinions of United Imaging Healthcare or the institutions with which the authors are affiliated unless this is clearly specified. Discussions of any brand, services, or products in the magazine should not be construed as promotion or endorsement thereof.

Articles published in this magazine are intended to inspire further general scientific research, investigation, understanding, and discussion only and are NOT intended to and should not be relied upon as recommending or promoting a specific medical advice, method, diagnosis, or treatment by physicians for any particular individual, nor to replace the advice of a medical doctor or other healthcare professional. Any individual wishing to apply the information in this magazine for the purposes of improving their own health should not do so without consulting with a qualified medical practitioner. All patients need to be treated in an individual manner by their personal medical advisors. The decision to utilize any information in this magazine is ultimately at the sole discretion of the reader, who assumes full responsibility for any and all consequences arising from such a decision. United Imaging Healthcare makes no representations or warranties with respect to any treatment, action, or application of medication or preparation by any person following the information offered or provided within or through the magazine. United Imaging Healthcare shall remain free of any fault, liability, or responsibility for any loss or harm, whether real or perceived, resulting from the use of information in this magazine.

The articles included in this magazine may contain work in progress, which represents ongoing research and development. Such technologies are not available for sale in China or the United States for clinical use and also may not available for such sales in other countries around the world.

Please note that the magazine is intended to be distributed only within a limited scope instead of publication.

If you have any questions about the magazine, or simply wish to reach out to us for any other reasons, you are welcomed to contact us at the following email address: compliance@united-imaging.com

About uINNOVATION GLOBAL

——

Welcome to uINNOVATION-GLOBAL, our new, recurring collection of perspectives from leading global experts in the medical imaging field. Technologies discussed in the articles of the inaugural RSNA 2022 edition of uINNOVATION-GLOBAL may contain work in progress, which represents ongoing research and development. Such technologies are not available for sale in the United States for clinical use and also may not available for such sales in other countries.

If you have any questions about the magazine, or simply wish to reach out to us for any other reasons, you are welcomed to contact us at the following email address: uinnovation-global@united-imaging.com

To download the inaugural RSNA 2022 edition, click on the links below.
https://usa.united-imaging.com/uinnovation-global-collaborative-research/

This magazine is 100% funded and edited by United Imaging Healthcare. Authors or their institutions may have received or currently receive financial support from United Imaging Healthcare, as indicated in each article.

About United Imaging Healthcare

——

United Imaging Healthcare is a provider of high-end medical equipment and medical IT solutions. From our headquarters in Shanghai's Jiading district to our network of research and development centers throughout the world, our global mission is to provide medical institutions with a full range of healthcare solutions, from diagnostic imaging and radiation therapy equipment to service, training, and medical IT solutions. We are dedicated to expanding access to high-quality medical care and improving the value of our services.

VISION

——

Leading Healthcare Innovation

MISSION

——

To Bring Equal Healthcare for All

To learn more,
visit https://www.united-imaging.com/

No. 2258 Chengbei Rd, Jiading District, Shanghai, 201807
Business Consultation: +86 (21)-67076666
Email: info.global@united-imaging.com
www.united-imaging.com

9370 Kirby Drive, Houston, Texas 77054
www.united-imaging.com

Editorial: The Future of Radiology

Omer Aras, M.D.
Department of Radiology, Memorial Sloan Kettering Cancer Center
New York, USA

Radiological images have become crucial in clinical practice for both diagnosis and treatment monitoring of a range of diseases. Considering the advancements in computing power, deep learning algorithms, and the availability of a large amount of data from medical imaging, clinical records, and wearable health monitors, artificial intelligence (AI) is poised to play an increasingly prominent role in medicine and healthcare. Specifically, in the field of radiology, every aspect of the imaging workflow can be improved by AI. AI has the potential to boost the value of medical images by improving imaging efficiency, image quality, and imaging assessment.

In chest radiology, multiple commercial algorithms (from several vendors) have been cleared by the United States Food and Drug Administration for clinical use to detect and segment nodules mainly on computed tomography (CT) images. In addition to lesion detection and segmentation, these AI algorithms can also provide information on nodule characteristics, improve the conspicuity of nodules, perform automatic LUNG-RADS reporting, and provide a lung cancer prediction score to assess the probability of the nodule being malignant in nature. In addition to the evaluation of cancer in the lung, AI algorithms can also evaluate pulmonary pathologies such as pneumonia, chronic obstructive pulmonary disease, pulmonary fibrosis, and pulmonary effusion. In this issue of uINNOVATION-GLOBAL, readers will find an interesting article on study of AI-based lung nodule detection from CT images[1] conducted on over 600 patients that shows that the use of AI resulted in better sensitivity and accuracy compared to subjective readings.

Among the available imaging modalities, magnetic resonance imaging (MRI) has many strengths for morphological and functional imaging, generating excellent soft tissue contrast at a high spatial resolution throughout the body. There have been efforts to reduce the examination time of MRI. Excessive scanning time reduces the daily average number of examinations that can be performed and causes patient discomfort. Deep learning has recently emerged as a tool to accelerate MRI examination time. United Imaging Healthcare 's AI-assisted Compressed Sensing (ACS) technology has been developed to provide an integrated MRI acceleration solution combining compressed sensing, parallel imaging, half Fourier analysis, and AI. An interesting article on this subject is presented in this edition of uINNOVATION-GLOBAL, in which the usage of ACS for different body organs demonstrates either superior or comparable image quality with reduced scanning time as compared to conventional MR acquisition.

In recent years, cardiovascular magnetic resonance (CMR) has emerged as a safe, non-invasive, radiation- and iodinated contrast medium-free technique allowing for a comprehensive assessment of cardiac function, dimensions, perfusion, and viability. As such, it may soon be among the most comprehensive and powerful imaging modalities for evaluating the cardiovascular system. CMR parameters are also potentially useful for repeat imaging and tracking disease progression or therapy efficacy. With the advancement of cardiac CT imaging technology, CT Coronary Angiogram (CTCA) is the most advanced diagnostic tool for detecting and monitoring coronary artery disease. In this issue, you will find two articles from Dr. Gregory Lanza and Dr. Rochita Venkataramanan sharing their experience using MRI and CT to manage patients with cardiovascular disease.

Molecular imaging provides a method for studying the biological processes at the cellular and molecular level in

[1] This product is a work in progress; the information in this article represents ongoing research and development. No 510k application has been filed with the FDA. This product is not available for sale in the U.S. for clinical uses and also may not be available for such sales in other countries

humans and in other living systems. ^{18}F-FDG PET is widely used in cancer imaging for diagnosis, staging, and monitoring of treatment response. In the past decade, several radiotracers have been introduced, including ^{18}F-Fluciclovine, ^{18}F-DCFPyL, ^{68}Ga-PSMA, ^{18}F-Fluoroestradiol, ^{68}Ga-DOTATATE, and ^{64}Cu-DOTATATE, improving the ability of PET to stage and characterize diseases. As more potential PET radiotracers are being discovered, they have the potential to expand the use of molecular imaging for further clinical disciplines. In this issue, you will find two articles from Dr. Remy Lim and Dr. Jun Zhao highlighting their clinical adoptions of PET/CT and PET/MR technologies in conjunction with novel radiotracers.

The availability of total-body PET devices has revolutionized the breadth of PET clinical and research studies. Since their introduction in 2018, total-body PET devices have attracted considerable attention in the medical community. The increased sensitivity of total-body PET allows faster imaging, use of a lower injected dose, and use of delayed scan start times to enhance lesion contrast. This edition of uINNOVATION-GLOBAL contains an interview with one of the creators of total-body PET, Dr. Simon Cherry, who gives us his personal insights into the technology and where it might be going in the future. Deep learning-based reconstruction and analysis algorithms are potentially immensely valuable to manage the increasing volumes of acquired imaging data that TB-PET generates. Dr. Kenta Miwa *et. al.* puts together a preliminary investigation on the evaluation of deep learning-based PET image reconstruction in an article included in this issue.

Notably, poor health outcomes can result from delays in diagnosis and treatment due to a lack of imaging equipment and personnel. More direction is needed for AI applications to help low- and middle-income countries (LMICs) in particular to increase their access to the diagnostic imaging and nuclear medicine tools and to address the rising burden of cancer. In the commentary article within this issue of uINNOVATION-GLOBAL, Dr. Harsh Mahajan and Dr. Vidur Mahajan have highlighted their important perspective on the future of radiology and how emerging technologies like AI can help LMICs.

Intelligent diagnostic imaging workflows have also become possible due to the rapid development of AI technology in recent years. With the goal of significantly reducing the repetitive work of radiologists and technologists and improving patient care, intelligent diagnostic imaging workflows may perform functions such as intelligent authentication of patient identity, intelligent voice interaction, intelligent patient positioning, and intelligent scanning parameter setting throughout the entire image scanning process. Although medical imaging has improved over the years, it still faces the challenges of long examination times and low acceleration rates. The future of radiology will undoubtedly see advances in precision medicine aided by AI tools. Future synergies with other emerging diagnostic tools will also be required.

Dr. Omer Aras
Guest Editor

Guest Editor Biography

Dr. Omer Aras

Dr. Aras is a physician-scientist with formal training in both clinical radiology/nuclear radiology and molecular imaging research. His clinical interests lie in oncologic imaging, with a focus on genitourinary and bone marrow cancer. His primary research interest involves developing novel and innovative molecular imaging approaches for cancer diagnostics and combining and utilizing the biology, nanotechnology, chemistry with advanced non-invasive imaging methods (predominantly PET/optical imaging) to create novel imaging agents that allow much earlier detection and improve therapy monitoring of cancer. As a result of translational work, much of it completed under his own initiative, he has published a number of peer-reviewed papers in biomedical journals and been invited to present his work at national and international venues.

Quantitative assessment of AI-based chest CT lung nodule detection in lung cancer screening: future prospects and main challenges

Marufjon Salokhiddinov[a], Ruth Awotwe[a], Munojat Ismailova[a]
[a]Radiology Department, Republic Zangiota No-2 COVID Specialized Hospital, Uzbekistan

1. Introduction

Lung cancer is the most common cause of cancer-related death. It is known for being particularly aggressive. Early detection of asymptomatic lung cancer is crucial for optimal treatment, which can greatly increase patients' survival rates. Since the beginning of the twentieth century, the incidence in the population has increased several times. Its growth is especially pronounced in industrialized countries, where lung cancer ranks first in the structure of oncological morbidity. Lung cancer also ranks among the top three cancers in terms of incidence rates for both men and women. As the precursor, lung nodules are the main indication of lung cancer. Therefore, lung screening by CT exams has been recommended for identifying and characterizing nodules to detect early lung cancer.

The manifestation of lung nodules in CT images is complicated because of their irregular shapes, broad gray value range, and varied scale [1]. It is a time consuming and challenging task to effectively detect nodules for Radiologists. Additionally, differentiating benign from malignant nodules is another challenging task. Currently, pulmonary nodules incidentally observed on CT exams are handled by following consensus standards [2, 3]. But that has several drawbacks. Because the Radiologist's interpretation of each lesion is a complicated process, the evaluation performance is highly dependent on the experience or skills of the Radiologist, so the diagnosis is not always consistent. Considering the low efficiency of human reading, some patients might miss the ideal opportunity for treatment [4,5,6,7].

The computer-aided automatic solution has been proposed and utilized to address these challenges. It is expected to be able to overcome physical human limitations, such as the limited gray level recognition of the human visual system, fatigue, and distraction [8]. It can also provide diagnostic results in a repeatable and reliable manner. It can therefore be used to reduce Radiologists' workloads, locate nodules that Radiologists might overlook, and improve diagnostic accuracy [4]. Recently-developed artificial intelligence (AI) technology has made the computer-aided automatic solution even more promising. Deep learning, as one subset of AI technology, allows the model to learn high-dimensional abstract features from vast amounts of data and empowers the model to handle complex tasks. AI has demonstrated many compelling advantages and accomplishments [9,10,11,12,13] in imaging diagnosis and/or evaluation.

In this study, we aim to quantitatively assess the performance of AI-assisted reading versus traditional radiology reports in detecting lung nodules and evaluate AI as a method of characterizing and classifying lung nodules in lung cancer screening.

2. Materials and Methods

2.1 Data Preparation and Categorization

The study included 635 patients with a mean age of 52±9 years old. They underwent chest CT exam from May to October 2021 at Republic Zangiota No-2 COVID Specialized Hospital, Uzbekistan. Scans were not included in the study if:

(a) All lung lobes were not fully visible in the field of view
(b) The image contained motion artifacts
(c) The image did not meet Digital Imaging and Communications in Medicine standards
(d) The Radiologists responsible for ground truth labeling were unable to confidently annotate the images [14]

2.2 CT Image Acquisition

For non-contrast-enhanced chest CT scanning, the uCT® 550 scanner (United Imaging Healthcare, Shanghai, China) was

used. The collimation of the CT detector was 256 x 0.625 mm, 64 x 0.625 mm, 96 x 0.6 mm, and 320 x 0 x 5 mm, respectively. In the supine position, each subject underwent an inspiratory CT scan during a single breath hold. The tube voltage was set to be either 120 kV or 100 kV depending on the patient size. The dose modulation was on, and the tube current ranged from 50 to 200 mAs. Slice thickness ranged from 0.625 to 1.0 mm.

2.3 Radiologist Interpretation

One Radiologist with over five years of experience reviewed the chest CT images. RadiAnt DICOM Viewer was used to review the studies. The Radiologist was given unlimited reading time and the option to adjust the display based on scan-specific characteristics to ensure optimal reading quality. Nodules in our dataset were divided into five types based on the National Comprehensive Cancer Network (NCCN) recommendations for lung cancer screening (version 2.2019): solid nodules (<5 or >5 mm), subsolid nodules (<5 or >5 mm), and calcified nodules.

2.4 Artificial Intelligence-assisted Reading

On chest CT images, uAI® Discover Chest[2] (United Imaging Healthcare, Shanghai, China) can automatically identify and measure lung nodules. The CT console automatically sends the CT images to the AI server for lung nodule detection once acquired. It took about 2 to 4 minutes to transfer and process the whole volume images of each patient. In short, this system automatically generates a bounding box that shows the characteristics of the suspected nodule, such as its diameter and volume, as well as its components (solid, part-solid, or nonsolid).

2.5 AI Model Development

Recent research [15,16,17] studies have proposed using deep learning approaches for the detection and classification of lung nodules with CT images, as such approaches have demonstrated significant improvements in both tasks. In this work, the automated processing was performed using United Imaging Intelligence's uAI Discover Chest AI-based approach. For automated nodule detection, the uAI Discover Chest employs cascading feature pyramids and a heterogeneous convolutional neural network in its algorithm. Conventional deep learning approaches can only identify objects at a single scale – they cannot handle items with significant size variations. As shown in Figure 1, the uAI Discover Chest approach uses a 3D feature pyramids network (FPN) with V-Net to specifically solve the large-scale variance problem.

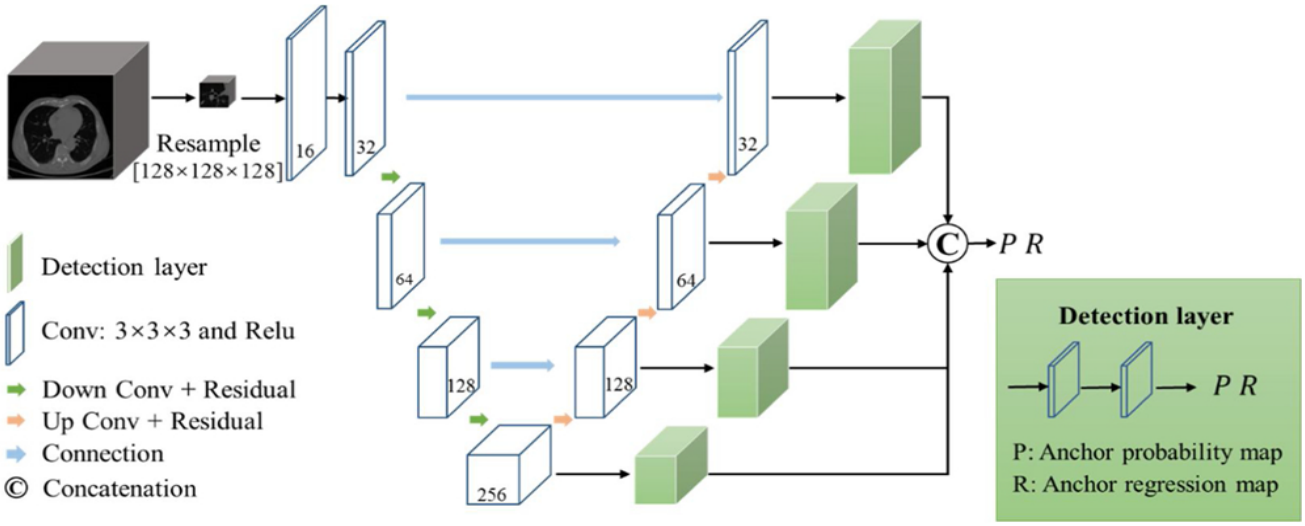

Figure 1. The architecture of the feature pyramid network (FPN).

[2] This product is a work in progress; the information in this article represents ongoing research and development. No 510k application has been filed with the FDA. This product is not available for sale in the U.S. for clinical uses and also may not be available for such sales in other countries

2.6 Nodule Categorization

Lung nodules are divided into three main types according to the NCCN guideline [18]: solid, part-solid, and non-solid nodules. Each type has a unique management process. Solid nodules are further divided into strata of <5 and >5 mm, part-solid nodules <5 and >5 mm, and calcified nodules. Typical nodules of different types are shown in Figure 2.

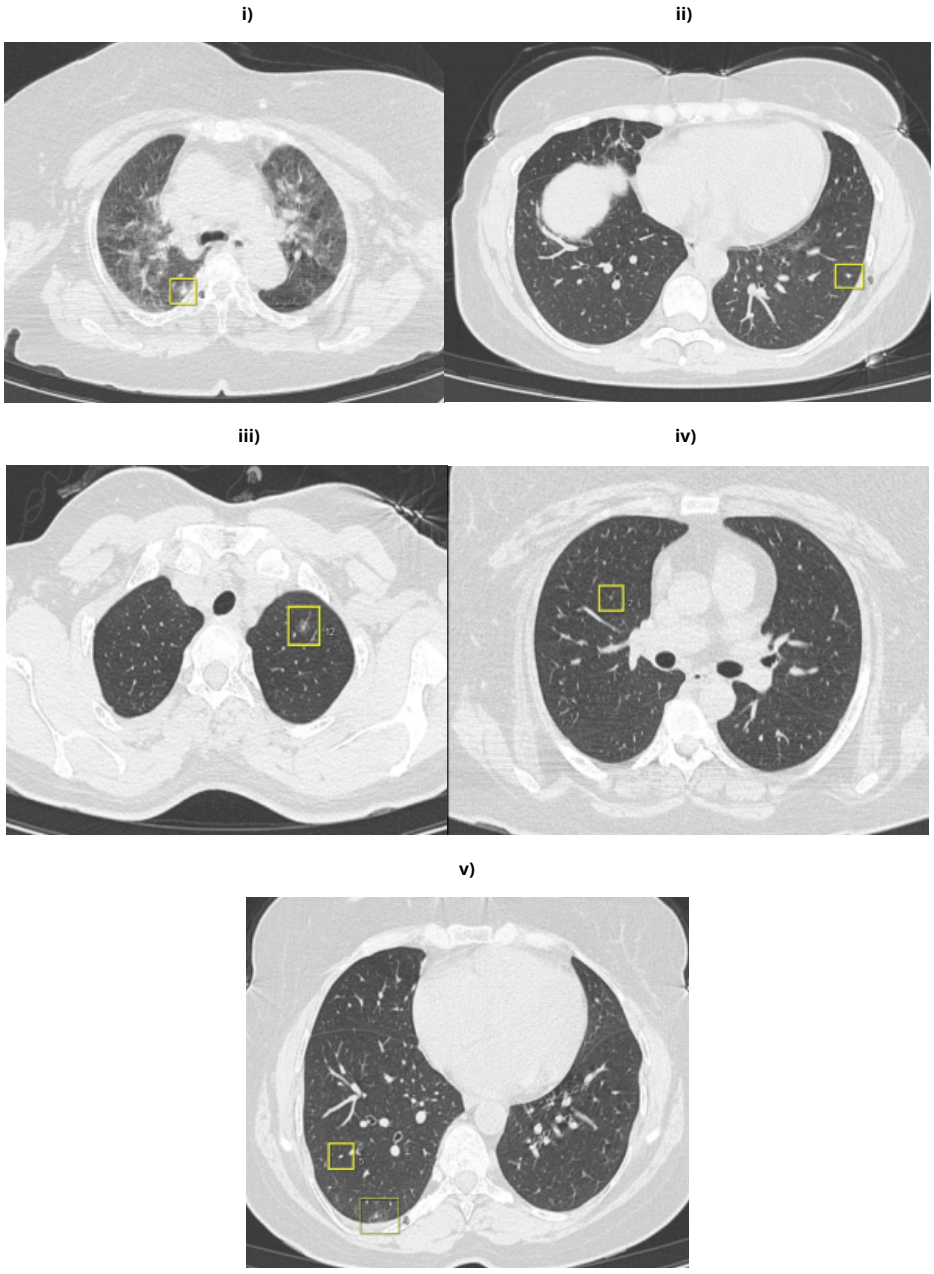

Figure 2. Nodule Categorization according to NCCN. i) Solid >5 mm, ii) Solid <5 mm, iii) Subsolid >5 mm, iv) Subsolid <5 mm, v) Calcified.

2.7 Panel Review

Two Radiologists with 15 and 20 years of experience in chest radiology were included in the review panel to evaluate the results reported by the Radiologist and AI system. The review panel was to establish a reference standard for the presence of nodules. Based on the standard, the figure of merit (FOM) could be calculated by including the number of false negatives, true negatives, false positives, and true positives. For instance, a lung nodule was regarded as a false-positive nodule if it was discovered by a Radiologist or detected by AI-assisted reading but was not confirmed by the review panel. The system interface of the uAI Discover Chest assisted lung nodule evaluation is shown in Figure 3.

2.8 Statistical analysis

In this study, 1082 nodules were included from the data of 635 patients, further classified as 778 (<5mm = 513 and >5 mm = 265) solid nodules, 283 (<5mm = 186 and >5 mm = 97) subsolid nodules and 21 calcified nodules. Statistical analysis was performed using MedCalc®, version 19.3 (MedCalc Software Ltd). Sensitivity and accuracy were measured to evaluate the performance of lung nodule detection, using the following equations, respectively:

$$Sensitivity = \frac{TP}{(TP+FN)} \quad (1)$$

$$Accuracy = \frac{TP+TN}{TP+FP+TN+FN} \quad (2)$$

where TP is the true positive, TN is the true negative, FP is the false positive, and FN is the false negative. FP is an outcome where the model incorrectly predicts a nodule in the lung CT without its existence.

3. Results

In the detection of solid nodules, the sensitivity and accuracy were 96.80% and 94.08% for AI-reading and 89.50% and 85.34% for radiological observation, respectively. The sensitivity and accuracy for <5 mm solid nodules were 96.80% and 94.34% with AI-reading and 91.70% and 88.65% with radiological observation, and for >5 mm solid nodules were 96.90% and 93.58% with AI-reading and 85.10% and 79.02% with radiological observation, respectively.

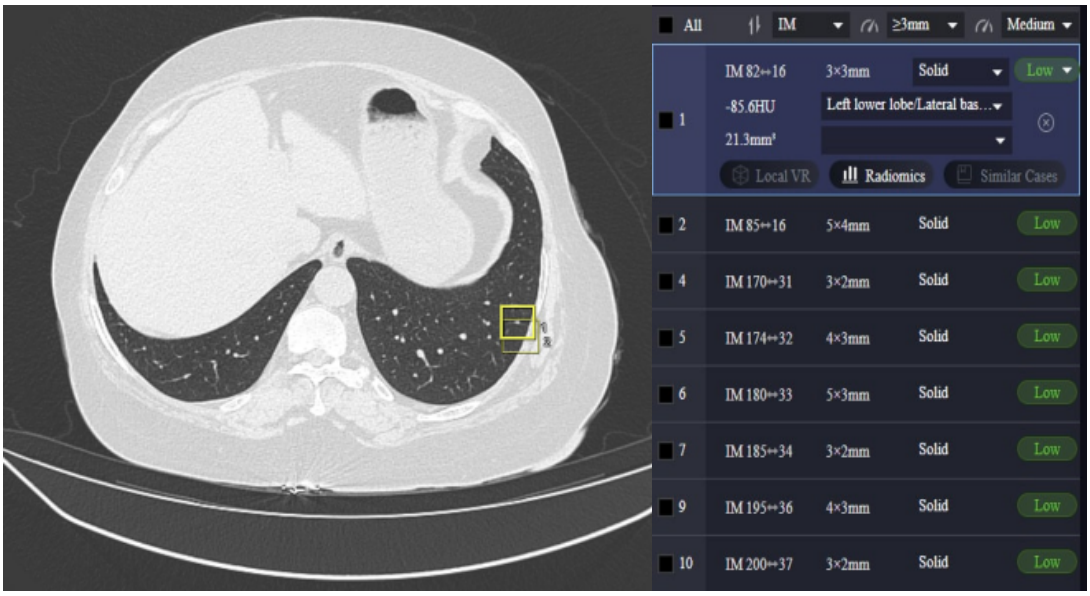

Figure 3. uAI® Discovery Chest-assisted lung nodule evaluation system interface

A similar analysis was performed for sub-solid and calcified nodules. The sensitivity and accuracy were 93.34% and 89.04% for AI-reading and 80.00% and 75.26% for radiological observation, respectively, in the sub-solid nodule detection. The sensitivity and accuracy for <5 mm sub-solid nodules were 93.80% and 90.21% with AI-reading

and 87.10% and 82.32% with radiological observation, and for >5 mm sub-solid nodules were 92.50% and 86.86% with AI-reading and 67.40% and 63.36% with radiological observation, respectively.

The sensitivity and accuracy of the AI-reading-based calcified nodule detection were 95.34% and 95.34%, and 88.90% and 76.19% for Radiologist observation, respectively. The comparison of the detection performance between AI reading and Radiologist observation for all solid, subsolid, and calcified nodules is shown in Figure 4. Figure 5 displays the bar graph of the sensitivity and accuracy of AI reading and Radiologist observation for <5 mm and >5 mm solid and subsolid nodules detection.

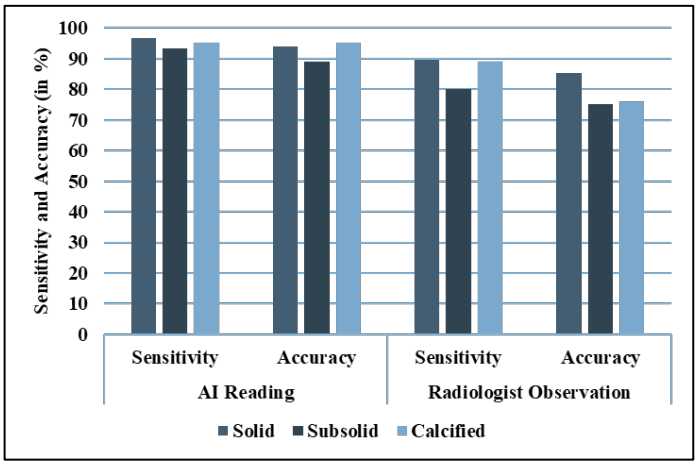

Figure 4. Bar graph of the sensitivity and accuracy of AI reading and Radiologist observation for solid, subsolid and calcified nodules detection.

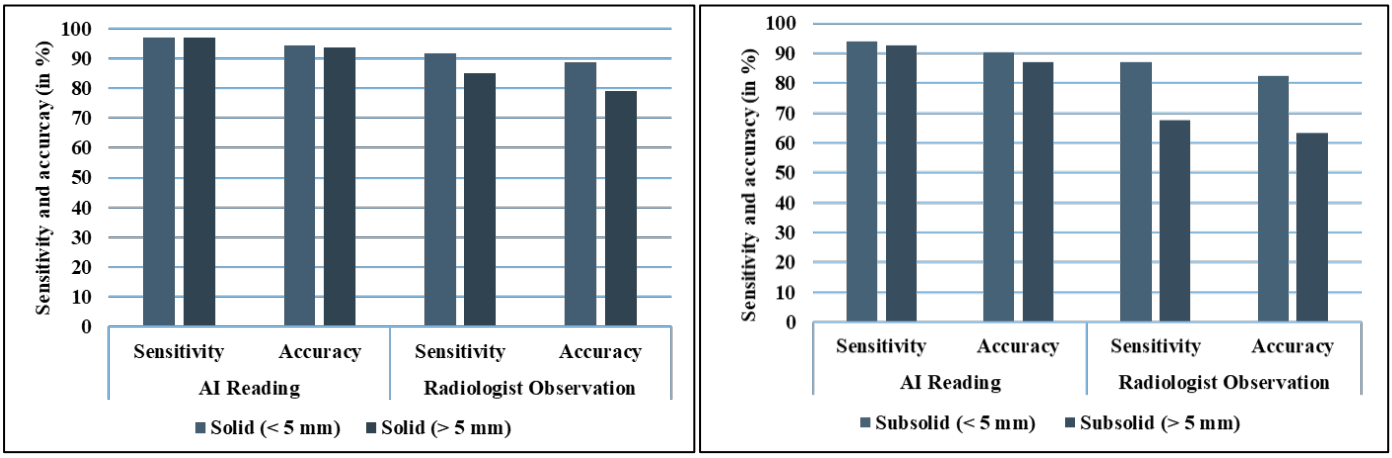

Figure 5. Bar graph of the sensitivity and accuracy of AI reading and Radiologist observation for a) <5 mm and >5 mm solid nodules and b) <5 mm and >5 mm subsolid nodule detection.

4. Discussion

The performance of AI reading and Radiologist observations were quantitively assessed in detecting multiple type nodules including solid, subsolid, and calcified ones. The assessment showed that the performance of AI was better than Radiologist performance in all nodule categories. This study suggests that AI was more sensitive and accurate in detecting the nodules. It is consistent with most other studies that AI is a reliable and sensitive method to use in lung nodule detection.

Compared to earlier studies [19,20,21], uAI Discover Chest introduced several key advanced techniques. First, it used a

classification network to further reduce false positives and to analyze large-scale data. The model demonstrated a significantly higher identification rate in sensitivity and accuracy than Radiologists achieved. By utilizing the threshold ReLU, this heterogeneous network not only reduced the overfitting problem but also improved detection performance. The detection of solid nodules had the highest sensitivity as compared to sub-solids and calcified lesions. The results obtained in this work showed that the overall performance of uAI Discover Chest algorithm in detecting lung nodules of different sizes and different types depicted better outcomes as compared to the Radiologist's assessment, especially in detecting nodules that the Radiologist missed.

Nevertheless, this study had a limitation that need to be addressed in the future. There was no true gold standard available for the comparison of outcomes. For the evaluation in this study, a reference standard was carried out by the two Radiologists having an experience of 8 years and 7 years respectively. In such cases, there is a possibility of missing out fewer lung nodules which may lead to an inconsistency of obtained results. According to recent research, the performance of a cutting-edge artificial intelligence system for lung nodule detection and characterization is comparable to that of skilled Radiologists. Numerous AI studies discuss cutting-edge architectures for finding lung nodules, with the Radiologists' consensus as the reference standard [22,23,24].

Finding all lung cancers, not all nodules, is the ultimate goal. Therefore, future research should concentrate on a reference standard that measures cancer detection and is based on histopathological evidence or follow-up imaging for at least 2 years (depending on morphology to judge the stability of lesions). Unfortunately, there are no publicly available datasets with a sizable number of CT-detected malignant nodules [25]. The NLST database is the largest database that is open to the public, but the metadata does not specify which nodules were biopsied. Therefore, even with all the available screening scans and knowledge of the pathological evidence, it is not always clear which CT lesions were cancerous.

However, the issue of lack of data is currently being addressed by a variety of approaches, one of which is the creation and dissemination of databases that are open to the public. For instance, in 2017, the National Institutes of Health disseminated one hundred thousand labeled chest radiographs [26,27] in their collection. The labels of the data were obtained by applying the technology of natural language processing into reading the radiology reports. It makes it possible to implement bigger databases and skip the human labeling step. It will also resolve the imperfection in statistical significance and make it conducive to further study.

The methods employed in lung nodule image classification have shown massive progress from user-defined to technological feature-based methods. Though the accuracy achieved with the user-defined features is over 90%, as seen in the work of Liu and Hou [28], and Wei and Cao [29], it is solely based on the professional understanding and analysis of nodules which is very subjective and lacks uniformity and standardization. Performance can be improved by combining it with other methods like generic features. Most research studies have resorted to using AI tools in developing algorithms, which are most efficient in identifying features of imaging and making precise differentiation, improving lung cancer detection [30]. AI can be employed to improve the efficiency of Radiologists in nodule detection. It must meet several requirements, such as processing speed, cost of training, maintenance, and implementation to detect various shapes, and low numbers of false positives, for Radiologists to use it routinely [31,32].

The use of a convolutional neural network (CNN) like the generative adversarial network (GAN) is another method that can be utilized to circumvent the lack of large datasets [33]. This method involves the generation of data sets that are fabricated to contain characteristics that are analogous to those of a specific training dataset. These GANs could be taught to learn representative features in a totally unsupervised fashion through the process of training [31]. The labeling step can be skipped entirely because the features are generated rather than chosen from images that already exist in the database. GANs can either be integrated into supervised strategies or used on their own without supervision.

5. Conclusion

In conclusion, the experiment's results demonstrated that the uAI Discover Chest outperformed the Radiologists' assessment on average in terms of lesion identification sensitivity. Furthermore, the performance of the uAI

Discover Chest algorithm to identify lung nodules is consistent and less subjective compared to assessments made by skilled Radiologists regardless of lung nodule size. Results obtained in this study also suggest that the use of uAI Discover Chest for clinical screening can greatly benefit Radiologists in making a substantial diagnosis. The uAI Discover Chest can be considered an effective tool due to its advantages such as consistent performance, faster processing, and high clinical efficiency.

6. Image/Figure Courtesy

All images are the courtesy of Republic Zangiota No-2 COVID Specialized Hospital, Taskent, Uzbekistan.

7. References

1. Liang F, Li C, Fu X. Evaluation of the Effectiveness of Artificial Intelligence Chest CT Lung Nodule Detection Based on Deep Learning. J Healthc Eng. 2021 Aug 17;2021:9971325. doi: 10.1155/2021/9971325. PMID: 34447527; PMCID: PMC8384550.

2. MacMahon H, Austin JH, Gamsu G, Herold CJ, Jett JR, Naidich DP, Patz EF Jr, Swensen SJ; Fleischner Society. Guidelines for management of small pulmonary nodules detected on CT scans: a statement from the Fleischner Society. Radiology. 2005 Nov;237(2):395-400. doi: 10.1148/radiol.2372041887. PMID: 16244247.

3. Callister ME, Baldwin DR, Akram AR, Barnard S, Cane P, Draffan J, Franks K, Gleeson F, Graham R, Malhotra P, Prokop M, Rodger K, Subesinghe M, Waller D, Woolhouse I; British Thoracic Society Pulmonary Nodule Guideline Development Group; British Thoracic Society Standards of Care Committee. British Thoracic Society guidelines for the investigation and management of pulmonary nodules. Thorax. 2015 Aug;70 Suppl 2:ii1-ii54. doi: 10.1136/thoraxjnl-2015-207168. Erratum in: Thorax. 2015 Dec;70(12):1188. PMID: 26082159.

4. Wang X, Mao K, Wang L, Yang P, Lu D, He P. An Appraisal of Lung Nodules Automatic Classification Algorithms for CT Images. Sensors (Basel). 2019 Jan 7;19(1):194. doi: 10.3390/s19010194. PMID: 30621101; PMCID: PMC6338921.

5. Kundel HL, Revesz G. Lesion conspicuity, structured noise, and film reader error. AJR Am J Roentgenol. 1976 Jun;126(6):1233-8. doi: 10.2214/ajr.126.6.1233. PMID: 179387.

6. Berbaum KS, Franken EA Jr, Dorfman DD, Rooholamini SA, Kathol MH, Barloon TJ, Behlke FM, Sato Y, Lu CH, el-Khoury GY, et al. Satisfaction of search in diagnostic radiology. Invest Radiol. 1990 Feb;25(2):133-40. doi: 10.1097/00004424-199002000-00006. PMID: 2312249.

7. Renfrew DL, Franken EA Jr, Berbaum KS, Weigelt FH, Abu-Yousef MM. Error in radiology: classification and lessons in 182 cases presented at a problem case conference. Radiology. 1992 Apr;183(1):145-50. doi: 10.1148/radiology.183.1.1549661. PMID: 1549661.

8. Firmino M, Morais AH, Mendoça RM, Dantas MR, Hekis HR, Valentim R. Computer-aided detection system for lung cancer in computed tomography scans: review and future prospects. Biomed Eng Online. 2014 Apr 8;13:41. doi: 10.1186/1475-925X-13-41. PMID: 24713067; PMCID: PMC3995505.

9. Esteva A, Kuprel B, Novoa RA, Ko J, Swetter SM, Blau HM, Thrun S. Dermatologist-level classification of skin cancer with deep neural networks. Nature. 2017 Feb 2;542(7639):115-118. doi: 10.1038/nature21056. Epub 2017 Jan 25. Erratum in: Nature. 2017 Jun 28;546(7660):686. PMID: 28117445; PMCID: PMC8382232.

10. Abedi V, Goyal N, Tsivgoulis G, Hosseinichimeh N, Hontecillas R, Bassaganya-Riera J, Elijovich L, Metter JE, Alexandrov AW, Liebeskind DS, Alexandrov AV, Zand R. Novel Screening Tool for Stroke Using Artificial Neural Network. Stroke. 2017 Jun;48(6):1678-1681. doi: 10.1161/STROKEAHA.117.017033. Epub 2017 Apr 24. PMID: 28438906.

11. Bejnordi, B.E., Veta, M., Van Diest, P.J., Van Ginneken, B., Karssemeijer, N., Litjens, G., Van Der Laak, J.A., Hermsen, M., Manson, Q.F., Balkenhol, M. and Geessink, O., 2017. Diagnostic assessment of deep learning algorithms for detection of lymph node metastases in women with breast cancer. Jama, 318(22), pp.2199-2210.

12. Gulshan V, Peng L, Coram M, Stumpe MC, Wu D, Narayanaswamy A, Venugopalan S, Widner K, Madams T, Cuadros J, Kim R, Raman R, Nelson PC, Mega JL, Webster

DR. Development and Validation of a Deep Learning Algorithm for Detection of Diabetic Retinopathy in Retinal Fundus Photographs. JAMA. 2016 Dec 13;316(22):2402-2410. doi: 10.1001/jama.2016.17216. PMID: 27898976.

13. Chen PJ, Lin MC, Lai MJ, Lin JC, Lu HH, Tseng VS. Accurate Classification of Diminutive Colorectal Polyps Using Computer-Aided Analysis. Gastroenterology. 2018 Feb;154(3):568-575. doi: 10.1053/j.gastro.2017.10.010. Epub 2017 Oct 16. PMID: 29042219.

14. Liu K, Li Q, Ma J, Zhou Z, Sun M, Deng Y, Tu W, Wang Y, Fan L, Xia C, Xiao Y, Zhang R, Liu S. Evaluating a Fully Automated Pulmonary Nodule Detection Approach and Its Impact on Radiologist Performance. Radiol Artif Intell. 2019 May 29;1(3):e180084. doi: 10.1148/ryai.2019180084. PMID: 33937792; PMCID: PMC8017422.

15. Wang YX, Gong JS, Suzuki K, Morcos SK. Evidence based imaging strategies for solitary pulmonary nodule. J Thorac Dis. 2014 Jul;6(7):872-87. doi: 10.3978/j.issn.2072-1439.2014.07.26. PMID: 25093083; PMCID: PMC4120179.

16. Xiao Y, Wang X, Li Q, Fan R, Chen R, Shao Y, Chen Y, Gao Y, Liu A, Chen L, Liu S. A cascade and heterogeneous neural network for CT pulmonary nodule detection and its evaluation on both phantom and patient data. Comput Med Imaging Graph. 2021 Jun;90:101889. doi: 10.1016/j.compmedimag.2021.101889. PMID: 33848755.

17. Dongdong Gu, Guocai Liu, and Zhong Xue. On the performance of lung nodule detection, segmentation and classification. Comput Med Imaging Graph. 2021; 89:101886. https://doi.org/10.1016/j.compmedimag.2021.101886

18. National Comprehensive Cancer Network. Lung cancer screening version 1. 2020. Available from: https://www.nccn.org/patients [Accessed on Feb 6, 2021].

19. Chen L, Gu D, Chen Y, Shao Y, Cao X, Liu G, Gao Y, Wang Q, Shen D. An artificial-intelligence lung imaging analysis system (ALIAS) for population-based nodule computing in CT scans. Comput Med Imaging Graph. 2021 Apr;89:101899. doi: 10.1016/j.compmedimag.2021.101899. Epub 2021 Mar 11. PMID: 33761446.

20. Chamberlin, J., Kocher, M.R., Waltz, J. et al. Automated detection of lung nodules and coronary artery calcium using artificial intelligence on low-dose CT scans for lung cancer screening: accuracy and prognostic value. BMC Med 19, 55 (2021). https://doi.org/10.1186/s12916-021-01928-3

21. Fukui Liang, Caiqin Li, Xiaoqin Fu, "Evaluation of the Effectiveness of Artificial Intelligence Chest CT Lung Nodule Detection Based on Deep Learning", Journal of Healthcare Engineering, vol. 2021, Article ID 9971325, 10 pages, 2021. https://doi.org/10.1155/2021/9971325

22. Yoo H, Kim KH, Singh R, Digumarthy SR, Kalra MK. Validation of a Deep Learning Algorithm for the Detection of Malignant Pulmonary Nodules in Chest Radiographs. JAMA Netw Open. 2020 Sep 1;3(9):e2017135. doi: 10.1001/jamanetworkopen.2020.17135. PMID: 32970157; PMCID: PMC7516603.

23. Espinoza JL, Dong LT. Artificial Intelligence Tools for Refining Lung Cancer Screening. J Clin Med. 2020 Nov 27;9(12):3860. doi: 10.3390/jcm9123860. PMID: 33261057; PMCID: PMC7760157.

24. Wang X, Peng Y, Lu L, et al. ChestX-Ray8: Hospital-Scale Chest X-Ray Database and Benchmarks on Weakly-Supervised Classification and Localization of Common Thorax Diseases, 2017 IEEE Conference on Computer Vision and Pattern Recognition (CVPR), Honolulu, HI, 2017:3462-71.

25. Schreuder A, Scholten ET, van Ginneken B, Jacobs C. Artificial intelligence for detection and characterization of pulmonary nodules in lung cancer CT screening: ready for practice? Transl Lung Cancer Res 2021;10(5):2378-2388. doi: 10.21037/tlcr-2020-lcs-06

26. Wang X, Peng Y, Lu L, et al. ChestX-Ray8: Hospital-Scale Chest X-Ray Database and Benchmarks on Weakly-Supervised Classification and Localization of Common Thorax Diseases, 2017 IEEE Conference on Computer Vision and Pattern Recognition (CVPR), Honolulu, HI, 2017:3462-71.

27. Tandon YK, Bartholmai BJ, Koo CW. Putting artificial intelligence (AI) on the spot: machine learning evaluation of pulmonary nodules. J Thorac Dis. 2020 Nov;12(11):6954-6965. doi: 10.21037/jtd-2019-cptn-03. PMID: 33282401; PMCID: PMC7711413.

28. Liu X.L., Hou F., Hao A. Multi-view multi-scale CNNs for lung nodule type classification from CT images. Pattern Recognit. 2018;77:262–275. doi: 10.1016/j.patcog.2017.12.022.

29. Wei G, Cao H, Ma H, Qi S, Qian W, Ma Z. Content-based image retrieval for Lung Nodule Classification Using Texture Features and Learned Distance Metric. J Med Syst. 2017 Nov 29;42(1):13. doi: 10.1007/s10916-017-0874-5. PMID: 29185058.

30. 22. Goodfellow I, Pouget-Abadie J, Mirza M, et al. Generative Adversarial Networks 2014.Availableonline:https://ui.adsabs.harvard.edu/abs/2014arXiv1406.2661G/abstract. Accessed March 2, 2020.

31. Tandon YK, Bartholmai BJ, Koo CW. Putting artificial intelligence (AI) on the spot: machine learning evaluation of pulmonary nodules. J Thorac Dis. 2020 Nov;12(11):6954-6965. doi: 10.21037/jtd-2019-cptn-03. PMID: 33282401; PMCID: PMC7711413.

Author Biography

Dr. Marufjon Salokhiddinov

Head of Department
Radiology Department,
Republic Zangiota №2 COVID Specialized Hospital
Uzbekistan

Dr. Marufjon Salokhiddinov completed his BSc in Medicine from Tashkent Medical Academy and a one-year internship in Neurology, followed by MSc in Medical Imaging, at the University of Aberdeen, UK. After the completion of his MSc, he was employed at the Department of Radiology, Tashkent Medical Academy. Since 2020, Dr. Marufjon has been working as an M.D. Radiologist at Republic Zangiota No-2 Clinical Hospital, Tashkent, Uzbekistan. Dr. Marufjon has been awarded with several prizes including "El-yurt Umidi" funded MSc by the Government of Uzbekistan, Young Investigator Award by WFN, and Best Poster Awards from WCN, ESR, WFITN, and AAN. He has published several research articles at national and international conferences/congresses.

Performance evaluation of the artificial intelligence assisted compressed sensing MR technique in routine clinical settings

Adiraju Karthik[a], Apoorwa Devappa[b], Dharmesh Singh[c], Dileep Kumar[c]
[a]Department of Radiology, Sprint Diagnostics, Jubilee Hills, Hyderabad, Telangana 500033, India
[b]Department of Radiology, Mahadevappa Rampure Medical College, Sedam Road, Mahadevappa Marg, Kalaburagi, Karnataka 585105, India
[c]Central Research Institute, Global Scientific Collaborations, United Imaging Healthcare

Abstract

Magnetic Resonance (MR) Imaging plays a valuable role in diagnosis and prognosis of diseases. However, the longer scanning time of MR examinations is considered one of the biggest challenges faced by radiology departments and their patients. Recently, the introduction of artificial intelligence (AI) and deep learning methods have made it possible to enable ultra-fast image acquisition while maintaining high resolution image quality. In this work, a deep-learning-based reconstruction technique by United Imaging Healthcare called AI-Assisted Compressed Sensing (ACS) was evaluated qualitatively and quantitatively for its utility in routine clinical settings for brain, knee, kidney, liver and spine. MR scans were conducted with ACS and without ACS sequences. Images were assessed by a Radiologist for their quality, artifacts, diagnostic efficacy and sharpness. A quantitative assessment was done by calculating signal to noise ratio (SNR) and contrast to noise ratio (CNR). A qualitative evaluation by a Radiologist showed that the overall quality and diagnostic information in images acquired with ACS was similar to images obtained without ACS. Similarly, the SNR and CNR values obtained from images with ACS demonstrates significantly higher values ($p < 0.05$) as compared with images acquired without ACS. Results obtained in this study also found that ACS-enabled images not only maintain good quality and high resolution with better sharpness but also takes much lesser time for acquisition. In conclusion, the ACS technique is easy to implement in routine clinical settings, provides considerable image quality as compared to those techniques with routine MR sequences, and saves significant time during acquisition, which helps Radiologists and imaging technologists plan more cases with an adequate quality of images for diagnostic purposes.

1. Introduction

MRI can provide multi-parameter and multi-directional imaging of organs, which has significant application value in disease diagnosis and prognosis monitoring. Much effort has been made in recent years to enhance the field of view (FOV), resolution, and acquisition time of MRI sequences. The long examination duration is one of the challenges faced by radiology departments and the patients being examined, making it difficult for some patients to hold still during the examination, leading to motion artifacts. Longer scanning time not only introduces artifacts in acquired images but also significantly increases health cost and availability, especially in countries where the number of MR scanners are limited [1]. The MR imaging cycle is repeated many times during the acquisition process and the number of cycles depends on the quality of the image that is required. Signal-to-noise ratio (SNR) is primarily used in MR for image evaluation and quality assurance; however, SNR in MR is inherently constrained. One must find an acceptable trade-off between spatial resolution and scan time in most clinical applications. With more clinical examinations being performed, innovative accelerated imaging is urgently needed to enable ultra-fast scanning while producing high-quality images [2]. In recent times, compressed sensing-based techniques, (nonlinear mathematical models that successfully suppress noise bands and acceleration-induced artifacts), have been developed and employed in several clinical studies [3-5]. These technologies effectively reduce imaging time, but at the cost of image quality. The number of studies examining the image quality of compressed sensing for therapeutic applications is growing. Nevertheless, image quality of compressed sensing for cardiac, brain, liver, cervical artery, and prostate MR is poorly studied, and analysis of its use in clinical routine is

lacking. Several attempts have been made to overcome issues faced in compressed sensing as well as in other acceleration techniques such as half Fourier and parallel imaging methods. Recently, a deep- learning-based reconstruction technique called uAI®-Assisted Compressed Sensing (ACS) was introduced that is integrated with conventional acceleration techniques to provide better quality and reduced scanning time [6]. Despite the fact that ACS has been successfully applied to most body organs, its utility in a routine clinical setting has not been specifically tested. This study is thus conducted to measure performance of ACS in terms of scanning time, qualitative and quantitative parameters in depicting image quality in clinical settings.

2. Materials and Methods

2.1 Subjects

In this study, 25 subjects were randomly selected to undergo MR examination of different body regions such as brain, spine, knee, liver and kidney prospectively. For each body region, five subjects were chosen so that five MR datasets were acquired for each body region, with and without the ACS technique, using different MR contrasts.

2.2 MR Examination & protocols

All MR exams were performed on the 3T uMR® 780 system (United Imaging Healthcare Shanghai, China) at Sprint Diagnostics in Hyderabad, India. Before the examination, a consent form was signed by all subjects. For brain MR scanning, a dedicated 24 channel head-neck coil was used, while spine exams were performed using a 32-channel spine coil. For knee MR, a dedicated 12 channel coil was used, while for liver and kidney a combination of 12 channel body coil and 12 channel spine coil was used. A complete detail of different contrast and protocols parameters used in this study are included in Table 1. All sequence parameters were kept identical to acquire data with ACS and without ACS in all body regions.

Table 1. Scanning protocols of all sequences.

Region	Sequence Name	ACS/Non-ACS	Plane	TR	TE	ST	FA	#slice	AD	AF_ACS
Brain	T1-weighted FSE Flair	Non-ACS	Axial	2023	22.96	5	90	23	02:01	
	T2-weighted FSE Flair with FS	Non-ACS	Axial	9000	103.32	5	90	23	02:24	
	T1-weighted FSE	Non-ACS	Axial	375	6.32	5	90	23	02:08	
	T2-weighted FSE	Non-ACS	Axial	5552	118.08	5	90	23	01:07	
	T1-weighted FSE Flair	ACS	Axial	2023	22.96	5	90	23	00:53	2.5
	T2-weighted FSE Flair with FS	ACS	Axial	9000	103.32	5	90	23	01:30	2.5
	T1-weighted FSE	ACS	Axial	375	6.32	5	90	23	00:57	2.5
	T2-weighted FSE	ACS	Axial	5552	118.08	5	90	23	00:39	2.25
Spine	T1-weighted FSE	Non-ACS	Sagittal	750	9.26	4	90	11	01:49	
	T2-weighted FSE	Non-ACS	Sagittal	5421	121.8	4	90	11	02:21	
	T1-weighted FSE	ACS	Sagittal	750	9.26	4	90	11	00:51	2.25
	T2-weighted FSE	ACS	Sagittal	5421	121.8	4	90	11	01:00	2.25
Liver	T2-weighted_NAVI	Non-ACS	Axial	2775	84.8	6	90	24	03:53	
	T2-weighted FSE with FS and BH	ACS	Axial	2950	98.42	6	90	24	00:17	2.25
Kidney	T2-weighted_NAVI	Non-ACS	Axial	2700	84.8	6	90	24	04:08	
	T2-weighted FSE with FS and BH	ACS	Axial	8220	121	6	90	24	00:12	2.75
Knee	Proton Density FSE with FS	Non-ACS	Coronal	2780	38.3	3	90	26	03:34	
	T2-weighted FSE	Non-ACS	Sagittal	3200	118.08	3	90	26	04:10	
	T1-weighted FSE	Non-ACS	Axial	686	7.64	3	90	26	04:13	
	Proton Density FSE with FS	ACS	Coronal	2780	38.3	3	90	26	01:54	2
	T2-weighted FSE	ACS	Sagittal	3200	118.08	3	90	26	01:49	2.25
	T1-weighted FSE	ACS	Axial	686	7.64	3	90	26	01:47	2.25

FSE- Fast Spin Echo, FS- Fat Supression, BH- Breathhold, TR- Repetition Time, TE- Echo Time, ST- Slice Thickness, FA- Flip Angle, AD- Acquistion Duration, Acceleration Factor for ACS

2.3 Qualitative Evaluation

After the MR scan, images were transferred to a local clinical picture archiving and communication system (PACS) system and uWS® MR workstation (United Imaging Healthcare, Shanghai, China) available on the premises. For the qualitative evaluation of images acquired in different body regions from all subjects, a standard scoring was designed to evaluate quality in terms of artifacts in images, sharpness of tissue edges, overall images quality and the diagnostic efficiency of images. The scores were given on a 5-point scale ranging between 0 to 4 based on the parameters. Detailed information on the scoring is given in Table 2 below. A Radiologist with around 5 years of overall experience was asked to read all images and provide a rating based on the parameters shown here.

Table 2. Scoring criteria for qualitative analysis.

Parameters	Scores				
	0	1	2	3	4
Image Artefact	Non-Diagnostic Image Quality	Major Artifacts	Moderate Artifacts	Mild Artifacts	No Artifacts
Image Sharpness	Poor	Intermediate	Acceptable	Good	Perfect
Overall Image Quality	Poor	Intermediate	Acceptable	Good	Perfect
Diagnostic Efficiency	Poor	Intermediate	Acceptable	Good	Perfect

2.4 Quantitative Evaluation

Following the Radiologist's evaluation of qualitative criteria, all images were anonymised and transferred to a workstation. The quantitative assessment was further performed by calculating Signal to Noise ratio (SNR) and Contrast to Noise Ratio (CNR) in all the sequences for all body regions. To calculate these image quality parameters, multiple regions of interest (ROIs) in different tissue locations were drawn in the images to obtain average signal intensities and standard deviation of those signal intensities. The SNR and CNR measurements were performed using MATLAB (v.2018; MathWorks) functions using the formula given in Equation 1 and Equation 2. In order to demonstrate the capabilities of ACS enabled imaging, scanning time was also included in study as a quantitative parameter.

$$SNR = \frac{Average\ Signal\ Intensities}{Standard\ Deviation\ of\ noise} \dots\dots\dots\dots\dots\dots (1)$$

$$CNR = \frac{Difference\ in\ signal\ intensities}{Standard\ Deviation\ of\ noise} \dots\dots\dots\dots\dots (2)$$

SNR and CNR values were obtained in all sequences for five regions obtained from the 25 subjects and further used to conduct statistical analysis and correlations with qualitative evaluations done by the expert Radiologist.

2.5 Statistical analysis:

All the statistical analysis was done in MedCalc®, version 19.3 software (MedCalc Software Ltd). Qualitative and quantitative results obtained from both ACS and Non-ACS enabled image assessments were then compared using Mann-Whitney U-test and unpaired Student's t-test. Using Pearson's correlation coefficient, SNR and CNR values from non-ACS sequences were compared with those obtained from ACS sequences (*r*).

3. Results

One Radiologist interpreted and scored the images acquired in five different regions of all 25 subjects included in this study and was asked to evaluate quality in terms of artifacts, sharpness, overall image quality and diagnostic efficiency for two groups (ACS vs. Non-ACS) of images. The mean score of all assessments done by the Radiologist for each body region examined in this study are presented in Figure 1. Mann-Whitney U-test conducted in this study shows no significant difference ($p > 0.05$) in qualitative image quality between images acquired with ACS and images acquired without ACS, which means comparable results for both groups. A Radiologist's qualitative evaluation found that the diagnostic quality with all four parameters such as image

artifact, image sharpness, overall image quality and diagnostic efficacy of images acquired with ACS was similar to or better than those obtained without ACS (Figure 1).

For the quantitative evaluation, SNR and CNR was measured in all sequences acquired with and without ACS as reported in Table 1 above for all body regions. The SNR values across all sequences for brain, spine, liver, kidney and knee were 37.92 ± 1.79, 44.2 ± 5.26, 43.26 ± 1.37, 43.41 ± 1.62 and 39.62 ± 3.63 in images acquired without ACS whereas the SNR values were 40.13 ± 2.00, 45.75 ± 4.90, 45.5 ± 2.20, 45.36 ± 2.56 and 41.60 ± 4.51, respectively in images acquired with ACS as shown in Figure 2. Similarly, CNR values obtained for brain, spine, liver, kidney and knee were 21.18 ± 5.23, 27.62 ± 5.90, 20.83 ± 3.62, 24.75 ± 2.95 and 24.75 ± 2.95 for images acquired without ACS and the CNR values were 22.10 ± 5.71, 29.70 ± 5.78, 22.54 ± 4.20 28.7 ± 3.68 and 28.80 ± 3.92, respectively for images acquired with ACS as shown in Figure 3. Both SNR and CNR values in 5 different regions were found to be slightly better in images acquired with ACS as compared to images acquired without ACS. According to the unpaired Student's *t-test*, ACS-based measurements showed substantially higher values ($p < 0.05$) for both SNR and CNR ac compared to non-ACS measurements. There was a good correlation ($r = 0.93$ for SNR and $r = 0.88$ for CNR) between non-ACS and ACS measurement.

In terms of scan time differences, total scanning time for all sequences acquired in each body region was calculated. For an example, T1-weighted FSE, T2-weighted FSE, T1-weighted FSE Flair, and T2-weighted FSE Flair with FS were acquired in the brain region with and without the ACS technique, and the total time was calculated for all 4 sequences acquired with ACS and without ACS. Similarly, the total scanning time was calculated for all five body regions for the respective sequences included in this study. Figure 4 shows the total scanning time values for each body region. The differences in scanning time of ACS enabled sequences showed significant improvements in scanning time compared to non-ACS sequences. For brain, spine, liver, kidney and knee examination, an improvement in scan time in terms of percentage of 48.10%, 55.52%, 92.80%, 95.15% and 54% respectively was observed, which shows impressive results while ensuring similar image quality. Examples of images acquired with ACS and without ACS technique in different body regions are shown in the Figures 5-9.

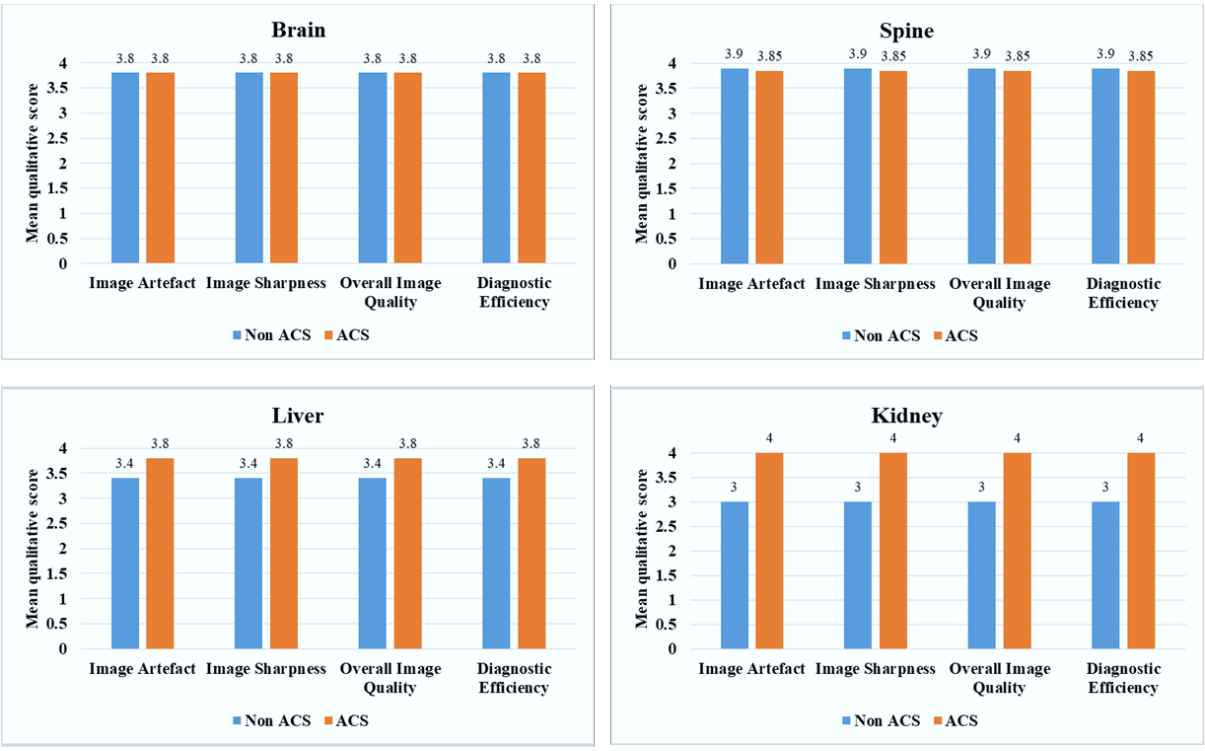

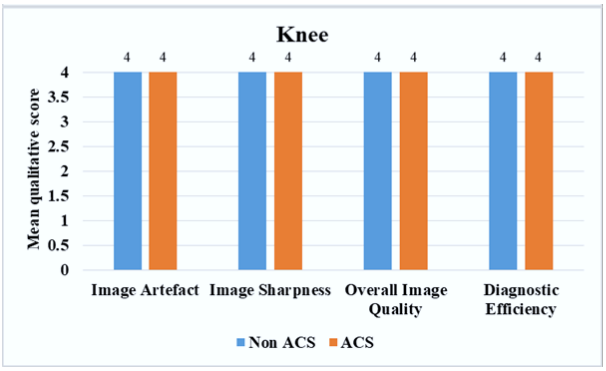

Figure 1. Mean qualitative score of ACS vs. Non-ACS for all body regions read by a Radiologist.

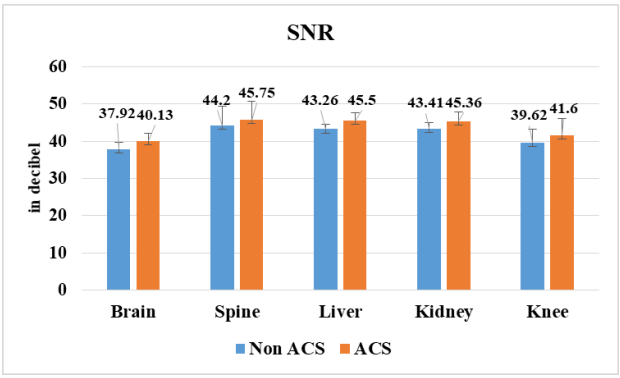

Figure 2. SNR across all body regions for non-ACS vs. ACS.

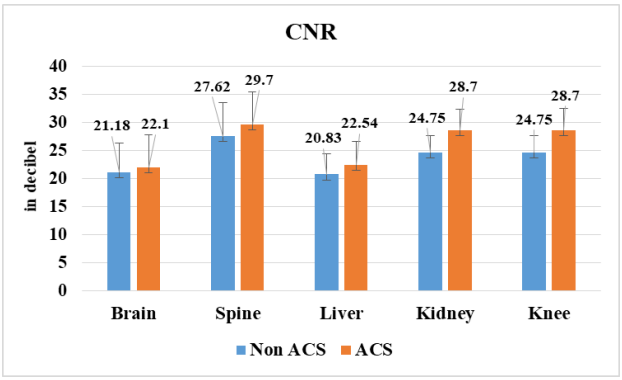

Figure 3. CNR across all body regions for non-ACS vs. ACS.

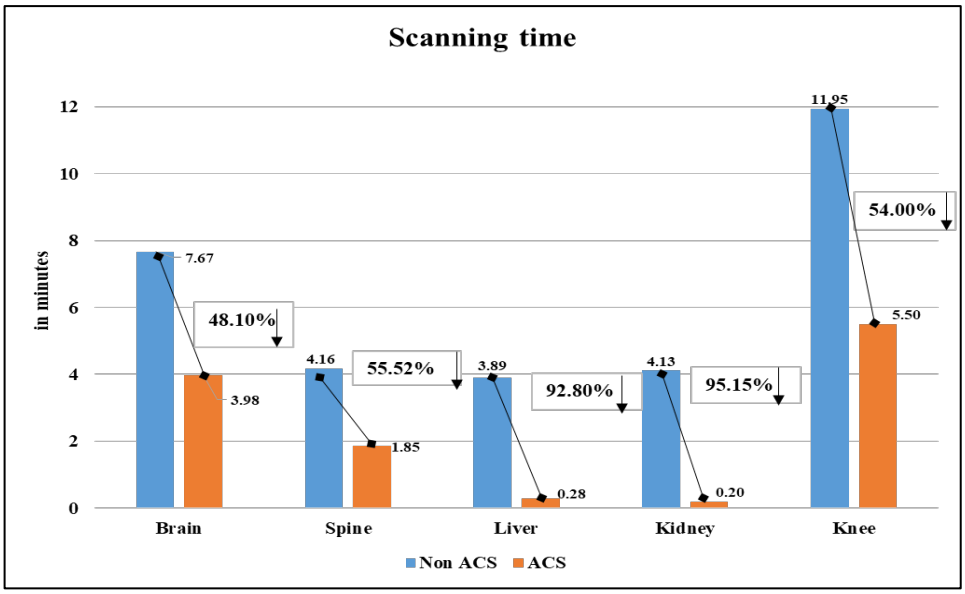

Figure 4. Total scanning time across all sequences for different body regions with percentage difference in scanning time between non-ACS and ACS in minutes.

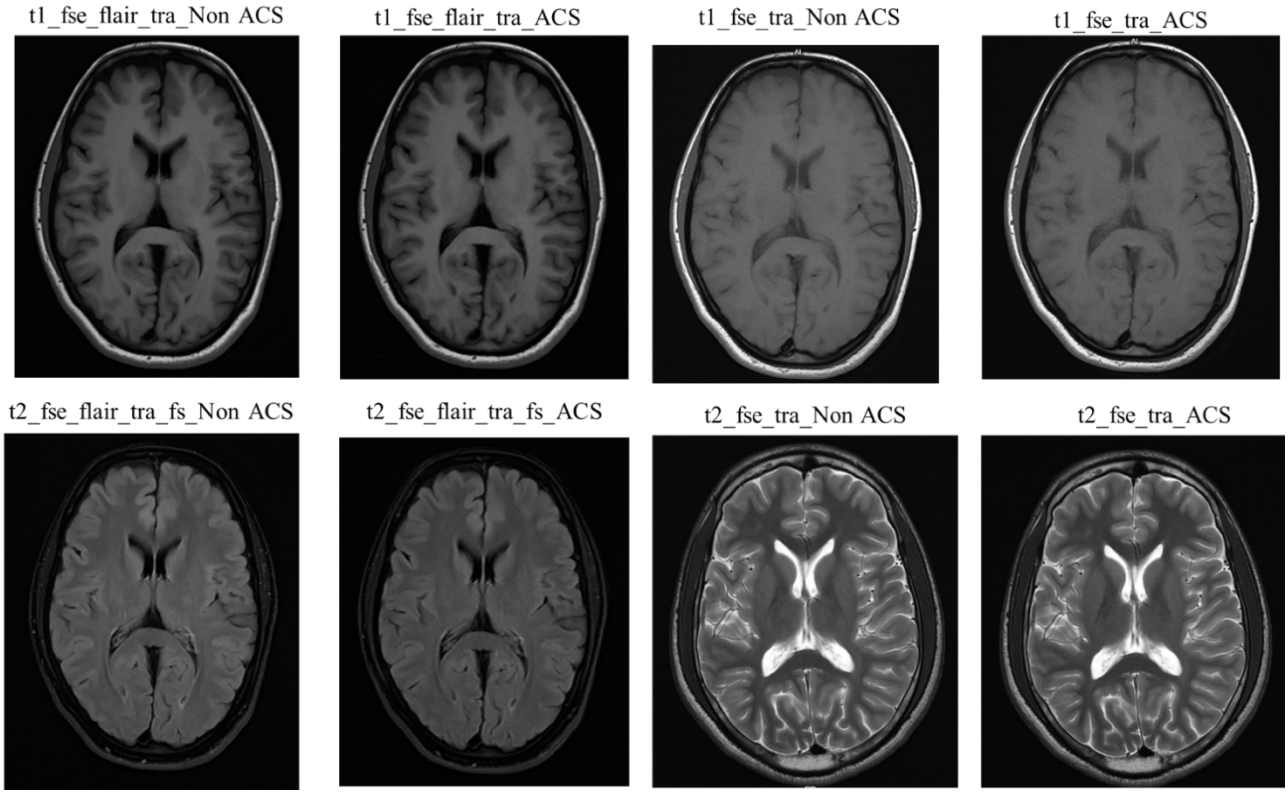

Figure 5. Brain MRI slices for all sequences of a representative subject.

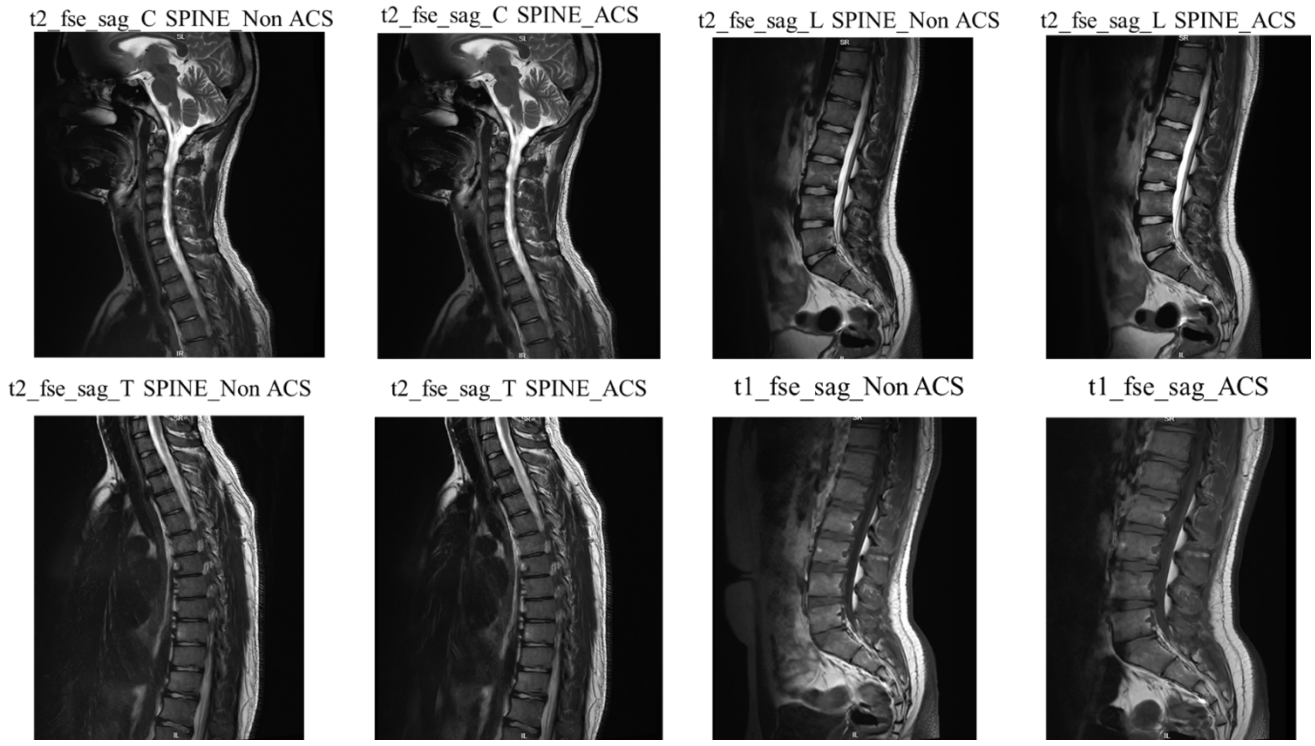

Figure 6. Spine MRI slices for all sequences of a representative subject.

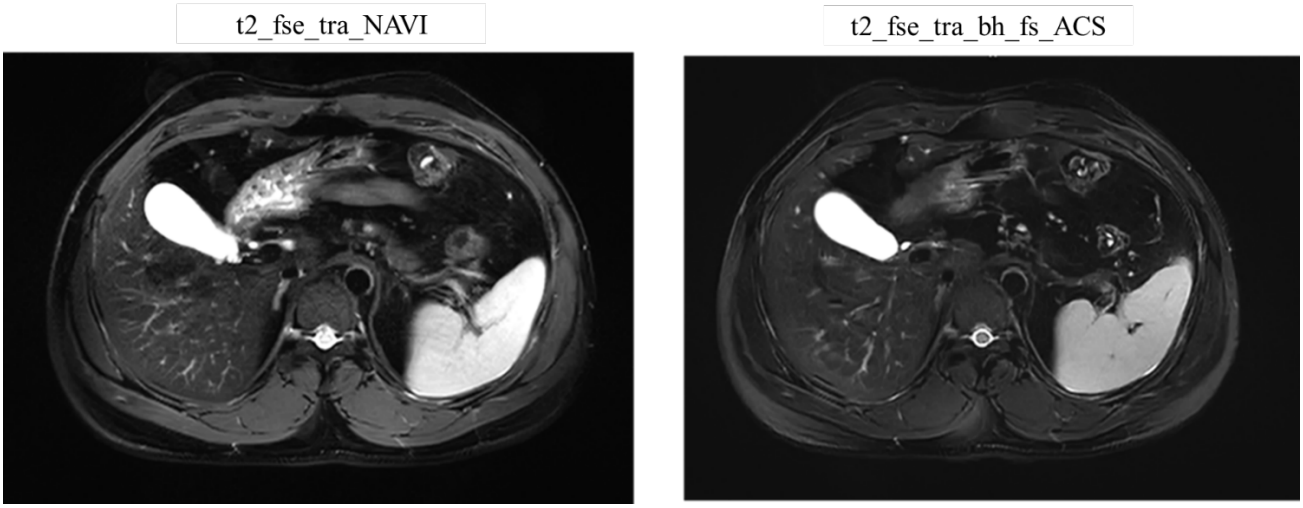

Figure 7. Liver MRI slice for all sequences of a representative subject.

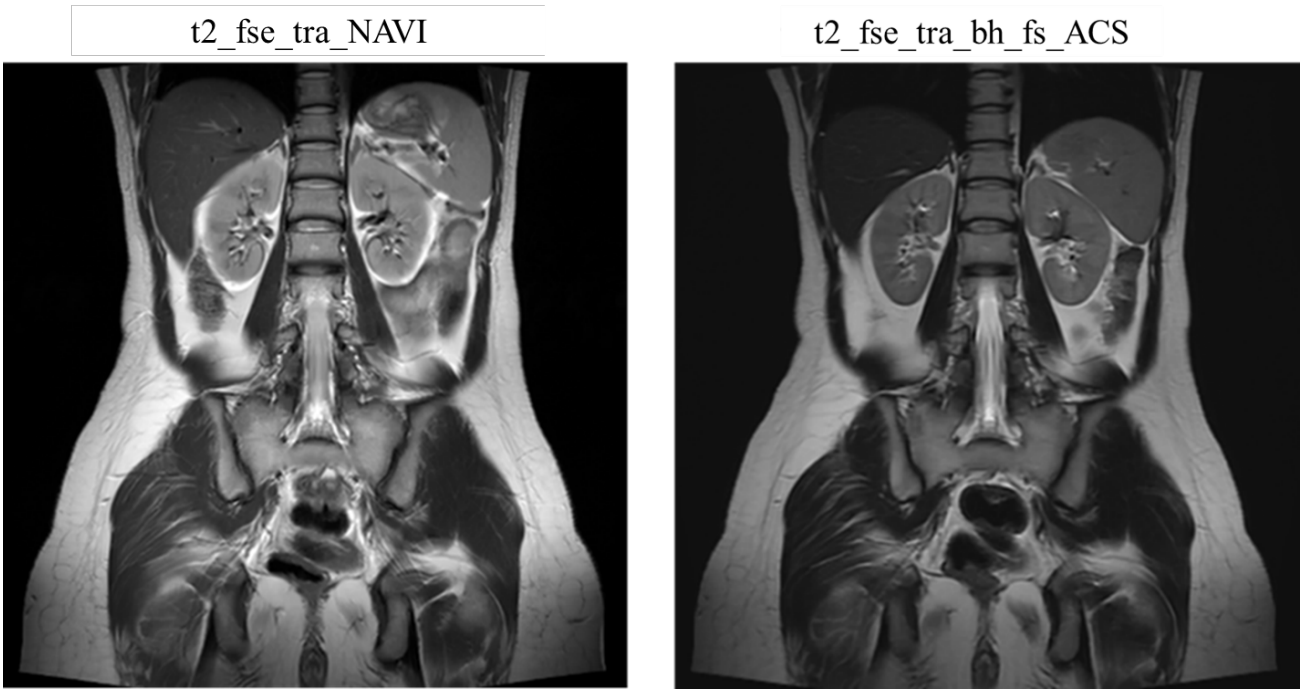

Figure 8. Kidney MRI slice for all sequences of a representative subject.

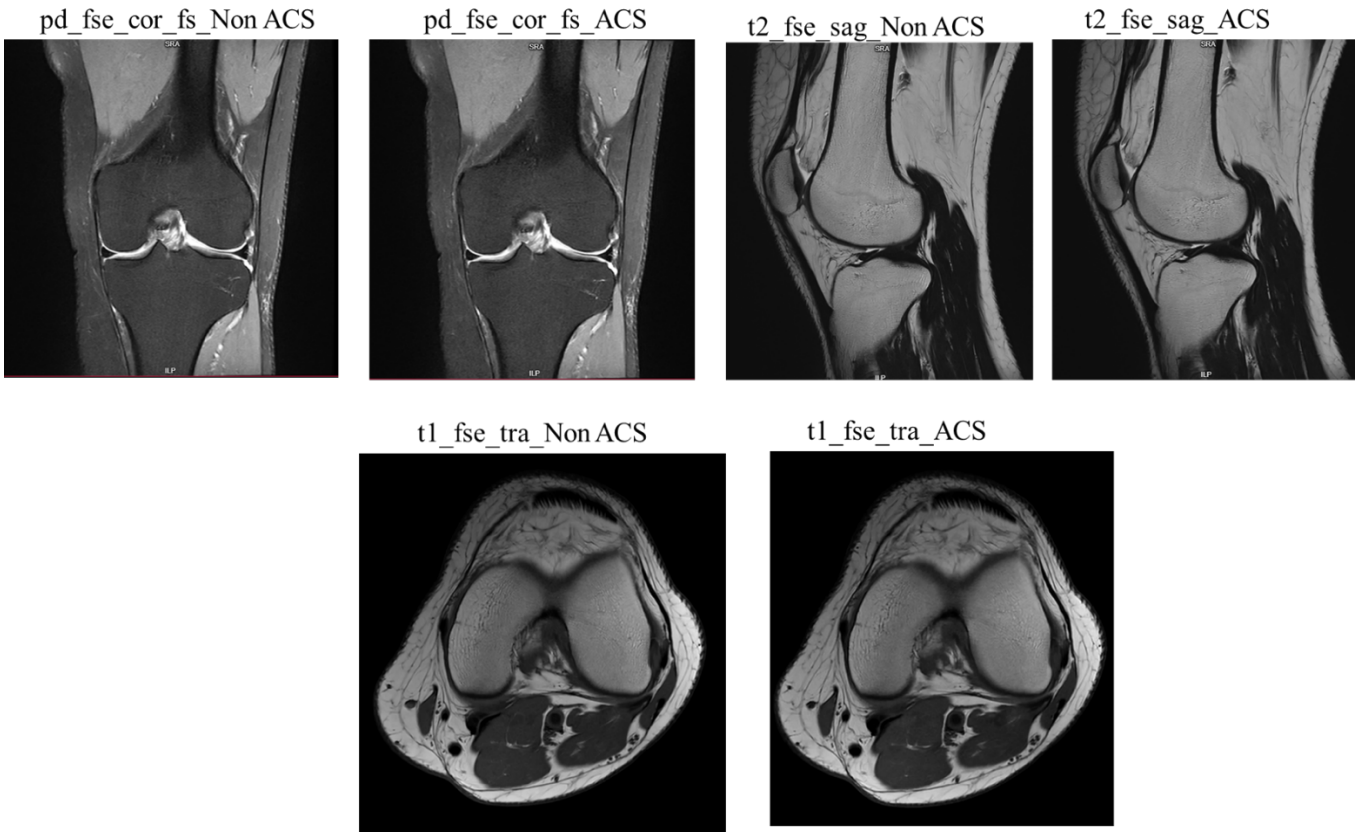

Figure 9. Knee MRI slices for all sequences of a representative subject.

4. Discussion/Conclusion

In this study, a clinical study of AI Assisted Compressed Sensing (ACS) magnetic resonance technology developed by United Imaging Healthcare was performed to measure its utility and effectiveness in routine clinical settings for different body regions (brain, spine, liver, kidney, and knee). Performance was measured in terms of scan duration, including both qualitative and quantitative parameters. The subjective image quality scoring parameters included artifacts in images, sharpness of tissue edges, overall image quality and the diagnostic efficiency of images and quantitative evaluation was done by measuring SNR and CNR. Often, compressed sensing methods are applied to different sequences, but they provide image artifacts and low quality of images for diagnostic purposes. In the past, several methods have also been introduced that help in image acquisition time reduction but lack in providing better outcomes for Radiologists to read or interpret those images for diagnostic accuracy. The findings of this study, on the other hand, revealed that the diagnostic quality of images acquired with ACS was similar to or better than images obtained without ACS.

Scan time, SNR, and CNR are the parameters traditionally used to demonstrate image quality with reasonable time for acquisition; there is typically a trade-off among all these parameters. Compared to non-ACS sequences, ACS has much shorter scan times for all body region sequences, enabling ultra-fast scans. Due to discomfort, disturbances in consciousness, and other factors, it might be difficult for some patients with severe disorders to maintain still for an extended period during imaging studies, which causes artifacts and lowers image quality. This issue can be resolved with ACS technology, which can also enhance image quality and clinical precision. Additionally, in line with literature [7], the SNR and CNR of the ACS subgroup were greater than those of the non-ACS or conventional group.

This study has some limitations. First, the data was acquired from a single institution and a small cohort, which may

influence the outcomes. A large cohort and multicentre study can provide stronger evidence for larger clinical applications. Second, the reference measurement was done by only one Radiologist; inter-observer and intra-observer variability were not evaluated.

In conclusion, ACS technology not only substantially lowered scan time duration, but also provided diagnostic quality images without artifacts -- which enables this method to be clinically suitable, especially for the routine clinical settings where workload is high and patients may be non-cooperative. Sequences enabled with ACS should more frequently be used in the clinical settings to improve image quality, diagnostic value, and the effectiveness of radiology imaging departments.

5. Image/Figure Courtesy

All images are the courtesy of Sprint Diagnostics, Jubilee Hills, Hyderabad, Telangana 500033, India.

6. References

1. Xiang L, Chen Y, Chang W, Zhan Y, Lin W, Wang Q, Shen D. Ultra-Fast T2-Weighted MR Reconstruction Using Complementary T1-Weighted Information. Med Image Comput Comput Assist Interv. 2018 Sep;11070:215-223. doi: 10.1007/978-3-030-00928-1_25. Epub 2018 Sep 26. PMID: 30906934; PMCID: PMC6430217.

2. Wang S, Su Z, Ying L, Peng S, Liang F, Feng D, Liang D: Accelerating magnetic resonance imaging via deep learning. In: IEEE 13th International Symposium on Biomedical Imaging (ISBI), pp. 514–517. IEEE; (2016).

3. Sheng RF, Zheng LY, Jin KP, et al. Single-breath-hold T2WI liver MRI with deep learning-based reconstruction: a clinical feasibility study in comparison to conventional multi-breath-hold T2WI liver MRI. *Magn Reson Imaging.* 2021;**81**:75.

4. Lei X, Yong C, et al. Ultra-fast T2-weighted MR reconstruction using complementary T1-weighted information. Medical image computing and computer-assisted intervention: MICCAI. In: International Conference on Medical Image Computing and Computer-Assisted Intervention, 2018.

5. Katayama M, Masui T, Kobayashi S, et al. Fat-suppressed T2-weighted MRI of the liver: comparison of respiratory-triggered fast spin-echo, breath-hold single-shot fast spin-echo, and breath-hold fast-recovery fast spin-echo sequences. *J Magn Reson Imaging.* 2001;**14**(4):439–449.

6. Wang, Shanshan & Cao, Guohua & Wang, Yan & Liao, Shu & Wang, Qian & Shi, Jun & Li, Cheng. (2021). Review and Prospect: Artificial Intelligence in Advanced Medical Imaging. Frontiers in Radiology. 1. 10.3389/fradi.2021.781868.

7. Zhao Y, Peng C, Wang S, Liang X, Meng X. The feasibility investigation of AI -assisted compressed sensing in kidney MR imaging: an ultra-fast T2WI imaging technology. BMC Med Imaging. 2022; 4;22(1):119.

Author's Biography

Dr. Adiraju Karthik

Consultant Radiologist
Department of Radiology,
Sprint Diagnostics,
Hyderabad, Telangana
500033, India

Dr. Adiraju Karthik is a young aspiring Radiologist with around four years of experience in the field. He is currently working as Consultant Radiologist in Sprint Diagnostics. He is holding a position as Director of Karthik Diagnostic Centre and as Assistant Professor in the Department of Radiology, Kamineni Institute of Medical Sciences. Dr. Karthik obtained his MBBS degree with honors and his M.D. with a Gold Medal. He has published several articles and case reports in national and international journals and conferences.

Dr. Apoorwa Devappa

Consultant Radiologist
Department of Radiology,
Sprint Diagnostics,
Hyderabad, Telangana
500033, India

Dr. Apoorwa Devappa obtained her MBBS degree with honors and is currently a Junior Resident at the Department of Radiology, Mahadevappa Rampure Medical College. She has a special interest in cross sectional imaging.

The use of artificial intelligence in cardiac magnetic resonance imaging

Mary Watkins[a#], Vidya Sridhar[b#], Xiao Chen[c], Anne Atteberry[a], Shanhui Sun[c], Terrence Chen[c], Gregory Lanza[a1]

[a]Washington University School of Medicine, St Louis, MO, USA
[b]UIH America, Inc., Houston, TX, USA
[c]United Imaging Intelligence, Inc., Cambridge, MA, USA
[#]Contributed equally to this work

Abbreviations:
Cardiovascular magnetic resonance – CMR; artificial intelligence – AI; magnetic resonance imaging – MRI; NN – neural network

Some of the artificial intelligence features discussed in this article are not available for clinical use in the U.S. and may not be available for such use in other countries.

1. Introduction

Cardiovascular magnetic resonance (CMR) imaging is considered the gold standard imaging modality for the assessment of cardiac structure and function [1,2] and the primary imaging modality of myocardial tissue characterization. However, CMR is riddled with intrinsic difficulties as its implementation is complex and requires specialized technologist training and expertise. Varying levels of operator expertise introduce non-uniformity between scans within a center and particularly serial studies in a specific patient. In addition, generating accurate and thorough myocardial characterization results can require long periods of limited physical motion as well as repeated breath holds. Consequently, patient throughput decreases and scanner productivity declines. Furthermore, image data post-processing techniques that take advantage of the modality's potential require image processing resources unavailable in most nonacademic institutions.

Artificial intelligence (AI) is increasingly used in healthcare. A recent literature review of AI identified five main health care areas where AI is expected to have significant impact [3]: health care systems management, diagnostics, clinical decision-making, patient data and predictive medicine. For CMR, AI will shorten and simplify workflows, preserve image quality, improve uniformity between scans, and enhance data interpretation for any MR center, regardless of its size or location.

The aim of this review article is to outline and describe some of the implementations of intelligent features for CMR imaging using a 1.5T United Imaging MRI (uMR 570) scanner in collaboration with Washington University School of Medicine in St Louis. The ongoing improvements strive not only for optimal image quality and study workflow but also overall for a simpler modality more accessible for the care of a broader patient population, for example individuals receiving cardiotoxic therapies for survival.

2. EasyScan

Obtaining scout scan acquisitions for CMR in the different orientation requires a skilled technologist. However, longitudinal studies for the image-guided management of patients are inherently subject to data inaccuracy, and variability exists when different technologists are involved. With the advent of automated or semi-automated slice adjustment methods, CMR studies have incorporated new geometric prescription processes [4-11]. For example, Lelieveldt et al [4,5] matched scout images to thoracic

[1] Washington University School of Medicine receives research support from United Imaging through a sponsored research agreement. Dr. Gregory Lanza is a principal investigator for the research.

anatomy models and estimated the left ventricular orientation for automatic view planning. The technique was limited to short-axis slice alignments and computational time was 3–5 min. While the concept was good, the methods were sensitive to the errors in landmarks.

In practice, the optimal position of the reference planes differ among individuals and they do not always pass through predefined landmarks.

Alternatively, United Imaging Healthcare implemented a slice alignment method (EasyScan) based on a deep learning regression network. Rather than relying on a few anatomical points, the image plane calculation utilizes all voxels in the region, reducing landmark detection errors and adding clarity to landmark annotation. The EasyScan AI planning algorithm[2] consists of three steps: (1) cardiac region segmentation using the Otsu method (Ref); (2) distance map calculation using the trained regression network; and (3) plane fitting using a least-squares method.

In our studies, EasyScan accelerated CMR imaging 13% (2.57 min, p<0.001, 95% CI [2.31, 2.83]) versus the traditional scout scan approach. Moreover, in contradistinction to the four-breath holds needed for typical plane prescriptions, EasyScan achieved the result with a single breath-hold scan and minimal operator dependence. EasyScan simplified cardiac image planning in all subjects and also achieved better scan accuracy with less plane angulation error, compared to previous reports for all four cardiac views (Fig. 1).

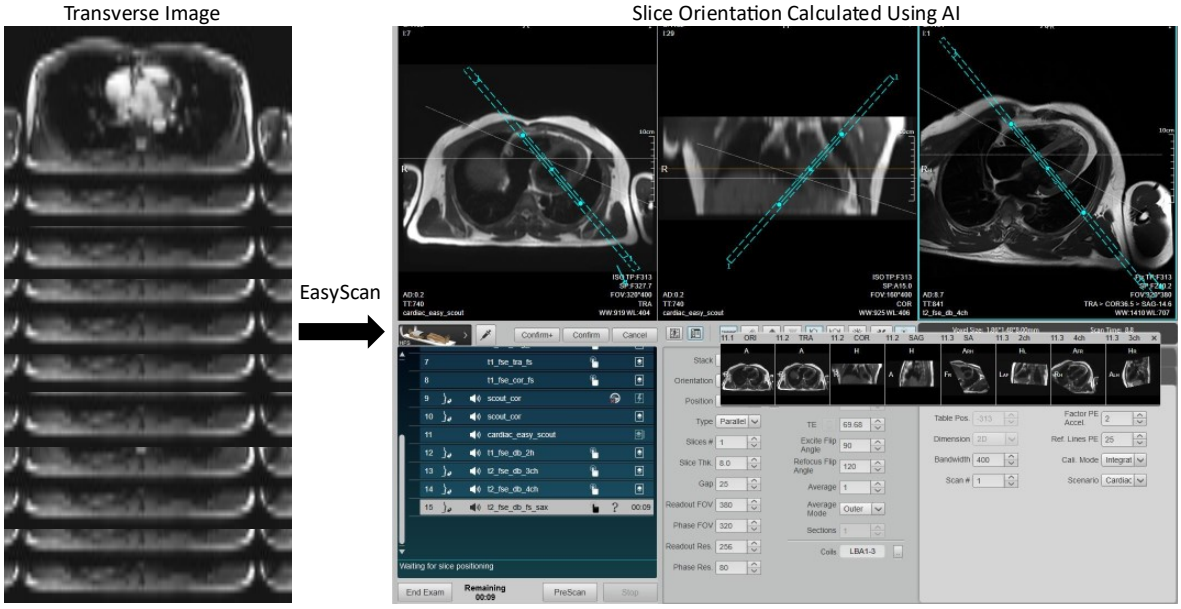

Figure 1. shows the Easy scan utilizing multiple 2D transverse slices to generate the standard views in a single breath hold, which results in faster imaging and greater reproducibility between scans.

3. AI Shim™

In CMR imaging, subject-induced magnetic field inhomogeneities can become pronounced due to susceptibility changes within the field of view [12]. Tissue-air boundaries compromise the B0 field, and careful shimming is required to establish a homogeneous and on-resonance B0 field around the heart.

This is particularly true when a balanced steady state free precession (bSSFP) sequence is used for acquisition, which is sensitive to the off-resonance effect [13]. In general, a "frequency-scout" scan is involved in the workflow.

[2]The EasyScan algorithm currently is not available for clinical use in the U.S. and also may not be available for such use in other countries.

Here, a series of images with different off-resonance frequencies are acquired that help the operator choose the best scanner frequency. Unfortunately, this process is time-consuming and operator dependent.

To address these issues, a generalized shimming tool using a mask-based AI segmentation technique (AI shim™) [3] was developed [14]. AI shim™ uses a dual echo 3D gradient sequence with breath-hold to collect the 3D anatomical structure and B0 field map of the cardiac

regions. A stack of transverse slices acquired at the beginning of the study is used to establish the shimming currents that automatically adjust the field for subsequent scans.

Compared with typical volume shimming, AI shim increased signal-to-noise ratio (SNR) in images obtained for all RV and LV myocardium cine planes. For instance, the mean SNR of LV myocardium SAX cine improved 17.75% with AI shim ($p<0.001$) among healthy volunteers and 10.40% ($p=0.006$) in referred patients. Similar findings were noted for contrast-to-noise (CNR) measurements. The improved SNR and CNR obtained through AI shim afforded better delineation of epicardial and endocardial borders, and the crisper AI shim images beneficially increased the efficiency and accuracy of automated contour detection algorithms utilized by the advanced CMR analysis software. Image sharpness over all four cardiac planes increased (2%) by AI shim and the relatively small improvement was notable along the thin RV free wall four-chamber and short-axis views (Fig. 2).

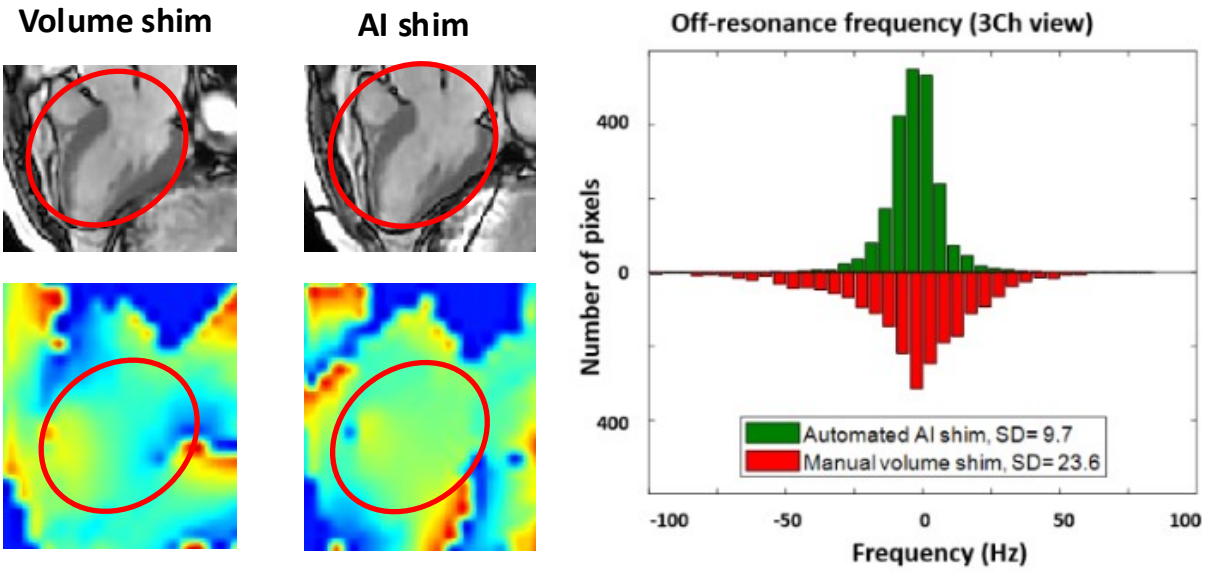

Figure 2. shows a three-chamber view example that highlights the superior image quality produced independent of the technologist with AI shim as compared to volume shim. The histograms also show the off-resonance distributions of the whole heart in the B0 field obtained with scans from 10 volunteers using two shimming methods: manual volume shim vs. AI shim. Histograms were separately generated for each cardiac plane with the standard deviation within the mask region, representing an improved field homogeneity with automated AI shim.

4. Fast-SENC

Fast-SENC Cardiac MR software operates efficiently on the United Imaging MRI scanner enabled by accelerated spiral k-space data acquisition. Fast-SENC technology is a rapid MRI scanning diagnostic feature that measures myocardium deformation from an unwound to a tense or contracted condition in one heartbeat per image plane. Breath-holds are not required, and a complete view of the ventricle is acquired in 6 seconds. This specialized pulse sequence reflects changes in the material properties cardiac muscle that can be harbingers of impending decreased contractility (Ejection Fraction, EF) [15-17]. The Fast-SENC pulse sequence quantifies circumferential (GCS) and longitudinal

[3]Not commercially available in the U.S. and some other countries for clinical use; sequence is still a work in progress.

(GLS) strain, varying with the plane of measurement, the latter being most utilized by cardiologists today (Fig. 3). The Fast-SENC has advantages of greater signal to noise ratio and more accurate strain calculation.

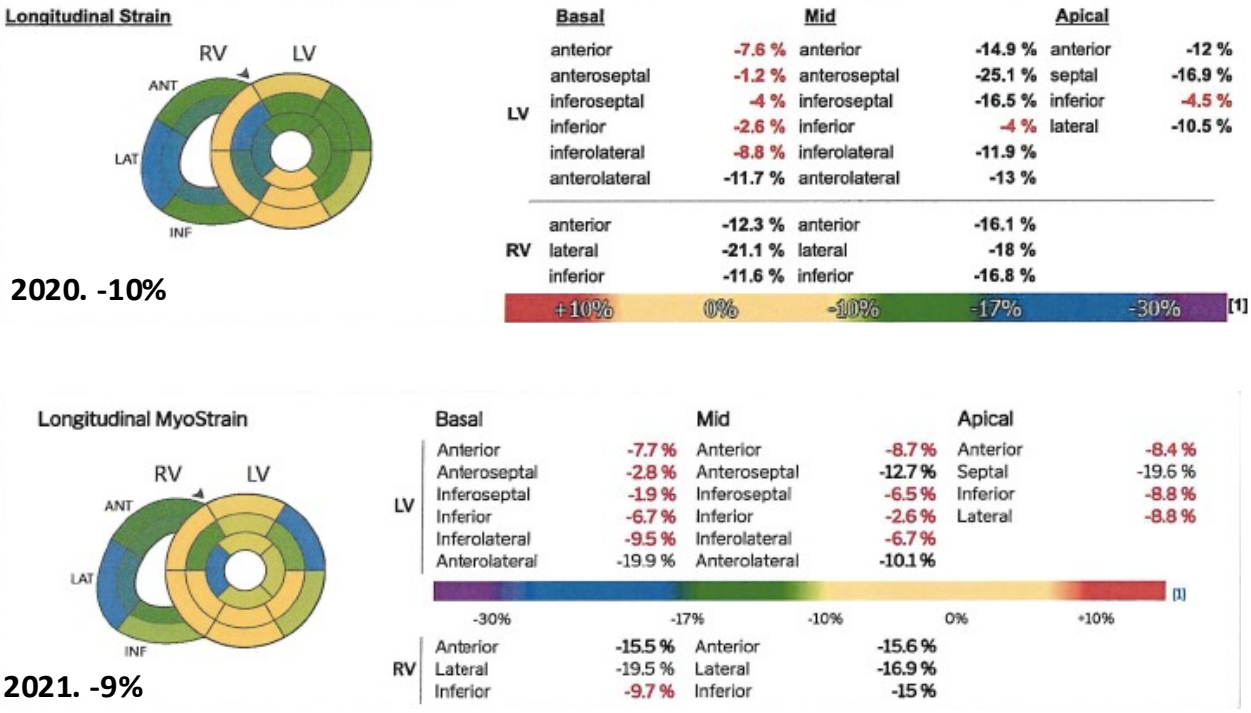

Figure 3. shows CMR results in a 84 year old patient with history of transthyretin amyloidosis in the spine. Ejection fraction was noted to be 63% in 2020 and had dropped slightly to 56% in 2021. The LV global longitudinal strain was noted to be 10% and 9% in 2021. The mapping shown below also helps to highlight the progression of myocardial involvement from the anterior, septal and posterior basal walls in 2020 to include more widespread left ventricular myocardial involvement in 2021.

5. Strain

Feature Feature-tracking (FT) [18] has been described as an alternative means of measuring myocardial strain using clinically routine cine CMR images, which require no special sequences such as tagging with DENSE or Fast-SENC [19-21]. Considerable effort has been focused on increasing the accuracy and reproducibility of FT strain assessment, but the process still requires human intervention. Moreover, performance and reproducibility of FT is directly related to observer's experience.

United Imaging Intelligence has created a deep-learning-based fully automated myocardium strain assessment system[4] (autoFT™, Fig. 4) that provides global and segmental strain estimates directly from cine CMR images without any human intervention, thereby removing observer variation or bias. The system was validated on patient data and compared to fast-strain-encoded (fast-SENC) imaging [22].

A neural network was established and trained to classify and group standard DICOM MRI images into short axis stacks, 2-chamber, 3-chamber and 4-chamber long axis images for assessment of cardiac anatomy and function. No additional MRI images are required. A convolutional neural network (UNet-like NN) detects anatomical landmarks on images to define and segment the myocardium according to the American Heart Association 17-segment model. A motion-pyramid NN is implemented to predict the dense motion field between two consecutive images. The motion tracking network is also equipped with anatomy-awareness such that the dense motion field from the network can maintain the heart anatomy through tracking [23]. Manual editing of the tracking is allowed at any frame to adjust the estimated motion and update the strain correspondingly. The myocardium, defined by the segmentation mask on the end-diastolic frame, is densely tracked through the entire cardiac cycle. Pixel-wise strains are calculated from the

[4]This product is a work in progress; the information in this article represents ongoing research and development. No 510k application has been filed with the FDA. This product is not available for sale in the U.S. for clinical uses and also may not be available for such sales in other countries.

dense motion field. Strain values along different directions (circumferential, radial and longitudinal) and at multiple spatial resolutions (global, segmental and pixel-wise) are provided in various formats, such as table, curves and bullseye.

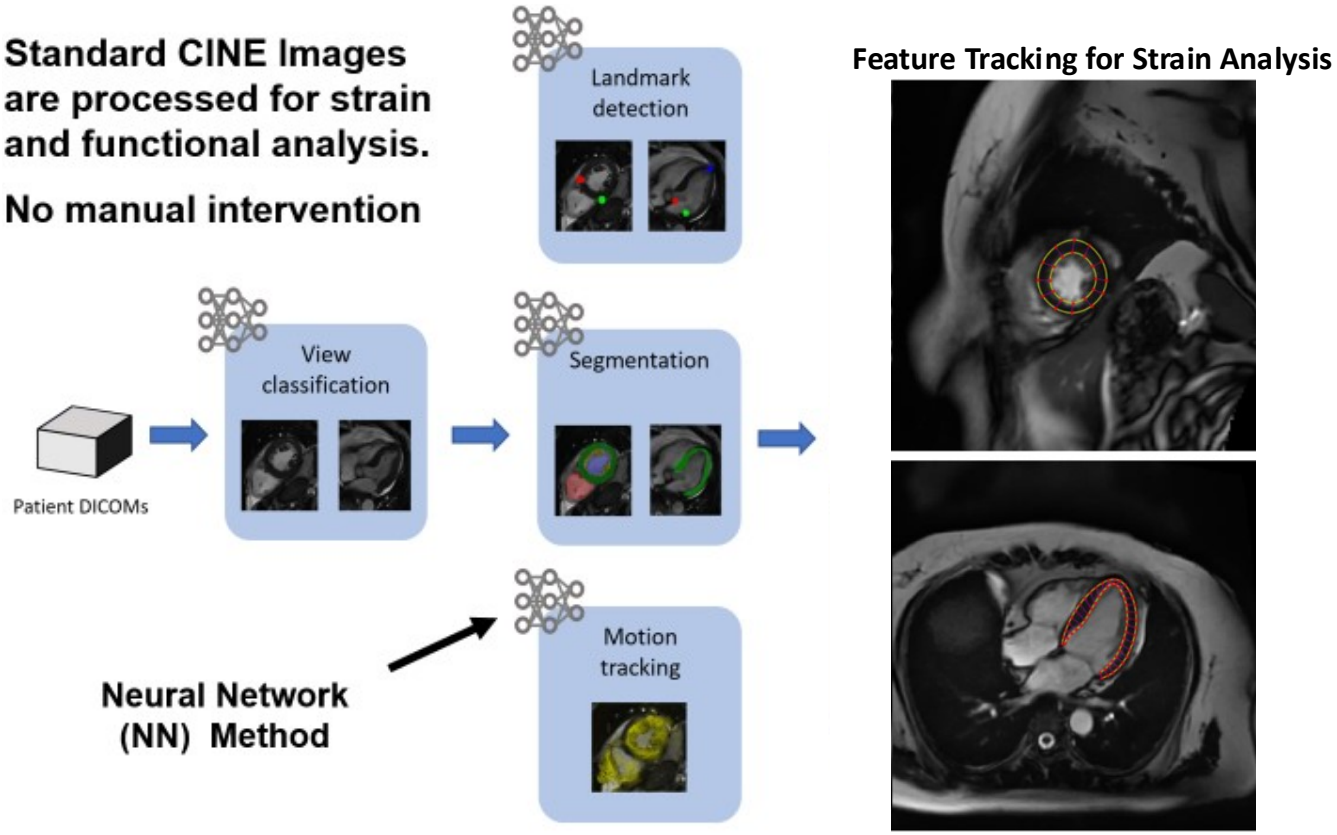

Figure 4. describes the workflow of the fully automated cardiac strain and function analyses.

The main components of this FT method include segmentation and motion tracking, which leverage the recent progress in computer vision and deep learning to achieve high accuracy, robustness, and computation speed. Repeatable preliminary results in serial studies have been obtained, in part because the short acquisition times minimize patient motion variability.

6. T1/T2 Mapping

MRI myocardial texture characterization using native T1 and T2 relaxation times can provide insight into changes in cardiac tissue. The normal practice of quantifying early changes in T1 and T2 parameters compares a subsampled region-of-interest (ROI) from the colorized T1 and T2 relaxation time maps with a ROI from chest wall muscle; the ratio of the magnetic parameter relaxation times determines the clinical significance. However, the technique is fraught with clinical variability and can be time-consuming to perform [24-25]. In the next edition of uINNOVATION-GLOBAL, a novel T1/T2 mapping feature re-envisions T1 and T2 relaxation data (Fig. 5) maps as automatic and intuitive quantitative reports.

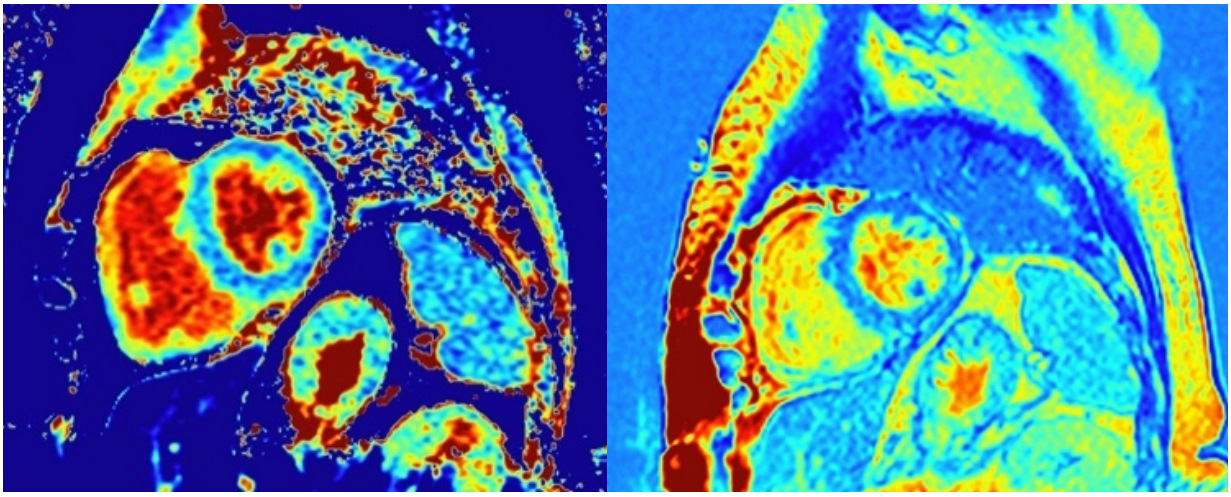

Figure 5. illustrates T1/T2 mapping of the cardiac myocardium.

7. Conclusion

CMR scans performed using the above-mentioned intelligent features are simplifying cardiac planning and image quality, decreasing the time for data processing and enhancing data interpretation. Collectively, the use of AI to achieve simpler and faster workflows will expand institutional availability, minimize technical complexity, and provide the best information for optimal patient care regardless of center location or size.

8. Image/Figure Courtesy

All images are the courtesy of Washington University School of Medicine in St Louis, USA.

References

1. Hundley WG, Bluemke DA, Finn JP, et al. ACCF/ACR/AHA/NASCI/SCMR 2010 expert consensus document on cardiovascular. magnetic resonance: a report of the American College of Cardiology Foundation Task Force on Expert Consensus Documents. Circulation. 2010;121(22):2462–2508.

2. Heckbert SR, Post W, Pearson GD, et al. Traditional cardiovascular risk factors in relation to left ventricular mass, volume, and systolic function by cardiac magnetic resonance imaging: the Multiethnic Study of Atherosclerosis.J Am Coll Cardiol. 2006;48(11):2285-2292.

3. Secinaro S, Calandra D, Secinaro A et al (2021) The role of artificial intelligence in healthcare: a structured literature review. BMC Med Inform Decis Mak 21:125

4. Lelieveldt BPF, van der Geest RJ, Ramze Rezaee M, Bosch JG,Reiber JHC. Anatomical model matching with fuzzy implicit sur-faces for segmentation of thoracic volume scans. IEEE Trans Med Imaging. 1999;18:218-230.

5. Lelieveldt BPF,van der Geest RJ,Lamb HJ,Kayser HWM,ReiberJHC. Automated observer-independent acquisition of cardiac short-axis MR images: a pilot study. Radiology. 2001;221:537-542.

6. Jackson CE, Robson MD, Francis JM, Noble JA. Automatic planning of the acquisition of cardiac MR images. Med Image Comput Assist Interv. 2003;2878:541-548.

7. Dwivedi S, Vaidya V, Mullick R, Foo T, Ho V. Methodology for rapid cardiac axis generation from non-gated cardiac MR images. Paper presented at: Proceedings of the 15th Scientific Meeting,International Society for Magnetic Resonance in Medicine; May19-25 2007; Berlin.

8. Darrow RD, Vaidya V, Govenkar A, Mullick R, Foo TK. One touch imaging for improved cardiac workflow. Paper presented at: Proceedings of the 16th Scientific Meeting, International Society for Magnetic Resonance in Medicine; May 3-9, 2008; Toronto,ON.

9. Darrow RD, Vaidya V, Mullick R, et al. Ground truth evaluation of one touch cardiac imaging. Paper presented at: Proceedings of the 17th Scientific Meeting, International Society for Magnetic Resonance in Medicine; April 18-24, 2009; Berkeley, CA.

10. Lu X, Jolly MP, Georgescu B, et al. Automatic view planning for cardiac MRI acquisition. Med Image Comput Comput Assist Interv. 2011;14(Pt 3):479-486.https://doi.org/10.1007/978-3-642-23626-6_59

11. Nitta S, Takeguchi T, Matsumoto N, et al. Automatic slice alignment method for cardiac magnetic resonance imaging. Magn Reson Mater Phy. 2013;26:451.

12. Simonetti OP, Ahmad R. Low-field cardiac magnetic resonance imaging: a compelling case for cardiac magnetic resonance's future. Circ Cardiovasc Imaging. 2017;10(6):e005446.

13. Oshinski JN, Delfino JG, Sharma P, et al. Cardiovascular magnetic resonance at 3.0 T: current state of the art. J Cardiovasc Magn Reson. 2010;12(1):55.

14. Edalati M, Zheng Y, Watkins MP, Chen J, Liu L, Zhang S, Song Y, Soleymani S, Lenihan DJ, Lanza GM. Implementation and prospective clinical validation of AI-based planning and shimming techniques in cardiac MRI. Med Phys. 2022 Jan;49(1):129-143.

15. Victoria Delgado, Laurens F. Tops, Rutger J. Van Bommel, Frank Van Der Kley, Nina Ajmone Marsan, Robert J. Klautz, Michel I.M. Versteegh, Eduard R. Holman, Martin J. Schalij, and Jeroen J. Bax. Strain analysis in patients with severe aortic stenosis and preserved left ventricular ejection fraction undergoing surgical valve replacement. European Heart Journal, 30(24):3037{3047, 2009.

16. Rose Khavari Nicholas Dias, Yung Peng and Angelo; Everaers, RalfRosa. Impaired systolic function by strain imaging in heart failure. Physiology & behavior. 176(12):139-148, 2014.

17. Henning Steen, Moritz Montenbruck, Blaz Gerzak, Arne Kristian Schwarz, Sebastian Kelle, Sorin Giusca, Grigorios Korosoglou, Susan Dent, and Daniel Lenihan. Cardiotoxicity during cancer treatment causes more regional than global dysfunction: the prefect study. Journal of the American College of Cardiology, 75(11):1824, 3 2020.

18. Chen X, Edalati M, Liu Q, Shou X, Sharma A, Watkins MP, Lenihan DJ, Hu L, Lanza, GM, Chen T, Sun S. Fully Automated myocardium strain analysis using Deep Learning. ISMRM abstract December 16, 2020.

19. E. A. Zerhouni, D. M. Parish, W. J. Rogers, A. Yang, and E. P. Shapiro. Human heart: Tagging with MR imaging - A new method for noninvasive assessment of myocardial motion. Radiology, 169(1):59{63, 1988.

20. Bruce S Spottiswoode, Xiaodong Zhong, Christine H Lorenz, Bongani M Mayosi, Ernesta M Meintjes, and Frederick H Epstein. NIH Public Access. 13(1):105{115, 2010.

21. Nael F. Osman, William S. Kerwin, Elliot R. McVeigh, and Jerry L. Prince. Cardiac motion tracking using CINE harmonic phase (HARP) magnetic resonance imaging. Magnetic Resonance in Medicine, 42(6):1048{1060,1999.

22. Li Pan, Matthias Stuber, Dara L. Kraitchman, Danielle L. Fritzges, Wesley D. Gilson, and Nael F. Osman. Real-time imaging of regional myocardial function using fast-SENC. Magnetic Resonance in Medicine, 55(2):386{395,2006.

23. Yu H, Sun S, Yu H, Chen X, Shi H, Huang T, Chen T. FOAL: Fast Online Adaptive Learning for Cardiac Motion Estimation, CVPR 2020 Anatomy-aware cardiac motion estimation, MICCAI workshop, 2020.

24. Roy C, Slimani A, de Meester C, Amzulescu M, Pasquet A, Vancraeynest D, Vanoverschelde JL, Pouleur AC and Gerber BL. Age and sex corrected normal reference values of T1, T2 T2* and ECV in healthy subjects at 3T CMR. J Cardiovasc Magn Reson. 2017;19:72.

25. Messroghli DR, Moon JC, Ferreira VM, Grosse-Wortmann L, He T, Kellman P, Mascherbauer J, Nezafat R, Salerno M, Schelbert EB, Taylor AJ, Thompson R, Ugander M, Van Heeswijk RB and Friedrich MG. Clinical recommendations for cardiovascular magnetic resonance mapping of T1, T2, T2 and extracellular volume: A consensus statement by the Society for Cardiovascular Magnetic Resonance (SCMR) endorsed by the European Association for Cardiovascular Imaging (EACVI). Journal of Cardiovascular Magnetic Resonance. 2017;1

Author Biography

Dr. Gregory Lanza

Professor of Medicine,
Biomedical Engineering,
and Biology and Biomedical
Sciences
Washington University
School of Medicine
St Louis, MO, USA

Dr. Gregory Lanza is a Cardiologist and Professor of Medicine, Biomedical Engineering, Biology and Biomedical Sciences at the Washington University School of Medicine in St Louis. His clinical areas of interest include echocardiography and cardiac magnetic resonance imaging, with specific research interests in the development of novel nanotechnologies for biomedical molecular imaging and targeted drug delivery in cardiovascular, neurological, inflammatory, and oncological disease.

He obtained his Doctor of Philosophy from University of Georgia, Athens and his Doctor of Medicine from Northwestern University Medical School, Chicago; he did his residency at Washington University School of Medicine in St Louis. He is also a recipient of numerous grants and prestigious awards.

Expert interview: Exploring the past, present, and future of total-body PET with Dr. Simon R. Cherry[1]

E: Dr. Cherry, thank you for joining us today to talk about your experience with total-body PET. Before we continue, we'd like to first congratulate you for winning the 2022 Benedict Cassen Prize from the Society of Nuclear Medicine and Molecular Imaging (SNMMI). We especially enjoyed your lecture titled "A Matter of Time" which showcased the development of PET over the years.

S: Thank you very much!

E: You have mentioned in your lecture, as well as in many of your past presentations, that the idea of total-body PET for adult human imaging is not new and can be dated back to 1990 when Dr. Terry Jones proposed the concept using parallel large detector panels. Can you please speak a bit about your early involvement in total-body PET and why you and Dr. Ramsey Badawi decided to pursue this concept?

S: That is a good question – if my memory serves me correctly, this all started about 18 years ago. At the time, the Department of Radiology at UC Davis was looking to hire someone well-versed in nuclear medicine physics. At the time I had no real connection with Radiology as my appointment was in the Department of Biomedical Engineering. However, I had known Ramsey from the time he was a graduate student at the University of London, and I was very pleased when Radiology recruited him to UC Davis.

Naturally, Ramsey and I quickly began chatting about research projects that we could collaborate on. Ramsey had done a lot of simulation work on longer axial field of view (FOV) PET systems up to 60 cm and studied effects such as random and scatter coincidences because the general consensus at the time was that the longer axial FOV PET systems would be dominated with these types of coincidence events, and therefore the idea would not be worth pursuing.

Ramsey's simulations on longer axial FOV PET systems showed that the effects of scatter and random coincidences did not grow as quickly as one might expect. Given Ramsey's interests in this phenomenon and my experience in preclinical instrumentation which already had relatively large axial FOV capable of covering an entire mouse, the conversation quite naturally turned to building longer axial FOV PET systems for human imaging.

I recall having the conversation about how long the system should be. At the time, the state-of-the-art clinical PET system was about 20 cm long. I am not sure who said it first, but we decided if we were going to build a long axial FOV PET system, we should take it to the extreme because otherwise you would always be left wondering what would happen if you built a longer system. The ability to capture the entire human body and watch the radiotracer move across the human body with improved sensitivity struck us as an exciting challenge that had never been attempted before. I think both Ramsey and I like big ideas and we are not afraid to take on those challenges. Shortly after, the total-body PET idea was born.

Looking back now I think we had no idea what the journey was going to be like. I would not have predicted that it would have taken so long. At the same time, I do not think I would have predicted that it would have been so successful either. So far, I have been very happy with what has transpired.

E: As many people know, the EXPLORER total-body PET system (now known as the uEXPLORER® system) was born out of a collaboration with United Imaging Healthcare. Can you please talk a bit about why you and Dr. Badawi decided to collaborate with a medical imaging device manufacturer? What are some advantages you saw with such collaborations compared to developing the system entirely in-house at UC Davis?

[1]The University of California, Davis (UC Davis) receives financial support from United Imaging Healthcare through a sponsored research agreement, in which Dr. Cherry is a principal investigator, and has a revenue-sharing license agreement with the company for jointly developed technology.

S: After we were awarded the $15.5 M transformative R01 grant from the National Institutes of Health in 2015, we quickly recognized that even though we had the funding, from the academic side we had little expertise or experience in building a PET system on an industrial scale. At the same time, we also realized we were going to receive a lot of attention due to the amount of funding we were awarded for this project. As many have experienced, academic projects can sometimes take longer than expected; and while the prototypes can produce images, they may not be stable or robust enough for routine clinical use. Therefore, we wanted to use the funding in a way that would lead to a lasting change in the field.

From the beginning, we were aware of the massive responsibility and that it was essential to collaborate with an industry partner. In fact, we have discussed the total-body PET idea with multiple companies even before we received the award. However, the response from industry at the time was generally lukewarm as they did not see a clear market need and were heavily invested in PET/MR technology at that time.

With that said, our first exposure to United Imaging Healthcare was at the IEEE Medical Imaging Conference in late 2015 where we met Dr. Hongdi Li (CTO of United Imaging Healthcare). I remember sitting down with him, and Hongdi was rapidly sketching ideas on the back of a napkin. He already had ideas about how to build a total-body PET scanner with United Imaging Healthcare technology and he offered to come to UC Davis to give a detailed presentation on how United Imaging Healthcare could help with the project within a couple of weeks, which he did. While we were impressed with his proposal, we did not know much about the company other than Hongdi. He then invited us to visit the United Imaging Healthcare headquarters in Shanghai several weeks later in January 2016. That was the pivotal point for us; in only 8 hours our perception of the company completely transformed despite its relatively young age. Although we had our doubts before visiting, after we toured the facilities and met the people we knew that we would move forward with United Imaging Healthcare, because we had found a team with *the same mindset* we had. I remember well that at the end of our visit, Min Xue, President of United Imaging Healthcare said "if you want to do this project with us, we will do it and we will do it well," and with those words and a handshake, the partnership was born. Total-body PET was an ambitious and difficult project, but it was worth doing. It was high risk, but United Imaging Healthcare leadership was willing to take the risk. They trusted and believed in us, and we trusted and believed in them, and it has worked out extremely well.

E: The term "total-body PET" has seen increased usage in the literature since the EXPLORER project was funded in 2015. Can you please talk about why you used the term "total-body PET" instead of the more common "whole-body" PET? What are the differences between the two?

S: The term "whole-body PET" has been in widespread use for a long time, and it typically refers to an eyes-to-thighs scan performed by stepping the patient through a conventional PET system in multiple bed positions. We needed a distinct terminology to denote the fact that we are not moving the bed and we are capturing the *entire human body at once*, and hence we created the term "total-body PET" to distinguish itself from "whole-body PET." The key distinction here is that "total-body PET" allows us to capture the kinetics across *all tissues in the body* by imaging the entire human *simultaneously* without moving the bed. Capturing kinetics across the entire human is very difficult and inefficient to achieve with "whole-body PET," especially when imaging radiotracers with faster kinetics.

E: Prior to the installation of the uEXPLORER system at UC Davis, you mentioned that total-body PET provides improved tradeoffs between scan time, radiation dose, and image quality. Having been the users of the first clinical total-body PET system in the world since 2019, what are some additional advantages of total-body PET that you and Dr. Badawi have realized?

S: Given the extensive amount of simulations we have previously performed, we had very high expectations for total-body PET and were not surprised by the image quality improvement achieved with the higher system sensitivity. However, after seeing the first images, we were amazed by the clarity and sharpness which were achieved with both high sensitivity *and* fine spatial resolution without the need to apply smoothing filters. In addition to the first dynamic total-body PET movie showing the radiotracer moving across the entire body, the ability to perform dynamic PET imaging of the entire body using 0.1 s time frames (which

has never been done before) and visualizing the cardiac cycle via PET was mind-blowing and eye opening.

E: What are some of the latest research projects you and Dr. Badawi are working on that were made possible using the uEXPLORER system?

S: One of the projects that we are involved in is the total-body imaging of CD8+ T cells for COVID-19 using ^{89}Zr-Df-Crefmirlimab-Berdoxam. This radiotracer has been used in cancer patients for immunotherapy, and the resulting radiation dose given to the patients, while justifiable, can be quite high. To use the same radiotracer to assess COVID-19 in recovering patients as well as in control groups (i.e., healthy volunteers), it is essential to utilize a PET system that can minimize the radiation dose administered to the patient.

To the best of my knowledge, we are currently the only people that have ^{89}Zr-radiolabled human imaging data with a control baseline from healthy human volunteers. This is because total-body PET is a necessity for imaging ^{89}Zr at greatly reduced injected radioactivity levels. The imaging of ^{89}Zr-radiolabled control groups would not have been possible without total-body PET systems. Also, with regards to the immune system, there are many chronic diseases where there may be value in scanning multiple time points (at 20 y/o, 30 y/o, 40 y/o, etc.) and performing interventional studies (e.g., before and after vaccination). These are new considerations that would not have previously been feasible without the large dose reduction enabled by total-body PET.

As always, we want to develop better and better next-generation PET systems to enable more novel clinical and research imaging applications. I hope this is just the beginning for these kinds of high-end PET systems, and I hope the field continues to push towards developing better systems in the future because we still have some ways to go.

E: When it comes to PET scanner performance, often the most discussed performance parameters are 1) sensitivity, 2) spatial resolution, 3) count rate performance, and 4) time of flight (TOF) performance. How would you rank the importance of each of these parameters to ensure the future success of total-body PET?

S: This is a difficult question – there needs to be a balance to a certain extent, because otherwise the PET system would be limited by its weakest link. Care must be taken to not overemphasize one performance metric over the other. There is no point in having spatial resolution if there are insufficient counts to support the spatial resolution, for example. The other way around is also sub-optimal – if there are tons of counts but the detectors have coarser spatial resolution, the annihilation photons are not being fully utilized. If there is excessive deadtime, there can be a problem with count rate performance. So, these metrics are all linked to each other.

Therefore, I am going to answer the question a bit differently and ask "Where would I put my efforts in going beyond the current total-body PET systems? Where can we improve further?" Obviously, TOF performance is an area where we can do better, and so I think in the next few years it is not unreasonable for current PET detector technology to reach 100 – 150 ps TOF resolution. Challenging for sure – but I am confident that there is a way to get there. Of course, we would like to go down to well below 100 ps, but that is going to require some technological advancements which will take a bit longer.

I think another area to emphasize is "How do we deal with Compton scattering within the detector?" When comparing the measured sensitivity of a detector versus the predicted sensitivity based on the stopping power and thickness of the scintillator, the measured sensitivity is often much lower. The reason is that a lot of those Compton scattered photons are rejected since they are captured outside the photopeak energy window, and the detector efficiency is much lower as a result. We need to have detectors that are thick enough so that all of the energy gets absorbed; however at the same time there needs to be a way to determine the energy and the location of each interaction to best determine the first interaction among multiple interactions. So, I think this is another area to improve – perhaps one that is not mentioned very much because it is a little bit more of a subtle effect.

One thing of note is that we are not going to be able to make much more improvements in geometric coverage. The uEXPLORER system is the epitome of ultra-high geometric efficiency, so little sensitivity improvement can be gained from extending the system beyond 2 m.

Finally, I think we need to continue searching for new

scintillator materials. If we can get materials with better photoelectric cross sections, then we can get fewer events where inter-crystal scattering occurs. While BGO is better than LYSO in terms of photoelectric cross section, we do not yet have a robust way to obtain timing resolution down to below 100 ps. However, there are other materials that are in the early stages of development that have very good photoelectric cross sections and can be very fast, so we need to see effort and funding going into these materials. It took a good decade of development for LSO and LYSO to get to a point where it is usable for a PET system, and it will likely take a similar number of years for some of these new materials.

E: One of the advantages of PET systems with increasing axial FOV is the increasing axial coverage with uniform sensitivity. With the uEXPLORER system the axial length with uniform sensitivity is about 1 m. Can you speak a bit about the advantage of having uniform sensitivity axially? Are there any advantages to further extending the PET axial FOV beyond 2 m so that the axial length with uniform sensitivity covers the entire adult human?

S: Good question – of course, there is a lot of debate about the optimal axial length of a total-body PET system. Proponents for the shorter axial length total-body PET systems suggest that only the major vital organs (e.g., from the brain to the pelvis) must be covered and not the lower limbs. If that is the goal, then a system that is slightly over 1 m should suffice for most adult humans. However, to have ultra-high and uniform sensitivity across that entire 1 m region, the system needs to be considerably longer than 1 m due to its geometric response. Otherwise, the sensitivity at the first few cm of either end of the system (where the brain and pelvic regions are located at) is no better than that of a conventional PET system. So, I think a total-body PET system needs to be least 1.4 – 1.5 m to have ultra-high and uniform sensitivity across all the major organs of the body.

Of course, it is a bit more complicated than that – as you accept more oblique lines of response, then those lines get more heavily attenuated. This leads to more scattered photons because they travel a much longer path length through the body. So, while for point sources one can continue to benefit from sensitivity gains as the axial length increases, the gain is not as dramatic when imaging adult humans. So, while the minimum length required I would suggest is 1.4 – 1.5 m, the optimal length beyond that depends on the intended application, because there are applications where there is a need to image beyond the 1 m "high sensitivity" region. Some examples of our own research projects requiring high sensitivity information outside the 1 m region include the assessment of rheumatoid arthritis where there is a need to survey all the joints in the body simultaneously, and where disease is present in the wrists, ankles, and the feet as well. So, if the goal is to survey all of that, and knowing the radiotracer uptake is not very high in these small structures, having a system with ultra-high sensitivity is essential. In such scenarios, a 2 m system will really help.

Another example is our T cell study in COVID-19 subjects. As many people know, one of the production sites of T cells is the bone marrow. There is lots of bone marrow in the long bones of the leg, and we have seen quite some differences in radiotracer uptake between human subjects in our studies. This is another case where there is a need to extend the axial coverage beyond the pelvis and into the legs while minimizing the radiation dose given to the human subjects by taking advantage of the ultra-high sensitivity of total-body PET.

So, if I want to have a high-end PET system that is also a high-end research instrument to support all types of research related to systems medicine, the human connectome, and the immune system, then I want to have a scanner that can see the entire body with ultra-high sensitivity, and that pushes me much closer to having a 2 m system. The optimal length may very well turn out to be a different number if the intended application of the PET system is only for routine clinical use, such as FDG clinical oncology. On the other hand, if the goal is to develop new clinical indications by understanding the processes and treatment effects using systems such as the uEXPLORER, I think we want the best instrument we can get.

It is a long answer – it is not a question that has a single correct answer, but I am very glad we are able to get the uEXPLORER system built to the length that it is because it shows us what is possible and allows us to do things that we could not do otherwise.

E: The current NEMA NU 2-2018 standard for evaluating the performance of clinical PET systems using phantoms with lengths of 70 cm or less is not designed to evaluate PET systems with axial FOV greater than 65 cm. As a result, longer phantoms have been used at UC Davis to better reflect the actual performance of total-body PET systems when imaging adult humans. Do you think that the next NEMA NU 2 standard should include tests appropriate for evaluating total-body PET systems? Is there a need to revise the standard so that the tests are suitable for clinical PET systems of all lengths?

S: I think the next NEMA NU 2 standard needs to account for total-body PET systems since the current measurements do not fully reflect the real-world performance of these systems. Although one of the approaches to address this concern is to image longer phantoms, the process is not a simple undertaking – long phantoms can be heavy and difficult to fill, which is a resource intensive process.

Therefore, the challenge for the NEMA committee and for those who are trying to contribute is "How do we come up with a meaningful set of measurement that is also practical to do?" I do not think there is an easy answer for that currently, but certainly the standard needs to be revised to account for the new class of systems so one can fairly assess their performance in comparison to shorter systems. Ideally, rather than developing a new NEMA standard for long axial FOV systems, there would be an integrated standard that works for any length of scanner. It will be interesting to see where that discussion goes and what ideas people come up with.

The other thing that is not properly captured with the current NEMA measurement is the impact of different TOF performance on the resulting reconstructed images, and that also needs to be considered in the new NEMA standard now that we have scanners with considerably better TOF. One could assume that TOF is going to get better and better in the coming generations of scanners, so we need to be ready for that.

E: Where are we going with total-body PET in the next 5 to 10 years? How can a medical device manufacturer help facilitate this process with academic researchers from both a scientific and logistical standpoint?

S: People may disagree with me on this – I think that it is not so challenging to operate total-body PET systems in the current clinical environment. At the same time, I feel that we are not using PET in the most quantitative way possible in the clinic – we are still largely using semi-quantitative metrics such as SUV_{max}! Therefore, my hope for the manufacturers is that they will recognize the opportunities and potential for PET to be an accurate measurement device for biomedical research, which means that the system must be precise and accurate over a massive dynamic range. Of course, while it is essential to achieve accurate quantification, it is not a trivial task.

Tomorrow's research will lead to future clinical applications. Once we can prove that we can accurately measure small changes in the human body, then perhaps later the semi-quantitative metrics can eventually be utilized in the clinic. If we consider the history of 2-Deoxy-D-glucose research, which began as a quantitative research tool in animals and certainly long before anyone considered its clinical role – I think we are going to need to do the same kind of deep investigation on new radiotracers to better quantify them and unveil their potential for future clinical applications. Total-body PET is going to be the measurement tool that I believe we are going to need; however, we must view it also as a scientific instrument, not simply a producer of pretty pictures. Too many people are only talking about its clinical role – about "Let's make it a little bit cheaper" or "Let's get the dose down" or "Let's make it a bit quicker." That is not changing the field, and we will never change the world that way.

E: Finally, what do you think the ultimate PET scanner would look like and when will it be developed?

S: As I have mentioned in the Cassen Lecture at the 2022 SNMMI meeting, I think the ultimate scanner will not require image reconstruction once the TOF resolution reaches 20 – 30 ps. This will create new possibilities for all kinds of novel system geometries and correspondingly detector usage because we will not be restricted by the traditional radial and angular sampling framework anymore. The systems may also be more patient friendly as well.

While we are on our way to developing the ultimate scanner, there are still a few things we need to first solve. One of the problems that stands out to me is motion. Even if we can make our scanner extremely quantitatively

accurate and get the best quality information possible from our data, the data is no good if the patient moves and we do not know where the motion comes from. Therefore, we need to find a robust way to measure and correct for motion of all types. I think motion correction is one of the greatest methodological challenges that will also take a long time to solve, but ultimately, I think motion artifacts can be drastically reduced. Thus, while developing the next generation of PET scanners, the software piece is critical as well.

As we approach the limit where every count is carrying the maximum information possible, if we keep the detector efficiency high and detect *as many photons as possible*, we will be close to doing as well as we can. The technology that will enable us to do this is not available yet – there are several ideas for how to get there, and I think the answer to "When will we get there?" is:

"It's just a matter of time."

E: With that, Dr. Cherry, thank you very much again for your time and I hope you enjoyed exploring the past, present, and future of total-body PET with us!

S: My pleasure.

Expert's Biography

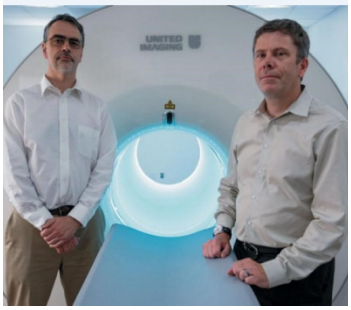

Dr. Simon R. Cherry
Distinguished Professor
Department of Biomedical Engineering
University of California,
Davis, CA, USA

Dr. Simon R. Cherry (right) is a distinguished professor in the Department of Biomedical Engineering and in the Department of Radiology at University of California, Davis (UC Davis). His work focused on various aspects of molecular imaging research, with an emphasis on position emission tomography (PET) instrumentation. As the co-director of the EXPLORER Molecular Imaging Center (with Dr. Ramsey D. Badawi, left), one of his most well-known research projects in the past several years includes the EXPLORER PET program, a $15.5 M transformative R01 project funded by the National Institutes of Health in 2015 to develop the first total-body PET system in the world. The program has led to the commercialization of the world's first and only total-body PET system capable of imaging the entire adult human in a single bed position (uEXPLORER) and has created new opportunities to study the human body using PET in ways that were previously not feasible due to the limited PET axial field of view.

Systematic evaluation of advanced PET image reconstruction algorithms according to the Japanese standard criteria – a preliminary phantom study

Kenta Miwa[a1], Masanori Watanabe[b], Masanobu Ishiguro[b], Tensho Yamao[a], Akira Hirayama[c], Hiroshi Toyama[d]

[a]Department of Radiological Sciences, School of Health Sciences, Fukushima Medical University
[b]Department of Radiology, Fujita Health University Hospital
[c]United Imaging Healthcare Japan K.K.
[d]Department of Radiology, Fujita Health University School of Medicine

Abstract

HYPER Iterative (Regularized OSEM), uAI® HYPER DLR (Deep Learning Reconstruction), and uAI® HYPER DPR (Deep Progressive Reconstruction) are advanced PET image reconstruction algorithms that have recently been introduced into clinical practice in Japan. We systematically determined the performance of these algorithms by measuring various indices of image quality and quantitative accuracy according to the Japanese Society of Nuclear Medicine (JSNM) guidelines derived from images acquired using a uMI® 550 PET/CT system (United Imaging Healthcare, Shanghai, China). The image quality index ($Q_{H,10\ mm}/N_{10\ mm}$) obtained using HYPER Iterative, DLR and DPR satisfied the JSNM criterion of ≥ 2.5. The $Q_{H,10\ mm}/N_{10\ mm}$ value for HYPER DPR with Enhance2 containing non-local mean and Metz filters as a postfiltering option was 11.5, which was the best among the evaluated reconstruction methods. Sphere detectability, on the other hand, was better with HYPER DPR than with the other reconstruction methods assessed. Quantitation of 10 mm spheres was improved with HYPER Iterative, DLR and DPR compared to OSEM. Overall, our results showed that the advanced image reconstruction algorithms can improve image quality and quantitative accuracy (particularly in 10 mm spheres), compared with OSEM-based reconstruction methods which may improve detectability of smaller lesions. HYPER DPR reduced noise, improved image contrast, and enhanced PET image quantitation.

1. Background

Positron emission tomography/computed tomography (PET/CT) using ^{18}F-fluoro-2-deoxy-D-glucose (FDG) has become an essential tool for diagnosing and staging cancer. Furthermore, PET/CT imaging is becoming more important as a means of providing quantitative biomarkers for monitoring therapeutic responses and evaluating new drug therapies. However, PET image quality and quantitative accuracy can be sensitive to various factors such as imaging protocols, PET scanner specifications, reconstruction methods and parameters [1]. The Japanese Society of Nuclear Medicine (JSNM) has published standard PET imaging protocols together with phantom test procedures and criteria for oncological PET imaging using FDG. The executive summary is available on the JSNM website (http://jsnm.org/archives/3071/). The JSNM standards for image quality and quantitative accuracy are regularly updated to account for advancements in hardware and software performance of PET scanners to ensure harmonization of various scanner models, which can improve the robustness of multicenter studies.

The JSNM has recently published new standards for oncological FDG PET studies based on phantom data obtained from 23 PET/CT scanners primarily reconstructed using ordered subset expectation maximization (OSEM)-based reconstruction methods [2]. However, the image reconstruction results using the latest clinically available advanced image reconstruction algorithms – including

[1]Kenta Miwa and Tensho Yamao received financial funding through a sponsored research agreement between Fukushima Medical University and United Imaging Healthcare Japan.

HYPER Iterative (Regularized OSEM), and deep-learning (DL)-based methods such as uAI® HYPER DLR (Deep Learning Reconstruction) and uAI® HYPER DPR (Deep Progressive Reconstruction) were not included. Therefore, we systematically performed qualitative and quantitative evaluations of PET image reconstructions using these algorithms according to the JSNM phantom test guidelines.

2. Materials and Methods

2.1 PET/CT scanner

All PET data were acquired using a uMI® 550 PET/CT system (United Imaging Healthcare, Shanghai, China). The system is comprised of a PET scanner coupled to an 80-slice CT scanner. One detector block of the PET scanner is comprised of a 7 × 6 LYSO array of 2.76 × 2.76 × 16.3 mm^3 crystals coupled to silicon photomultiplier (SiPM) sensors. The uMI 550 has axial and transaxial fields of view (FOV) of 24 and 70 cm, respectively. The time-of-flight (TOF) timing resolution is 395 ps. The spatial resolution and sensitivity of the uMI 550 according to National Electrical Manufacturers Association (NEMA) NU 2-2018 standard are 2.95 mm/2.97 mm (transverse/axial) at 10 mm off center and 10.3 cps/kBq, respectively [3].

2.2 Phantom experiments

Phantom data were acquired according to the JSNM phantom test procedures [4]. We used a NEMA body phantom comprising six spheres with diameters of 10, 13, 17, 22, 28, and 37 mm. The sphere-to-background activity ratio (SBR) in the phantom was 4:1 with a background activity concentration of 2.53 kBq/mL.

2.3 Data acquisition and image reconstruction

We acquired PET images in three-dimensional list mode for 30 min and reconstructed them using OSEM + point spread function (PSF) + time-of-flight (TOF) (3 iterations; 20 subsets; postfilter, non-local mean and Gaussian filter 6 mm), HYPER Iterative (β values of 0.01, 0.07, 0.14, 0.21, 0.28, 0.35, 0.42, 0.49, 0.56, 0.63, 0.7, 0.77, 0.84, 0.91, and 0.98; PSF+TOF, on), HYPER DLR (2 iterations; 20 subsets; postfilter, combined non-local means, Gaussian and Metz filters, 4 mm; PSF+TOF, on), and HYPER DPR (smoothing strength, 1–5 (Smooth to Sharp); postfilter; combined non-local means; Gaussians and Metz filters, 4 mm; PSF+TOF, on). The reconstruction parameters for each algorithm were chosen to account for differences in convergence speeds to ensure that the algorithms were compared under optimal conditions, similar to our previous studies. The parameters for OSEM were derived from the existing clinical protocol at Fujita Health University Hospital; the parameters for HYPER DLR were based on the work performed by Xing *et al*. [5]; and the same Gaussian filter was used for both HYPER DLR and HYPER DPR for direct comparisons. Images were reconstructed in a 256 × 256 matrix, with a slice thickness of 2.68 mm. Data acquired in 30 min list mode were re-binned into acquisition durations of 2 and 10 min. All standard data corrections were applied.

2.4 Image analyses

We assessed image quality by evaluating the contrast of the 10 mm hot sphere and background variability on PET images acquired for 2 min using PMOD software version 3.8. A circular ROI was placed on the 10 mm sphere on an axial slice of the sphere center. We also placed twelve 10 mm diameter circular ROIs on the background on a slice of the sphere center and on slices ± 1 cm and ± 2 cm away from the center slice (60 ROIs total). The percent contrast (% contrast) for the 10 mm hot sphere ($Q_{H,10\,mm}$) was calculated as:

$$Q_{H,10\,mm} = \frac{C_{H,10\,mm}/C_{B,10\,mm} - 1}{a_H/a_B - 1} \times 100\,(\%),$$

where $C_{H,10\,mm}$ and $C_{B,10\,mm}$ are the average activity concentration in the ROI for the 10 mm sphere and in the background 10 mm diameter ROIs, respectively, and a_H/a_B is the known activity concentration ratio between the hot spheres and the background. The percent background variability ($N_{10\,mm}$) for the 10 mm circular ROIs was calculated as:

$$N_{10\,mm} = \frac{SD_{10\,mm}}{C_{B,10\,mm}} \times 100\,(\%), \text{ and}$$

$$SD_{10\,mm} = \sqrt{\frac{\sum_{k=1}^{K}\left(C_{B,10\,mm,k} - C_{B,10\,mm}\right)^2}{K-1}}, K = 60,$$

where $SD_{10\,mm}$ is the standard deviation of the mean activity concentration for the 60 background ROIs.
We assessed the quantitative accuracy of the data by measuring the mean standardized uptake value (SUV_{mean}),

the relative recovery coefficient (RC) for the hot spheres, and the average SUV in the background ($SUV_{B,ave}$) on PET images acquired for 10 min.

3. Results

Figure 1 shows the % contrast, background variability, and image quality index ($Q_{H,10\ mm}$/ $N_{10\ mm}$) as a function of the β value in PET images reconstructed using HYPER Iterative.

The % contrast increased as the β value decreased. The % contrast was higher than that of OSEM + PSF + TOF at ranges of β = 0.01–0.70. Background variability decreased as the β value increased and was lower than that in OSEM + PSF + TOF when β = 0.63–0.98. The image quality index ($Q_{H,10\ mm}/N_{10\ mm}$) from HYPER Iterative satisfied the JSNM criterion of ≥ 2.5. The $Q_{H,10\ mm}/N_{10\ mm}$ value reached maximum at β = 0.63, then decreased as a function of increasing β values.

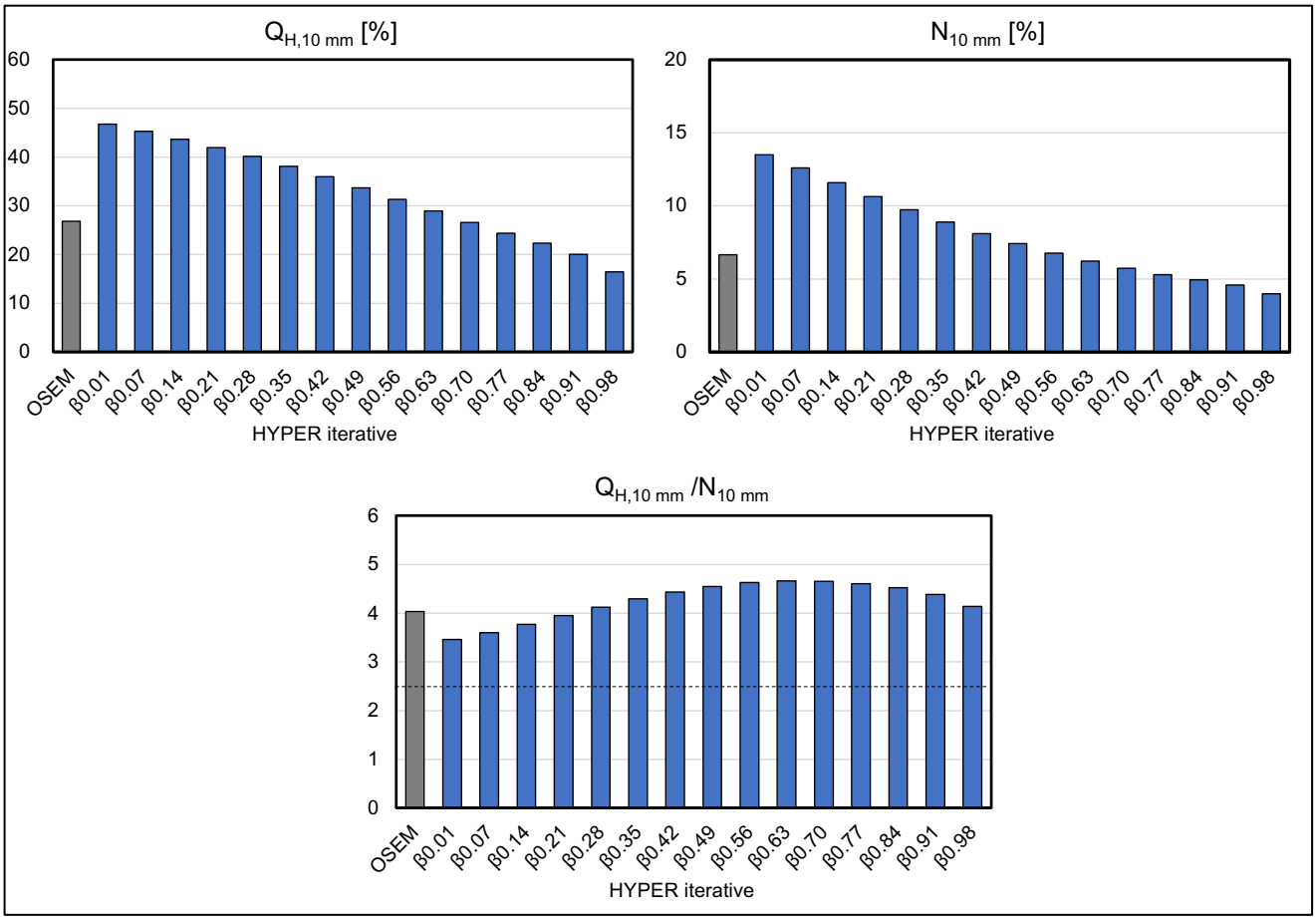

Figure 1. Percent contrast ($Q_{H,10\ mm}$), background variability ($N_{10\ mm}$), and image quality index ($Q_{H,10\ mm}$/ $N_{10\ mm}$) as a function of β in PET images reconstructed using HYPER Iterative. The dotted line represents the reference standards for the JSNM image quality acceptance. OSEM represents OSEM + PSF + TOF.

Figure 2 shows the % contrast, background variability, and image quality index ($Q_{H,10\ mm}/N_{10\ mm}$) with various postfilter options in PET images reconstructed using HYPER DLR. The % contrast in DLR was lower than that in OSEM + PSF + TOF without a postfilter. On the other hand, % contrast in DLR was almost identical to that in OSEM + PSF + TOF with a postfilter containing a non-local mean filter. The background variability was lower in DLR than in OSEM + PSF + TOF. Regardless, the image quality index ($Q_{H,10\ mm}/N_{10\ mm}$) in DLR satisfied the JSNM criterion for all configurations. The $Q_{H,10\ mm}/N_{10\ mm}$ values for DLR with Smooth1, Smooth3, and Enhance2 containing the non-local mean filter were higher than those of OSEM + PSF + TOF. The $Q_{H,10\ mm}/N_{10\ mm}$ value for DLR with Enhance2 was maximal among all configurations.

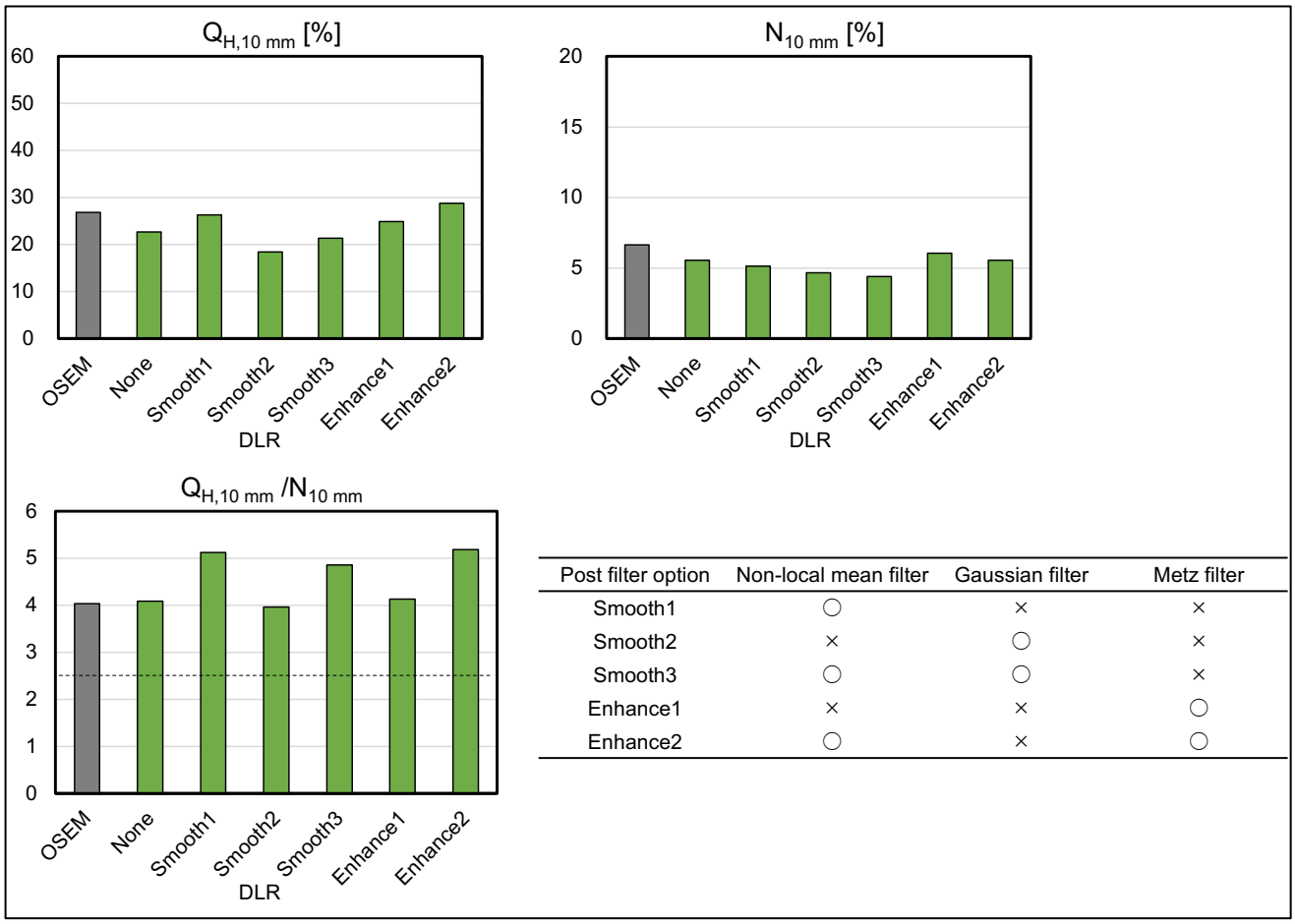

Post filter option	Non-local mean filter	Gaussian filter	Metz filter
Smooth1	○	×	×
Smooth2	×	○	×
Smooth3	○	○	×
Enhance1	×	×	○
Enhance2	○	×	○

Figure 2. Percent contrast, background variability, and quality index ($Q_{H,10\ mm}/N_{10\ mm}$) of PET images reconstructed using HYPER DLR with various postfilter options. The dotted line represents the reference standards for the JSNM image quality acceptance. OSEM represents OSEM + PSF + TOF; none represents no postfilter.

Figure 3 shows the % contrast, background variability, and image quality index ($Q_{H,10\ mm}/N_{10\ mm}$) with different smoothing strength and postfilter options in PET images reconstructed using HYPER DPR. The % contrast and background variability in DPR increased with increasing smoothing strength. The % contrast and background variability tended to be lower in DPR with Smooth2 and Smooth3 with a Gaussian filter, than in other postfilter options. The image quality index ($Q_{H,10\ mm}/N_{10\ mm}$) in DPR satisfied the JSNM criterion. The $Q_{H,10\ mm}/N_{10\ mm}$ values for DPR under all conditions were better than those for OSEM + PSF + TOF. The $Q_{H,10\ mm}/N_{10\ mm}$ values for DPR with Smooth1, Smooth3, and Enhance2 with a non-local mean filter were substantially better than those with other postfilter options. The $Q_{H,10\ mm}/N_{10\ mm}$ value for DPR with Enhance2 was maximal among all configurations.

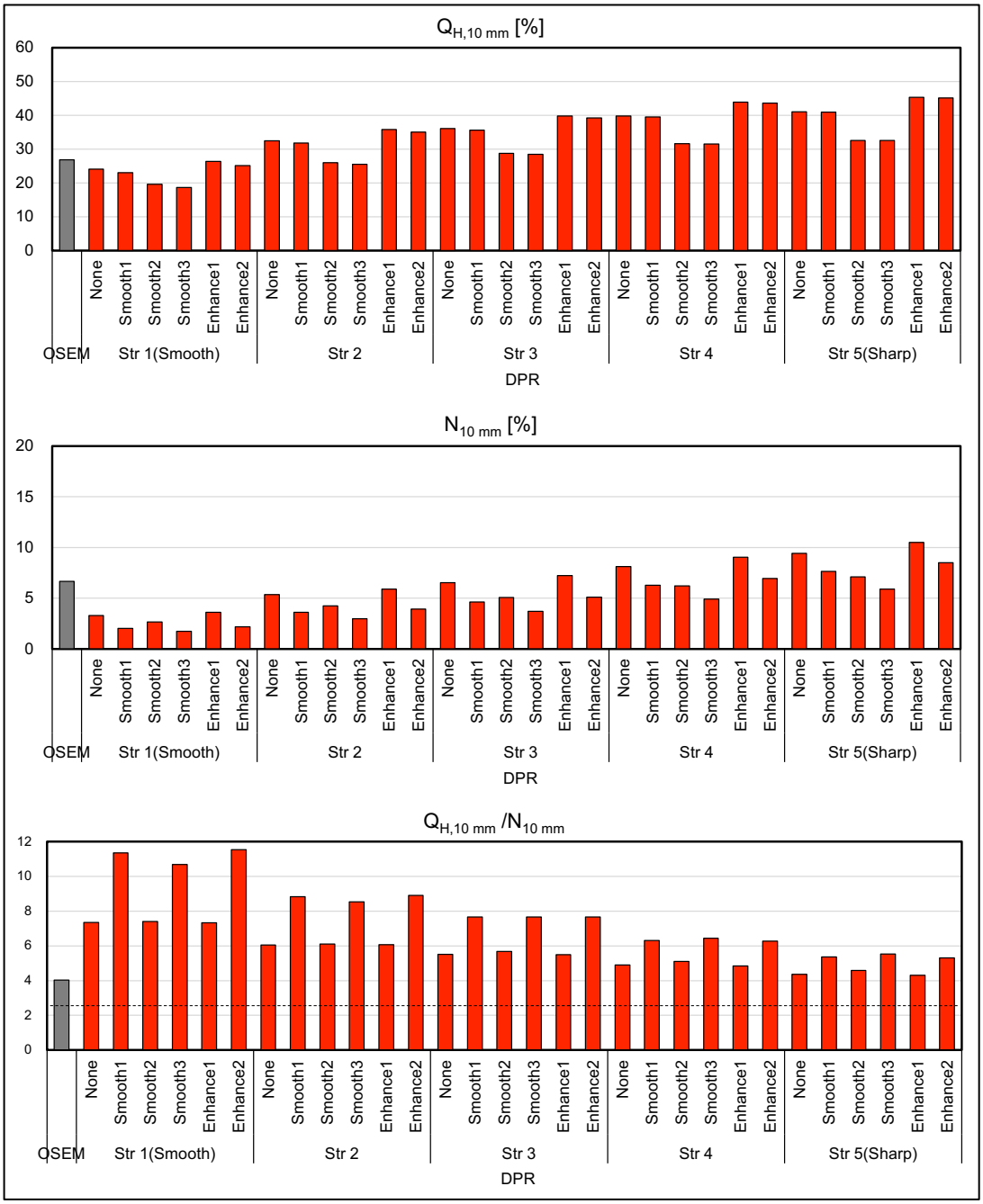

Figure 3. Percent contrast, background variability, and image quality index ($Q_{H,10\ mm}/N_{10\ mm}$) with different smoothing strength and postfilter options in DPR PET images. The dotted line represents the reference standards for the JSNM image quality acceptance. None represents no postfilter; OSEM represents OSEM + PSF + TOF; Str represents smoothing strength.

Figure 4 shows the relationship between % contrast and background variability for all reconstructed algorithms. The % contrast was plotted as a function of the background variability of hot spheres with diameters of 10 mm. Thus, a choice was needed between increased % contrast and decreased background variability. Ideally, these points on the graph would lie in the top left of the figure [6,7]. The balance between contrast and image noise was better in this descending order: HYPER DPR, HYPER Iterative, HYPER DLR, and OSEM.

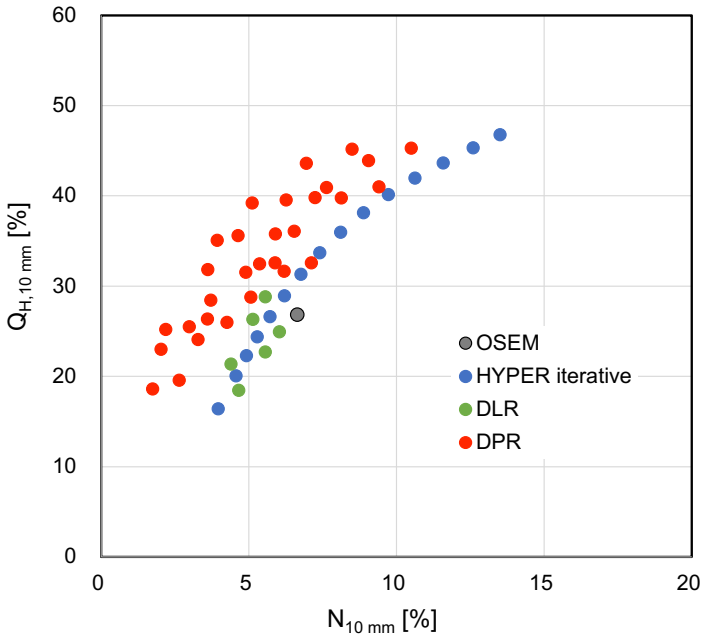

Figure 4. Relationship between % contrast and background variability for all reconstructed algorithms evaluated. OSEM represents OSEM + PSF + TOF.

Figure 5 shows PET images acquired for 2 min and reconstructed using various methods. Statistical noise in PET images was more apparent when OSEM + PSF + TOF was applied, but lower with HYPER DPR. Sphere detectability on PET images was visually better for HYPER DPR than the other types of algorithms evaluated.

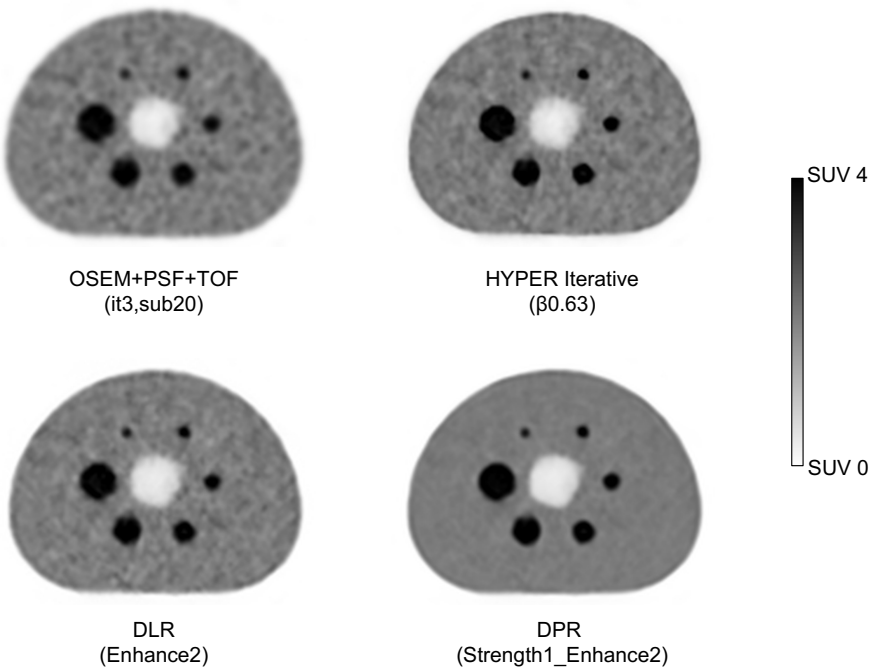

Figure 5. Examples of PET images reconstructed with OSEM +PSF +TOF (3 iterations; 20 subsets), HYPER Iterative (β = 0.63), HYPER DLR (Enhance2), and HYPER DPR (Strength1_Enhance2) acquired for the routine clinical duration of 2 min. The SBR was 4. All images are displayed as SUV on a scale of 0–4.

Figure 6 shows the SUV_{mean} and RC of hot spheres on images acquired for 10 min and reconstructed using OSEM (3 iterations; 20 subsets), HYPER Iterative (β = 0.63), DLR (Enhance2), and DPR (Strength1_Enhance2). The SUV_{mean} and RC differed considerably depending on the reconstruction method. Quantitation of 10 mm spheres was improved by HYPER Iterative, DLR and DPR. The tendency of sphere size dependence was similar among OSEM, HYPER DLR and HYPER DPR except for HYPER Iterative. The $SUV_{B,ave}$ of all reconstructions was within 0.95–1.05 (OSEM, 1.02; HYPER Iterative, 1.02–1.03; HYPER DLR, 1.02–1.03; HYPER DPR, 1.02–1.03). These results indicated that the scanner and reconstruction methods were appropriately calibrated, with quantitative accuracy within ± 5% error.

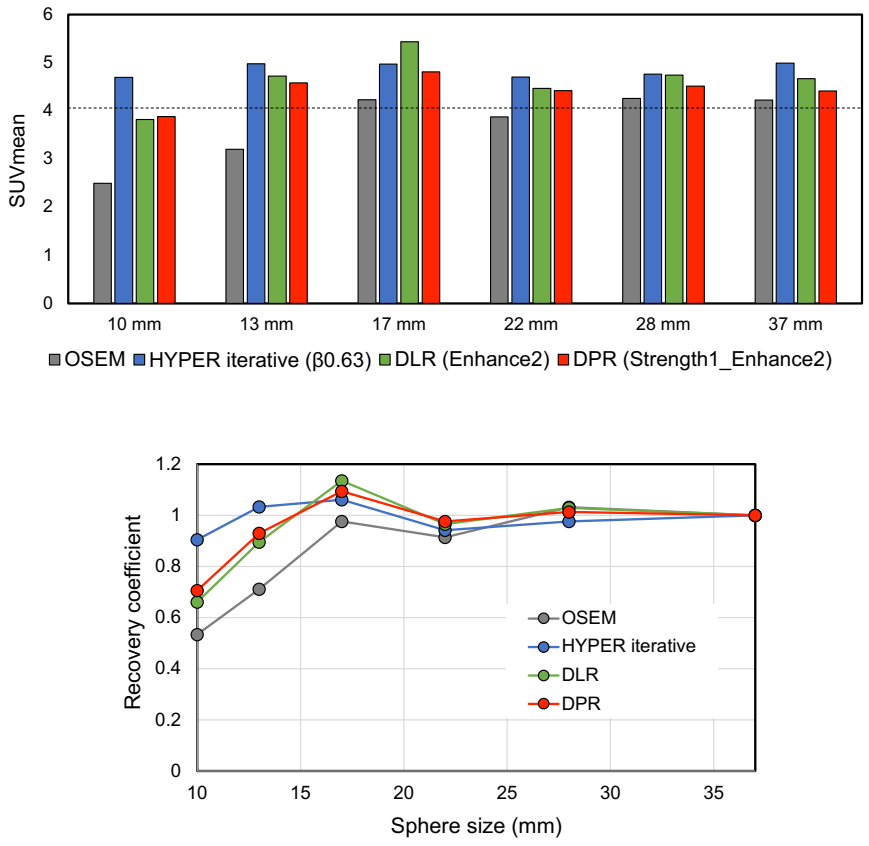

Figure 6. Results of SUV_{mean} and relative recovery coefficient of SUV_{mean} of hot spheres on images reconstructed with OSEM +PSF +TOF (3 iterations; 20 subsets), HYPER Iterative (β value, 0.63), HYPER DLR (Enhance2), and HYPER DPR (Strength1_Enhance2).

4. Conclusions

Our phantom results showed that the advanced image reconstruction algorithms can improve image quality and quantitative accuracy compared with traditional OSEM-based methods. In our evaluations, HYPER DPR reduced noise, improved image contrast, and enhanced PET image quantitation in 10 mm spheres, which may help improve detectability of smaller lesions. However, image quality and quantitation substantially differed according to the reconstruction parameters. The parameters of the new reconstruction methods may require optimization tailored to each institution and scanner, which will also be our next step. Further assessment using human data is needed to evaluate the performance of these advanced image reconstruction algorithms in various imaging scenarios.

5. Image/Figure Courtesy

All images are the courtesy of School of Health Sciences, Fukushima Medical University, Japan.

6. References

1. Miwa K, Wagatsuma K, Iimori T, Sawada K, Kamiya T, Sakurai M, et al. Multicenter study of quantitative PET system harmonization using NIST-traceable ^{68}Ge/^{68}Ga cross-calibration kit. Phys Med. 2018;52:98-103.
2. Akamatsu G, Shimada N, Matsumoto K, Daisaki H, Suzuki K, Watabe H, et al. New standards for phantom image quality and SUV harmonization range for multicenter oncology PET studies. Ann Nucl Med. 2022;36(2):144-61.
3. Chen S, Hu P, Gu Y, Yu H, Shi H. Performance characteristics of the digital uMI550 PET/CT system according to the NEMA NU2-2018 standard. EJNMMI Phys. 2020;7(1):43.
4. Japanese Society of Nuclear Medicine. Standard PET imaging protocols and phantom test procedures and criteria: executive summary. 2017: http://jsnm.org/wp_jsnm/wp-content/themes/theme_jsnm/doc/StandardPETProtocolPhantom20170201.pdf
5. Xing Y, Qiao W, Wang T, Wang Y, Li C, Lv Y, et al. Deep learning-assisted PET imaging achieves fast scan/low-dose examination. EJNMMI Phys. 2022;9(7).
6. Miwa K, Wagatsuma K, Nemoto R, Masubuchi M, Kamitaka Y, Yamao T, et al. Detection of sub-centimeter lesions using digital TOF-PET/CT system combined with Bayesian penalized likelihood reconstruction algorithm. Ann Nucl Med. 2020.
7. Yoshii T, Miwa K, Yamaguchi M, Shimada K, Wagatsuma K, Yamao T, et al. Optimization of a Bayesian penalized likelihood algorithm (Q.Clear) for ^{18}F-NaF bone PET/CT images acquired over shorter durations using a custom-designed phantom. EJNMMI Phys. 2020;7(1):56.

Author Biography

Dr. Kenta Miwa

Professor
Department of Radiological Sciences
School of Health Sciences, Fukushima Medical University, Fukushima, Japan

Kenta Miwa is a Professor of Radiological Sciences at Fukushima Medical University. He obtained his Bachelor of Health Science and Master of Medical Science degrees from Kitasato University, Japan, and his Ph.D. degree in Health Sciences from Kyushu University in 2015. He became an Assistant Professor of Radiological Sciences at Kyushu University, and then he moved to Fukushima Medical University in 2021. He has served the Japanese Society of Nuclear Medicine (JSNM), the Japanese Society of Nuclear Medicine Technology (JSNMT), the Society of Nuclear Medicine and Molecular Imaging (SNMMI), and the European Association of Nuclear Medicine (EANM) in several capacities.

Coronary CT angiogram – An evolving valuable diagnostic tool

Rochita Venkataramanan[a], Akash Venkataramanan[b]

[a]Advantage Imaging and Research Institute, Mylapore, Chennai, India
[b]Internal Medicine PGY1, Cook County Hospital, Chicago, USA

1. Introduction

Ischemic cardiovascular disease has evolved to become the leading cause of morbidity. Despite effective treatments like statins and other preventive efforts, it has led to the loss of useful life years and global mortality. Cardiovascular disease is no longer confined to the developed world; it is also a problem for developing nations. Despite receiving the best possible care from modern interventional and pharmacologic therapies, 10% of acute coronary syndrome patients experience recurrent episodes during the first year (1).

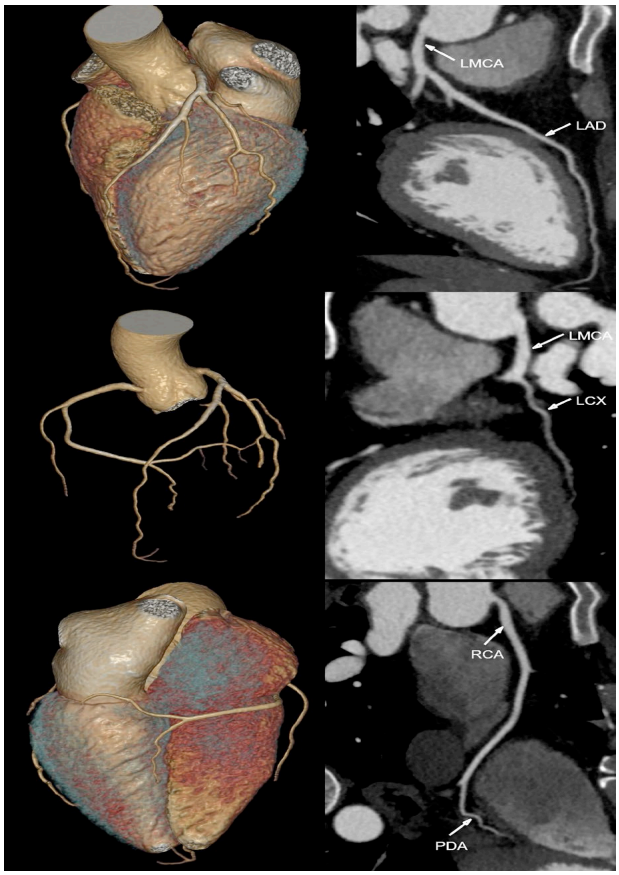

Figure 1. Curved and 3D reconstructions in a 32-year-old man who is a smoker with dyslipidaemia and comes with acute onset chest pain and a normal ECG, reveals a normal coronary arterial tree ruling out an acute coronary event. Scanning was performed on a uCT® 780 (United Imaging Healthcare, Shanghai, China) 160 slice CT scanner.

The CT Coronary Angiogram (CTCA) is the most advanced diagnostic armamentarium of tests for detecting and monitoring coronary artery disease. Patients with stable and unstable anginal symptoms benefit greatly from CTCA, which has a 99% sensitivity and 97% negative predictive value (2) for severe coronary artery disease (CAD) detection, shown in Figure 1.

The National Institute for Health and Care Excellence (NICE) provides independent evidence-based guidance for England's National Health Service. Its 2016 updated guideline for the assessment and diagnosis of recent onset chest pain or discomfort of suspected cardiac origin recommends CCTA as the first-line investigation for all patients with angina (or non-anginal pain but an abnormal electrocardiogram) and no prior CAD, with second-line functional imaging if the CCTA is equivocal (3) as shown in the Figure 2.

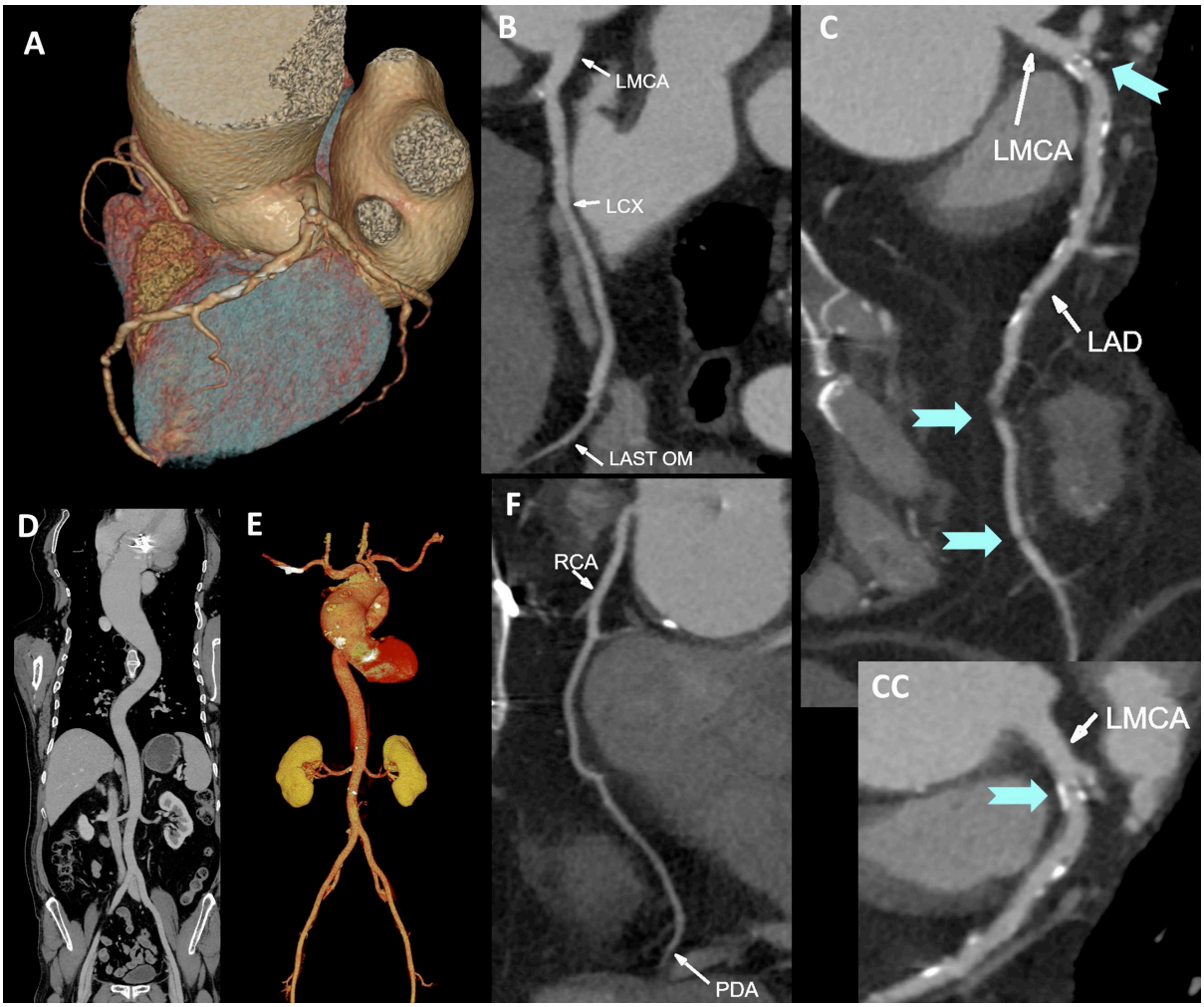

Figure 2. A 63-year-old man with an aortic valve replacement done 10 years ago and no prior coronary artery disease comes with recent onset chest pain. The Echocardiogram showed a normal left ventricular function but a dilated ascending aorta. The ECG showed no new changes. CTCA reveals no stenosis in the left circumflex (LCx) artery and right coronary artery (RCA) (panels B and F). However, left anterior descending (LAD) shows a 90% ostial as well as two short more than 90% stenosis in the distal segments marked by arrows (panels C and CC). The venous phase run through the chest and abdomen after the CTCA with no additional intravenous contrast shows a dilated ascending aorta with no dissection, dilatation or stenosis in the rest of the aorta (Panels D and E). The patient was scanned on a uCT 780 (United Imaging Healthcare, Shanghai, China) 160 slice cardiac CT scanner.

The SCOT-Heart Investigators trial was an open-label, multicenter, parallel-group trial that followed 4146 patients with stable chest pain for 3 to 7 years. The study showed that adding CCTA to standard care in patients with stable chest pain resulted in a significantly reduced rate of CAD or nonfatal MI at five years than standard care alone, without increasing the rate of coronary angiography or coronary revascularization (4) (Figure 3).

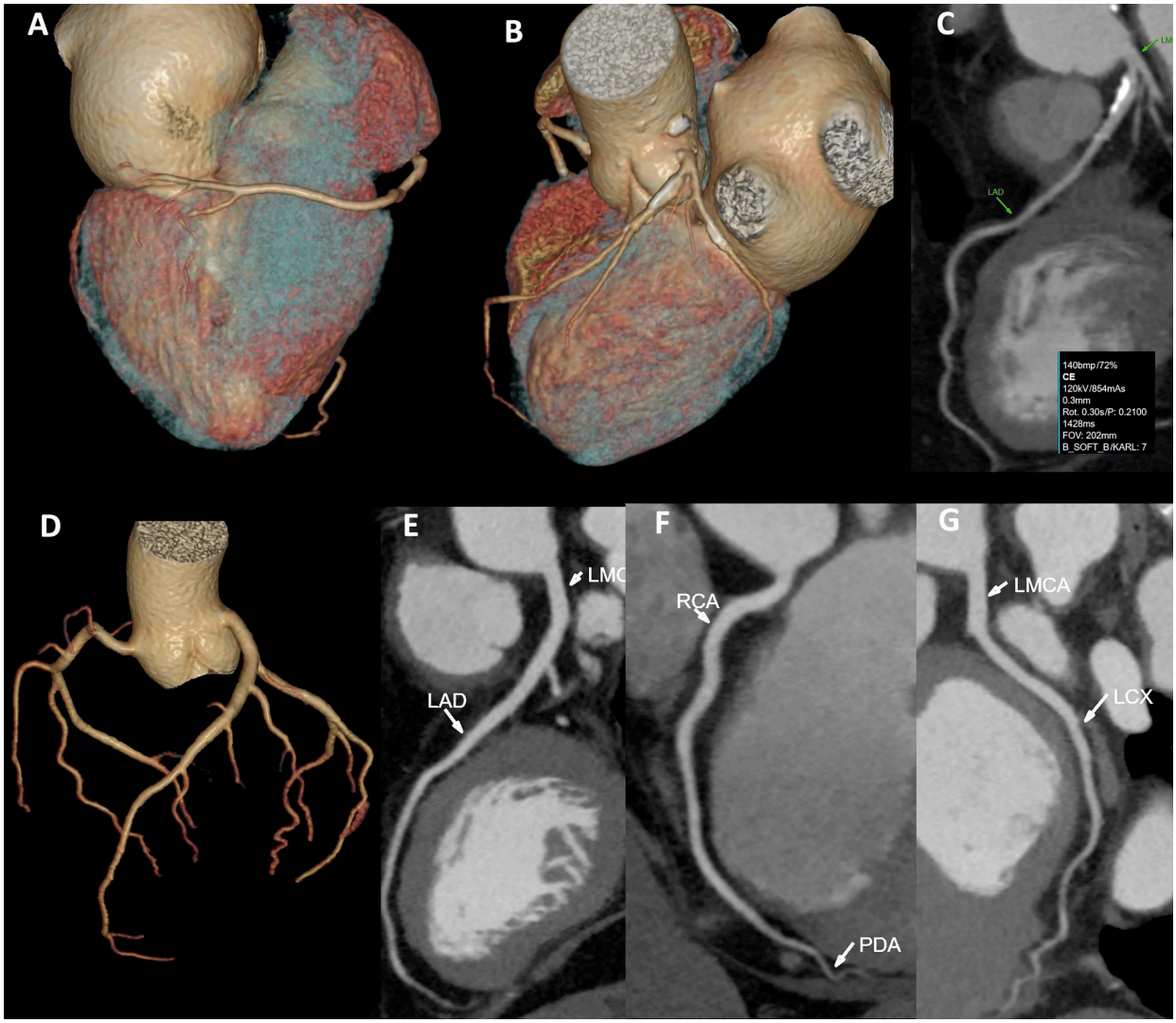

Figure 3. Panels A, B and C show CTCA in a 40-year-old lady with palpitations and chest pain. She was scanned on a uCT 780 (United Imaging Healthcare, Shanghai, China) 160 slice cardiac CT scanner. ECG and Echocardiogram were normal. Despite a high heart rate of 140 beats/minute, the image quality we obtain was excellent. A mild to moderate stenosis was seen by calcified plaques in proximal LAD and LCx. She was managed medically. Panels D, E, F and G show a normal CTCA in a 49-year-old woman without any risk factors for coronary artery disease but with recurrent chest pain and an abnormal ECG with a borderline positive treadmill test. Chest pain from cardiac cause was ruled out.

2. Recent improvements in CTCA hardware and software

The clinical value of CTCA has continued to increase because of considerable developments in CT technology, software, and machine learning in recent years. Increasing gantry rotational rates enables imaging that was not achievable with older machine models. Iterative reconstruction techniques with improved temporal resolution for patients with high heart rate have been utilized to drastically lower the radiation dose to the patient without affecting the image quality. High, near-isotropic spatial resolution is also required for coronary artery imaging. The accuracy of CTCA is improved by using the advanced detector features a thin 0.5 mm element size that can fundamentally improve the spatial resolution. And the detector has a coverage of 4–16 cm in z direction which enables simultaneously acquiring imaging date of the entire heart in a single breath-hold. Such developments are underway and will undoubtedly increase the use of CTCA. (5) (Figure 4)

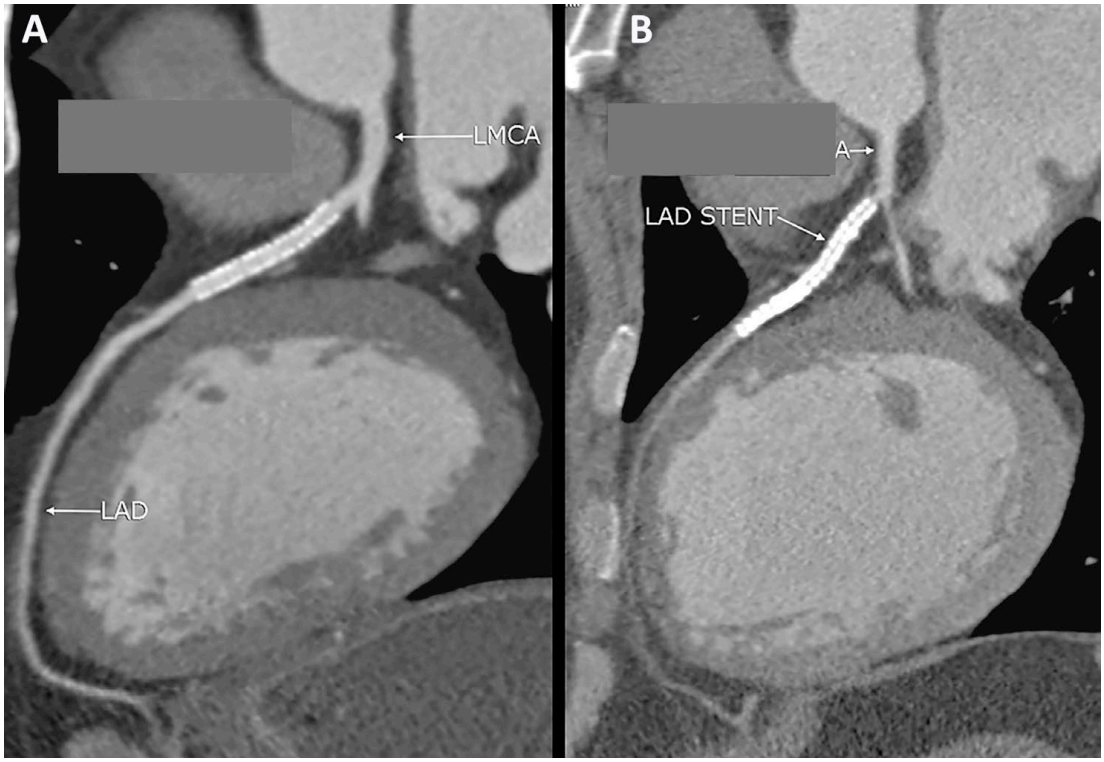

Figure 4. The LAD stent imaged in a higher version machine, the uCT 780 (United Imaging Healthcare, Shanghai, China) 160 slice cardiac CT scanner. Panel A shows remarkable clarity of the in-stent lumen as compared to the lower version machine study performed a few years earlier shown in Panel B.

3. The usefulness of coronary artery calcium scoring (CACS)

CACS is widely accessible, less complicated to operate (e.g., not depending on heart rate), does not need contrast, is less costly, and provides highly reproducible results. Although this test has been available for the past 20 years, there has recently been increased interest in its possible use of CACS in patients with low-risk symptomatic and the clinical importance of non-calcified plaque and stenosis in the absence of calcium. It has been shown that only 1 to 2% of symptomatic patients with CACS zero have potentially obstructive CAD, and only 0.4% of these patients have >70% stenosis. None of these patients will need coronary revascularization or have a bad prognosis within two years. (6) Patients with low and intermediate risk of CAD who appear with chest discomfort and have a normal Electrocardiogram, normal cardiac biomarkers, and a CACS of zero may be considered for early discharge without further screening in the emergency department (7).

CACS has been shown to continue improving discrimination and risk revaluation for major CAD and CVD in community-dwelling people who do not exhibit symptoms, even when Framingham risk factors are considered. It correctly reclassified two-thirds of the people in the Framingham Heart Study who were in the intermediate-risk group. Of those, 77% were moved down to low risk, and 23% were moved up to high risk (8). The ability to identify asymptomatic occult CAD in community residents who appear to be at low risk based on the Framingham risk scoring and to prevent CAD progression and incidents is a crucial addition of CACS.

4. CTCA value in the emergency room (ER)

Patients with low to intermediate-risk chest discomfort have found CTCA to be helpful in the ER. Those individuals without visible plaque can be discharged from the hospital immediately and securely. After a negative 6-hour troponin level, patients with non-obstructive plaque and mild to moderate stenosis can be discharged, whereas patients who have severe stenosis must be hospitalized to the hospital for further care (Figure 5). It has been determined that there are no fatalities or incidences of acute coronary syndrome

during the follow-up period. It has been demonstrated that patients without a CTCA have a greater rate of chest pain-related rehospitalization. The average stay period is similarly shorter for patients having a CTCA (9).

5. CTCA usefulness for percutaneous coronary interventions (PCI)

More than 2cm long, over severely angulated segments, heavily calcified, across ostia or bifurcations, with uneven surfaces and adherent thrombi, past tortuous segments, or completely blocked coronary artery lesions are considered complicated and have limited effectiveness following stenting (10). Therefore, it is essential to recognize these lesions. Brett M. Wertman et al. (11) revealed that CTCA was able to recognize Type C complex lesions well, which was related with increased contrast use and procedure duration during PCI. (Figure 6)

CTCA can differentiate angiographic TIMI grade 3 (normal) flow from TIMI grade 2 (sluggish) flow in patients with acute MI by comparing the contrast density at the distal end of the thrombolyzed artery with that proximal to the stenotic lesion. For TIMI 3, the ratio of CTCA number distal to CTCA number proximal should be greater than 0.54. CTCA can be used to check on coronary reperfusion after thrombolysis without any invasive procedure.

6. Plaque composition on CTCA and risk prediction

Due to the high resolution of CTCA images, the atheroma's composition can be depicted in exquisite detail. (Figure 7) Instead of exclusively soft plaques, we discovered that mixed plaques with soft and calcific portions are substantially more likely to rupture (13). It is now established that plaque morphology influences primary prevention, predictors of ischemia, and prognosis. Plaque composition, namely calcified vs soft and/or mixed plaques, as well as the presence of soft or mixed plaques, have been proven to be the highest predictor of events as a likely measure of plaque vulnerability, regardless of lesion severity. (Figure 8) (14, 15). The complete coronary tree is visible, and the overall plaque load and extent of diseased segments are assessed.

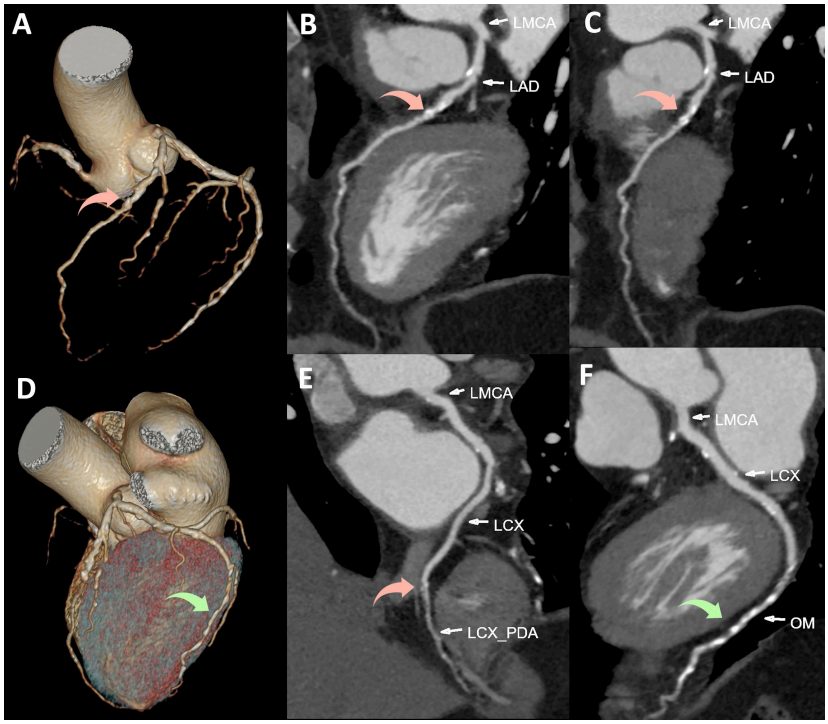

Figure 5. A 57-year-old man presented to the emergency room with chest discomfort. The ECG, echocardiogram and cardiac biomarkers were negative. However, CTCA revealed significant calcified plaque burden in the coronary arteries. Panels A, B and C show calcified mid LAD plaque causing more than 80% stenosis (pink arrow). Panels D and F show diffuse distal disease of the major OM branch (green arrow). Panel E shows a significant stenosis at the LCx- (posterior descending artery) PDA ostium (pink arrow). The patient was treated with a three vessel CABG with grafts to LAD, Diagonal and the LCx – PDA.

7. Plaque regression assessment by CTCA

The detection of early CAD on CTCA would be useless if it could not be resolved with medication. Several multicenter, randomized lipid-lowering trials utilizing both invasive catheter angiography (ICA) and clinical assessment, on the other hand, found a minimal change (1 to 3%) in luminal diameter on ICA. Nonetheless, these same studies found a 25% to 75% reduction in severe occurrences, such as myocardial infarction (16,17).

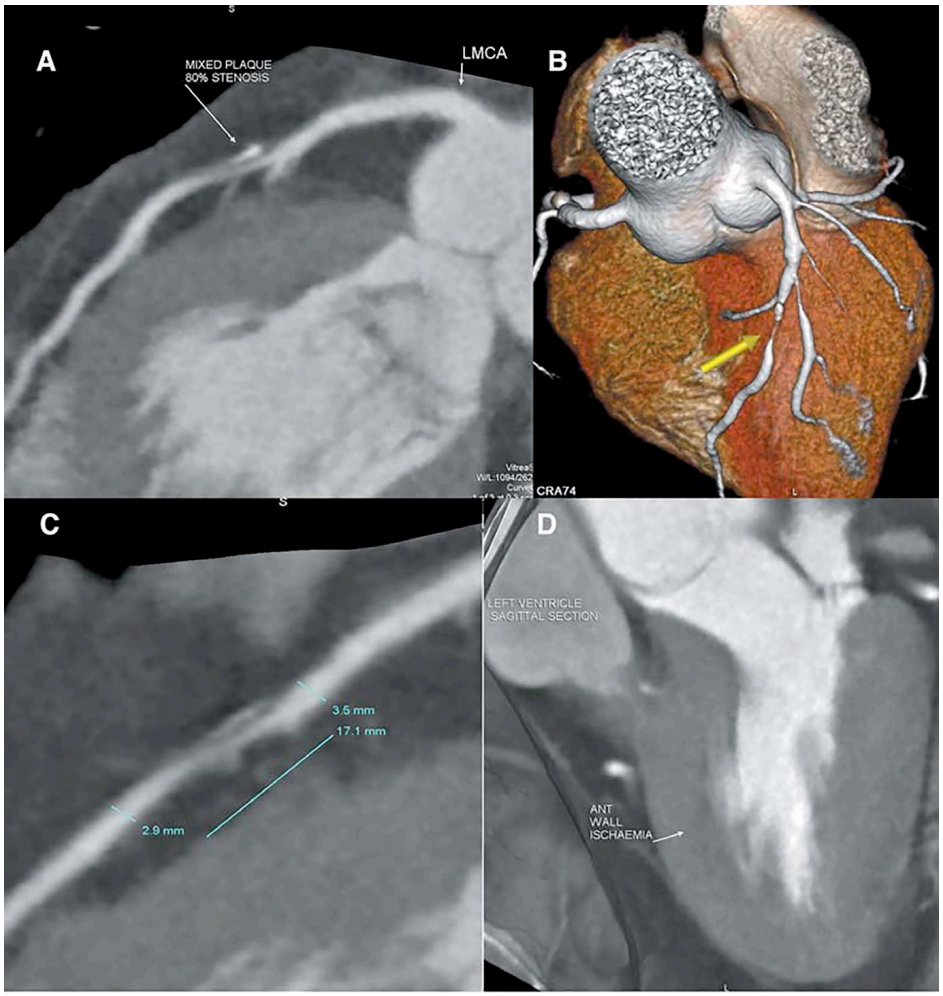

Figure 6. Panel A shows a curved reconstruction with a mixed plaque in the mid LAD. The 3D image gives the relation of the stenotic segment to side branches as well as the curvature of the artery in panel B. The lesion length and vessel diameter can be measured in Panel C. Panel D shows the myocardium in the 2 chamber long axis view revealing a dark area in the sub-endocardium of the anterior wall representing a perfusion defect at rest. Patient was scanned on a uCT 780 (United Imaging Healthcare, Shanghai, China) 160 slice cardiac CT scanner.

This shows that the benefits of lowering lipids come from stabilizing lipid-rich plaques, not from changes in the size of the ICA lumen. CTCA is able to accurately measure the diminution in plaque size. Even at modest doses, the administration of statins may cause significant changes in the CTCA plaque shape, an absolute reduction in plaque volume without a discernible change in lumen size, and variations in lipid profile that are not statistically meaningful. This shows that plaque morphological changes may emerge early on, even with only modest alterations to the lipid profile, as a result of statin therapy (18).

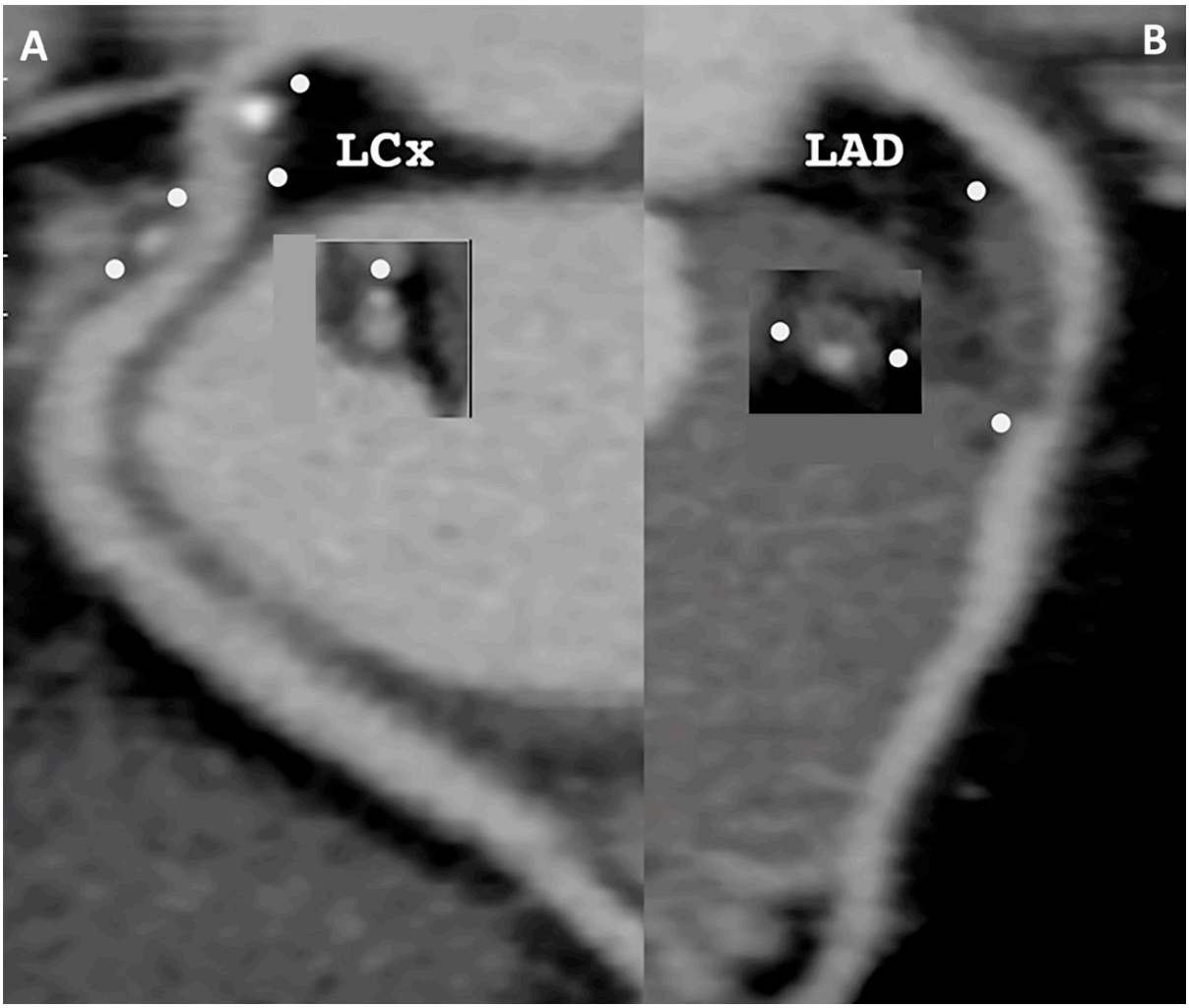

Figure 7. Panel A shows two eccentric mixed plaques marked by white dots in the proximal LCx artery with a soft component and a small, calcified nodule. Inset shows the cross section of one of the plaques. Panel B shows a thick eccentric soft plaque with no calcified component marked by white dots in the proximal LAD artery. Inset shows the plaque in cross section.

8. Stress myocardial CT perfusion (CTP)

CTP contains anatomic as well as physiological information (i.e., myocardial perfusion). The viability of stress myocardial CTP has been shown in multiple single-center studies. In addition, it has been demonstrated that a combination CCTA/CTP strategy increases the diagnostic accuracy for detecting hemodynamically severe stenosis compared to CTCA individually. Stress and reversible myocardial perfusion deficits detected by CTP utilizing a visual semi-quantitative technique and a visually guided software-based method are comparable to those assessed by SPECT (19,20).

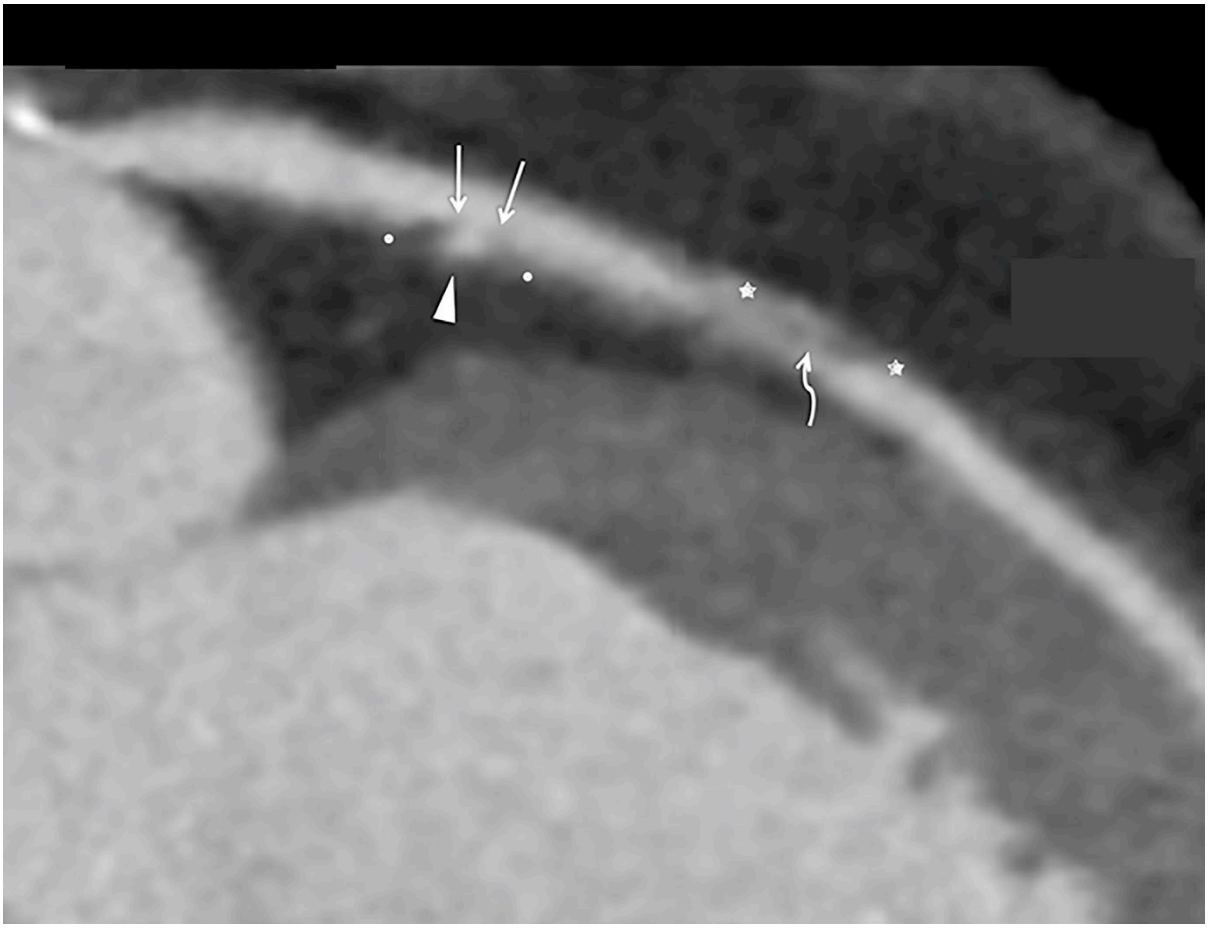

Figure 8. An eccentric ruptured plaque is seen along the inferior wall of the LAD marked by white dots. The straight arrows show the central ulceration on the plaque luminal surface. The arrowhead marks the cavity within the plaque filled with intraluminal contrast. Another plaque is seen marked by stars in the anterior wall of the LAD. This shows an ulceration along the inferior shoulder (curved arrow). Patient was scanned on a uCT 780 (United Imaging Healthcare, Shanghai, China) 160 slice cardiac CT scanner.

9. CT fractional flow reserve (CT-FFR)

CT- FFR predicts the functional relevance of coronary artery lesions using computational fluid dynamics. The strongest indicator of a positive CT-derived FFR, according to the Assessing Diagnostic Value of Non-invasive FFRCT in Coronary Care (ADVANCE) Registry, is stenosis greater than 70%. However, the ADVANCE Registry, like invasive FFR studies, demonstrates that there is a gap between morphological assessment of coronary stenosis and the physiological consequences of such lesions. 28.4% of severe lesions were found to have no functional significance. Similar to this, there is a positive CT- FFR rate of 20.8% in patients with non-obstructive coronary structure (stenosis grade 30-49%) (21).

10. Coronary Bypass Graft (CABG) imaging on CTCA

CTCA is quite reliable for determining graft patency after CABG. In a 3D picture, it shows every graft together. Studying the native arteries in relation to the failed grafts enables a therapeutic strategy to determine whether a PCI is warranted. In our study, we discovered that regardless of the number of years following CABG, 72% of all grafts, including LIMA, SVG, RIMA, and LRA, failed when placed on coronary arteries with less than 75% stenosis as opposed to 22.8% of grafts failing when positioned on coronary arteries with more than 75% stenosis ($p < 0.0001$) (Figure 9) (22).

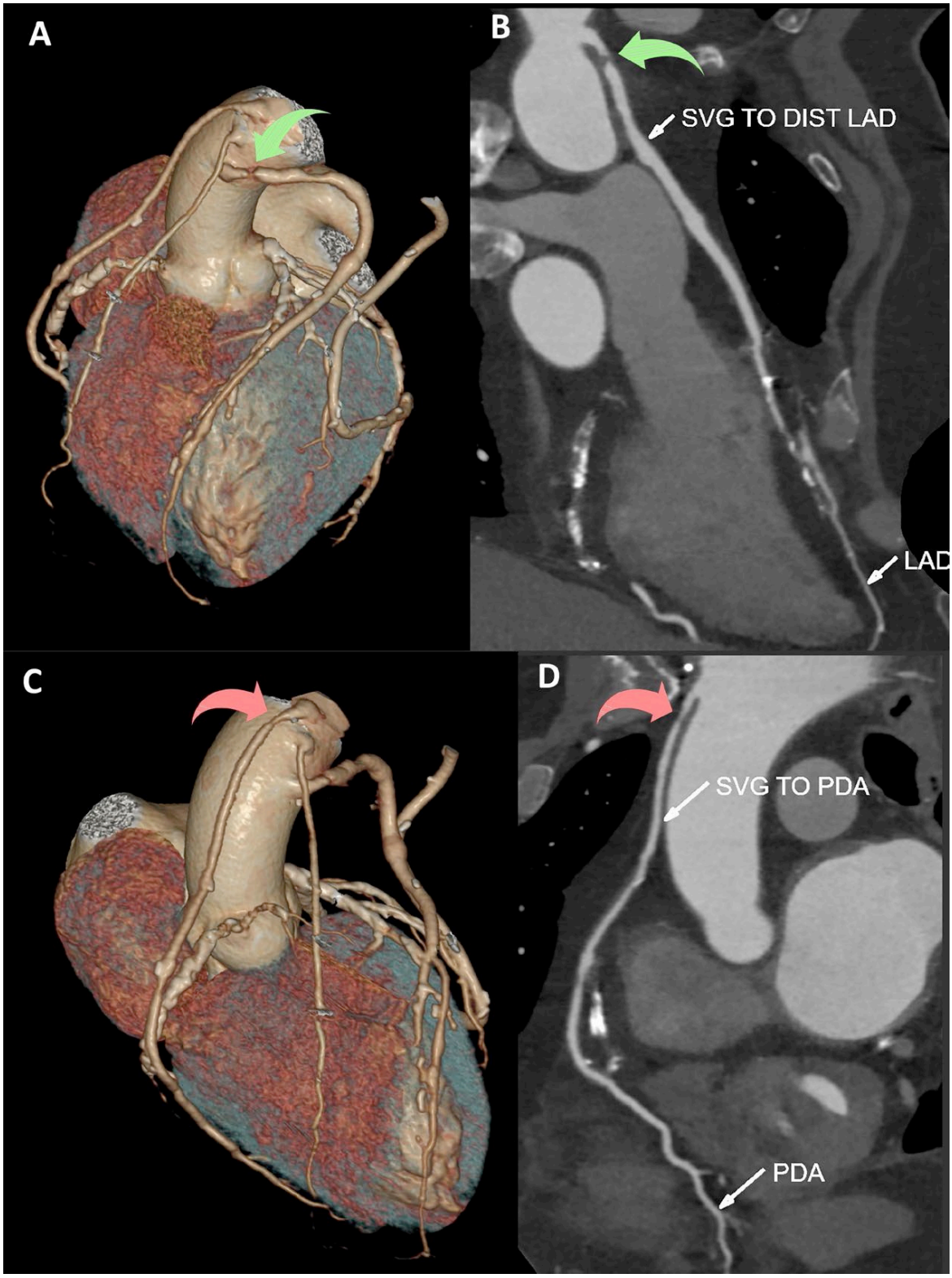

Figure 9. A 67-year-old man 6 years post CABG comes with recurrence of angina. Sequential LIMA to Diagonal and Obtuse marginal as well as saphenous vein grafts (SVG) to LAD, right ventricular branch and right PDA are patent. However, short critical stenosis is seen in the proximal segment of the SVG to LAD (green curved arrow) as well as the SVG to PDA (orange arrow). These were successfully stented. Patient was scanned on a uCT 780 (United Imaging Healthcare, Shanghai, China) 160 slice cardiac CT scanner.

11. Conclusion

In the modern era, CCTA has developed into an ideal test that can accurately and consistently image the true severity of coronary artery stenosis, a detailed representation of the atheroma causing this, the downstream impact on the myocardium, and functionality of the heart with minimum contrast dose and radiation in a short time with no patient discomfort.

CTCA demonstrates that the existence of soft and mixed plaques can result in higher major cardiovascular events score than a clinical risk model, regardless of the severity of the lesion. CTCA can be utilized in the emergency unit to check the coronary arteries and determine who needs to be hospitalized for an acute cardiac problem quickly and noninvasively. For patients who do not experience a cardiac incident, it is confidently concluded that a secure and early discharge is appropriate. By demonstrating a decrease in plaque volume, CTCA could be able to show a meaningful effect at lower statin doses.

It has been demonstrated that CACS improves risk categorization and discrimination for significant CAD and CVD irrespective of Framingham risk variables in asymptomatic community-dwelling individuals. CT-FFR, in conjunction with CTCA, could become the optimum test for assessing the functional relevance of a stenosis and guiding therapies.

12. Image/Figure Courtesy

All images are the courtesy of Advantage Imaging and Research Institute, Mylapore, Chennai, India.

13. References

1. Libby P, Bornfeldt KE, Tall AR. Atherosclerosis: successes, surprises, and future challenges. Circulation research. 2016 Feb. 19;118(4):531-4.

2. Meijboom WB, Meijs MF, Schuijf JD, Cramer MJ, Mollet NR, van Mieghem CA, Nieman K, van Werkhoven JM, Pundziute G, Weustink AC, de Vos AM. Diagnostic accuracy of 64-slice computed tomography coronary angiography: a prospective, multicenter, multivendor study. Journal of the American College of Cardiology. 2008 Dec 16;52(25):2135-44.

3. Kelion AD, Nicol ED. The rationale for the primacy of coronary CT angiography in the National Institute for Health and Care Excellence (NICE) guideline (CG95) for the investigation of chest pain of recent onset. Journal of cardiovascular computed tomography. 2018 Nov 1;12(6):516-22.

4. SCOT-Heart Investigators. Coronary CT angiography and 5-year risk of myocardial infarction. New England Journal of Medicine. 2018 Sep 6;379(10):924-33.

5. Commandeur F, Goeller M, Dey D. Cardiac CT: technological advances in hardware, software, and machine learning applications. Current cardiovascular imaging reports. 2018 Aug;11(8):1-2.

6. Hulten E, Bittencourt MS, Ghoshhajra B, O'Leary D, Christman MP, Blaha MJ, Truong Q, Nelson K, Montana P, Steigner M, Rybicki F. Incremental prognostic value of coronary artery calcium score versus CT angiography among symptomatic patients without known coronary artery disease. Atherosclerosis. 2014 Mar 1;233(1):190-5.

7. Tota-Maharaj R, McEvoy JW, Blaha MJ, Silverman MG, Nasir K, Blumenthal RS. Utility of coronary artery calcium scoring in the evaluation of patients with chest pain. Critical Pathways in Cardiology. 2012 Sep 1;11(3):99-106.

8. Hoffmann U, Massaro JM, D'Agostino Sr RB, Kathiresan S, Fox CS, O'Donnell CJ. Cardiovascular event prediction and risk reclassification by coronary, aortic, and valvular calcification in the Framingham Heart Study. Journal of the American Heart Association. 2016 Feb 22;5(2):e003144.

9. Arthur Nasis, Ian T. Meredith, Nitesh Nerlekar, et al. Acute Chest Pain Investigation: Utility of Cardiac CT Angiography in Guiding Troponin Measurement. http://radiology.rsna.org/lookup/suppl/doi:10.1148/radiol.11110013/-/DC1

10. SG Ellis, MG Vandormael, MJ Cowley, et al. Coronary morphologic and clinical determinants of procedural outcome with angioplasty for multivessel coronary disease. Implications for patient selection. Multivessel Angioplasty Prognosis Study Group. Circulation 1990,82:1193-1202.

11. Brett M. Wertman, Victor Y. Cheng, Saibal Kar, et al. Characterization of complex coronary artery stenosis morphology by Coronary Computed Tomographic Angiography. J. Am. Coll. Cardiol. Img. 2009: 2; 950-958.

12. Makoto Yamashita, Souki Lee, Shuichi Hamasaki, et al. Noninvasive evaluation of coronary reperfusion by CT Angiography in patients with STEMI. J Am Coll Cardiol Img. 2011: 4; 141-149.

13. Ramanan RV. Plaque rupture relationship to plaque composition in coronary arteries. A 320-slice CT angiographic analysis. Apollo Medicine. 2015 Jun 1;12(2):115-22.

14. Vincenzo Russo, Andrea Zavalloni, Maria Letizia Bacchi Reggiani, et al. Incremental Prognostic Value of Coronary CT Angiography in Patients With Suspected Coronary Artery Disease. Circ Cardiovasc Imaging 2010;3: 351-359.

15. Nance Jr JW, Schlett CL, Schoepf UJ, Oberoi S, Leisy HB, Barraza Jr JM, Headden GF, Nikolaou K, Bamberg F. Incremental prognostic value of different components of coronary atherosclerotic plaque at cardiac CT angiography beyond coronary calcification in patients with acute chest pain. Radiology. 2012 Sep;264(3):679-90.

16. Brown BG, Zhao XQ, Sacco DE, et al. View of treatment to achieve regression of coronary atherosclerosis and to prevent plaque disruption and clinical cardiovascular events. Br Heart J. 1993: 69: S48-S53.

17. Scandinavian Simvastatin Survival Study Group. Randomized trial of cholesterol lowering in 4444 patients with coronary heart disease: the Scandinavian Simvastatin Survival Study. Lancet. 1994: 344: 1383-1389.

18. Kaori Inoue, Sadako Motoyama, Masayoshi Sarai, et al. Serial Coronary CT Angiography – Verified changes in plaque characteristics as an end point: Evaluation of effect of statin intervention. J Am Coll Cardiol Img 2010:3; 691-698.

19. Tust Techasith, Ricardo C Cury. Stress Myocardial CT Perfusion: An Update and Future Perspective. J Am Coll Cardiol Img 2011: 4; 905-916.

20. Balaji K. Tamarappoo, Damini Dey, Ryo Nakazato, et al. Comparison of the Extent and Severity of Myocardial Perfusion Defects Measured by CT Coronary Angiography and SPECT Myocardial Perfusion Imaging. J Am Coll Cardiol Img 2010: 3; 1010-1019.

21. Kitabata H, Leipsic J, Patel MR, et al. Incidence and predictors of lesion-specific ischemia by FFR CT: learnings from the international ADVANCE registry. J Cardiovasc Comput Tomogr 2018;12:95–100. https://doi.org/10.1016/j.jcct.2018.01.008; PMID: 29422416.

22. Ramanan RV, Ramalingam A. Coronary artery bypass graft failure and its relationship to target artery percentage stenosis and competitive flow. A CT angiographic analysis. Apollo Medicine. 2014 Dec 1;11(4):245-54.

Author Biography

Dr. Rochita Venkataramanan

Founder and Chief
Radiologist
Advantage Imaging and
Research Institute,
Mylapore, Chennai, India

Dr. Rochita Venkataramanan completed her undergraduate studies at the prestigious Grant Medical College and Sir J. J. group of Hospitals in Mumbai in 1989. She was selected for postgraduate training in Radiology at the Tata Memorial Hospital, Mumbai which is the leading institution for Oncology in India. She completed her M.D. and DNB in 1993. Dr. Rochita is a passionate clinical researcher and has five new radiology signs to her name published in leading International and National Medical Journals. These signs help to accurately diagnose specific diseases and are used by Radiologists all over the world. She also founded the Journal of Gastrointestinal and Abdominal Radiology (JGAR) and is the Editor-in-Chief. She has led the journal to indexation at the DOAJ within a short period of three years.

Future of radiology in developing countries

Harsh Mahajan[a] and Vidur Mahajan[b]
[a]Mahajan Imaging Private Limited, Delhi-110016, India
[b]CARPL.AI Inc, San Francisco, CA-94107, USA

The association between technical breakthroughs and human well-being in terms of life expectancy has been well established through the past several centuries. Since its development in the 19th century, radiology has expanded swiftly to improve diagnosis and thereby treatment of disease for hundreds of millions of patients all over the world. The medical sector has been revolutionized by the introduction of cutting-edge technologies and methods that have increased productivity, decreased costs, and increased patient safety. Radiology, in conjunction with pathology, has become an essential component of both the diagnostic and treatment processes utilized for a wide variety of diseases.

Radiology services are now a crucial component of every hospital, including in small hospitals and nursing homes, to find the root cause of illness in patients. It includes X-rays, Ultrasonography, Computerized Tomography (CT) scans and Magnetic Resonance Imaging (MRI) scans, Positron Emission Tomography (PET), Ultrasound etc. There are around 50,000 MRI[1] and over 300,000 CT systems installed worldwide. Furthermore, there are roughly 1,600 PET/CT systems in use worldwide. Access to modern imaging systems like CT is restricted in low- and middle-income countries (LMIC), with most available models being 16-slice or less, although a trend to higher-end imaging systems is emerging. The current standard for magnetic field strength in LMIC is 1.5T MRI. 3T MRI access is considerably more limited. Japan has the largest per capita number of MRI (55.21 per million population) and CT systems among developed nations, followed by the United States and Germany. For LMICs like South Africa, India, Mexico, and the Middle East, the MRI systems per million population are 0.23, 1.50, 2.57, and 1.90, respectively[2].

According to a survey, there are currently about 30,000 CT systems and 3,500 MRI[3] systems in India. Now, multi-detector CT systems are commonly seen in use and 64- and 128-slice systems have become a reality. It will not be surprising if the figure doubles in the next ten years. The next decade will be dominated by molecular imaging worldwide, and developing nations are quickly catching up. There are currently 222 PET/CT[4] systems in India performing around half million PET/CT scans annually.

The International Agency for Research on Cancer (IARC) estimates that 18 million new cases of cancer and 10 million cancer deaths were reported in 2020. The load may increase in the future because of a number of factors, including sedentary lifestyles, unhealthy diets, and fewer births in nations that are transitioning economically. We are currently observing good trends in developed countries; the expansion of healthcare facilities will undoubtedly promote the expansion of radiology services, which can aid Radiologists in the diagnosis of life-threatening disease like cancer. However, many developing and underdeveloped nations experience difficulties in effectively implementing sub-specializations of radiology. These difficulties include a lack of money, inadequate infrastructure and equipment, a lack of knowledge, politics, the emigration of radiologists, perfectionism, and others. The other two problems are a) accessibility and b) awareness, both of which are equally crucial. Access to hospitals is another concern, as people from remote areas may have to travel for several days to reach a city hospital. This, along with the high cost of care, causes many people to visit hospitals only as a last option, resulting in poor outcomes for many diseases.

[1]Ogbole GI, Adeyomoye AO, Badu-Peprah A, Mensah Y, Nzeh DA. Survey of magnetic resonance imaging availability in West Africa. Pan Afr Med J. 2018 Jul 31;30:240. doi: 10.11604/pamj.2018.30.240.14000. PMID: 30574259; PMCID: PMC6295297.
[2]Qin C, Murali S, Lee E, Supramaniam V, Hausenloy DJ, Obungoloch J, Brecher J, Lin R, Ding H, Akudjedu TN, Anazodo UC, Jagannathan NR, Ntusi NAB, Simonetti OP, Campbell-Washburn AE, Niendorf T, Mammen R, Adeleke S. Sustainable low-field cardiovascular magnetic resonance in changing healthcare systems. Eur Heart J Cardiovasc Imaging. 2022 Jun 1;23(6):e246-e260. doi: 10.1093/ehjci/jeab286. PMID: 35157038; PMCID: PMC9159744.
[3]https://www.indianradiologist.com/index.php/review/made-in-india-mri
[4]Tharma AR. Nuclear Medicine in India: A Historical Journey. Indian J Nucl Med. 2018 Nov;33(Suppl 1):S5-S10. doi: 10.4103/0972-3919.245053. PMID: 30533977; PMCID: PMC6243721.

Over the past few years, Artificial Intelligence (AI) has attracted immense attention in the field of medicine, particularly in radiology. In the next ten years, the use of AI in radiology will be a significant advancement that will result in a massive paradigm shift in how radiology is managed globally. We believe that the introduction of AI into clinical practice is the only way to bend the current demand-supply mismatch between the number of scans that need to be read and the Radiologists available to read them. With vast amounts of data now readily available, and a new wave of AI algorithms which are much more sophisticated and holistic than before, it is clear that the radiology department of the future will run hundreds of AI systems in tandem. AI will contribute to the global development of personalized precision medicine and provide individualized treatment alternatives. Radiologists around the world must understand these potential AI areas of application and should be strongly encouraged to help shape the future of Radiology and medicine by becoming the driving force behind the development and implementation of AI in clinical practice. India is uniquely positioned in this AI race for two key reasons. First, India has highly skilled physicians that are trained in challenging clinical settings. Secondly, India is extremely heterogenous in terms of the diseases / patient-base – with the presence of both western and eastern diseases in a single country. This combination allows for India to be best suited for AI implementation in the clinical setting.

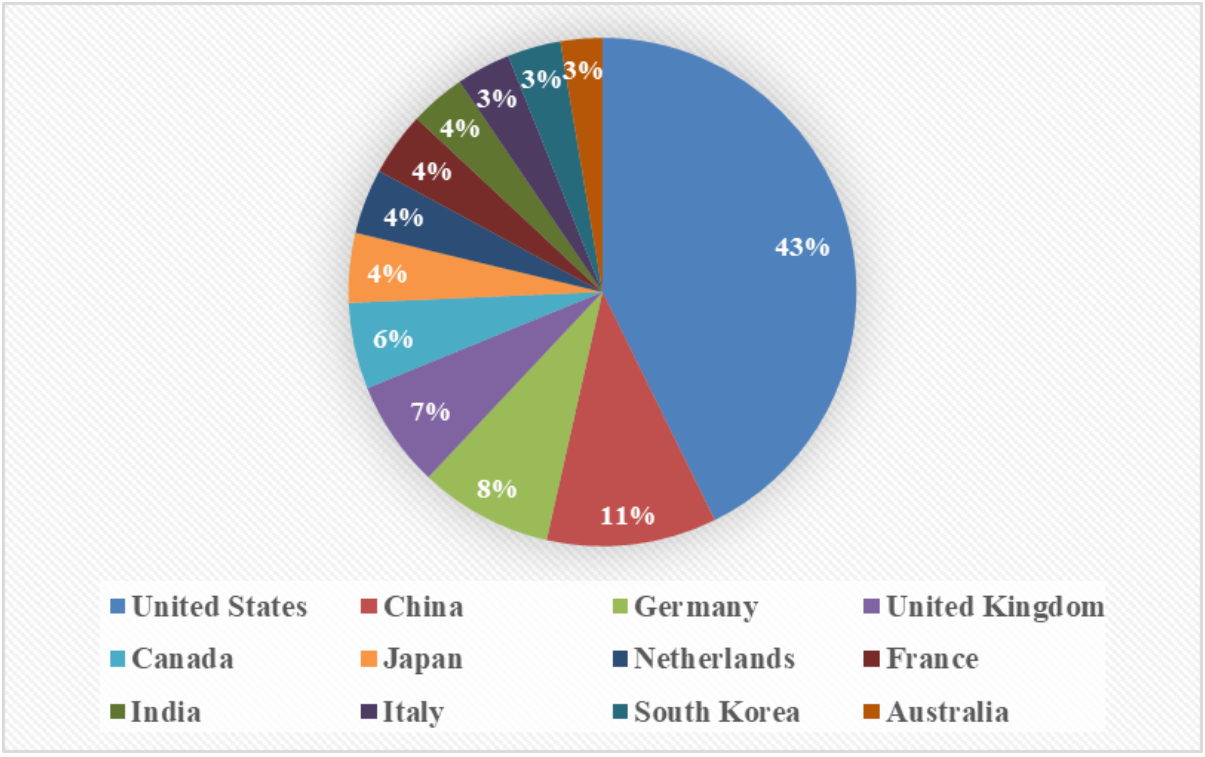

Figure 1. Graph of number of AI in Radiology based publications by country from year 2000 to 2019.

The market size[5] for AI in healthcare surpassed USD 4.2 billion in 2020 and is predicted to expand at a CAGR of approximately 33.7% between 2021 and 2027. In 2020, the medical imaging & diagnosis market sector held around 24.6% market share. The uses of AI in modern healthcare practices continue to grow.

[5]https://www.gminsights.com/toc/detail/healthcare-artificial-intelligence-market

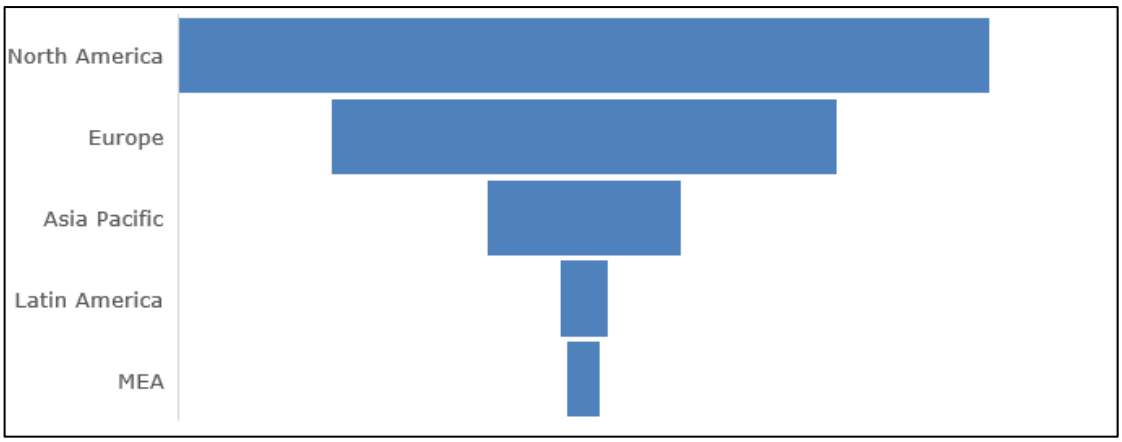

Figure 2. AI in the Radiology market, 2022 (million USD) by region, based on usage and growth.

Healthcare is expensive, and cost is widely regarded as the industry's most significant impediment worldwide. This major impediment can be overcome by lowering scanning and operational expenses without compromising system quality. The training of more imaging specialists to fulfill the excessive demand, the transformation of existing Radiologists into subspecialty Radiologists, and the reduction of the high operating, scanning, and equipment expenses of MRI and CT scans are a few potential solutions. New solutions can be achieved by expanding exchange programs among Radiologists and residents from various countries and sharing their expertise. In less developed nations, the availability of subspecialist radiology training is limited. To overcome this shortcoming, cost-effective and innovative training methods are required. MRI systems that can detect diseases and injuries presently cost up to $3 million and have monthly operating costs of roughly $15,000, making them inaccessible for 70% of the world's population[6]. The image quality resulting from earlier attempts to create more economical scanners has not been sufficient to be used for medical applications. However, technical improvements in the last two years have raised the prospect of "generating brain images with low-cost hardware[7]."

Current CT systems with 32 or 64 slices are up to four times faster than earlier models[8]. Machine learning has created the great potential to advance medical imaging, specifically CT scanning, by reducing exposure to radiation and by harnessing the power of AI. Newer digital technologies, including voice recognition and structured formatted reporting, also improve Radiologists' workflow, productivity, and reporting accuracy. Over the next decade, we will see more and more imaging departments across the world recognize the need to embrace digital technologies and profit substantially as a result. Tele-Radiology will be increasingly implemented in less developed nations, allowing for three changes: increased reach of high-quality radiologic services to remote regions, more sub-specialization within the field of radiology, and increased availability of emergency radiology services.

The time has come for developing countries to implement continuing medical education programs for professional Radiologists, and improve access to imaging equipment, workforce capacity, digital technologies, and PET radiopharmaceuticals. In recent years, a growing number of similar programs have emerged in low- and middle-income nations to produce substantial health and economic benefits and reduce the cancer burden globally. In fact, United Imaging's entry into India with the latest technology is testament to the fact that India is now ready to receive attainable innovative imaging systems. We have been using their PET/CT (uMI® 550) system for the past year and everyone – from patients to clinicians to Nuclear Medicine Physicians – is amazed at the quality of images, and reduction in ^{18}F-FDG dose and scan time.

[6]https://www.natureasia.com/en/research/highlight/13913
[7]Liu, Y., Leong, A.T.L., Zhao, Y. et al. A low-cost and shielding-free ultra-low-field brain MRI scanner. Nat Commun 12, 7238 (2021).
[8]https://www.neurologica.com/blog/advances-ct-scan-technology

Author's Biography

Dr. Harsh Mahajan
Founder and Chief
Radiologist, Mahajan
Imaging Pvt. Ltd.
President of NATHEALTH
Past President, IRIA

Dr. Harsh Mahajan is the Founder and Chief Radiologist at Mahajan Imaging, a chain of high-end medical imaging centers in New Delhi. He is the Honorary Radiologist to the President of India and a recipient of the Padma Shri award from the Government of India. He has been President of the Indian Radiology and Imaging Association and Indian Society of Neuroradiology. He is also a Consultant to the International Atomic Energy Agency (IAEA) and is a post-graduate teacher and examiner in Radiology and Nuclear Medicine. He also serves as Chairman of CARING - The Centre for Advanced Research in Imaging, Neuroscience and Genomics - which is Mahajan Imaging's research division. He is also the President of the Healthcare Federation of India. He did his MBBS from Maulana Azad Medical College, Delhi, M.D. in Radiology from PGI, Chandigarh and Fellowship in MRI from the MD Anderson Cancer Institute, Houston.

Dr. Vidur Mahajan
CEO, CARPL.AI

Dr. Vidur Mahajan is the Chief Executive Officer of CARPL.ai – the world's first end-to-end platform for testing and deployment of medical imaging AI solutions. CARPL works with more than 60 partners across the world spanning leading research groups in academia, industry and startups. In the past, he ran Mahajan Imaging, India's leading Radiology chain and has published more than 120 academic and conference papers in the field of AI and imaging. He has done an MBA with dual majors in finance and healthcare management from the Wharton School of Business and studied medicine from Sion Hospital, Mumbai.

PET/MR in the assessment of non-ischemic heart disease

Haiyan Wang[a#], Vidya Sridhar[b#], Qing Wan[a], Xing Chen[a], Zhiwen You[a], Zheng Zhang[b], Jianmin Yuan[b], Lingzhi Hu[b], Jun Zhao[a]
[a]Department of Nuclear Medicine, Shanghai East Hospital, Tongji University School of Medicine, 200120
[b]UIH America, Inc., Houston, TX, USA
[#]Contributed equally to this work

Abbreviations:

CMR – cardiac MR; LGE – late gadolinium enhancement; PET – positron emission tomography; MR – magnetic resonance; CT – computed tomography; FLASH – fast low angle shot

1. Introduction

PET/MR has been utilized as an important medical imaging technology in clinical radiology for more than a decade. The introduction of the integrated PET and MR modalities has made it possible to simultaneously acquire high-resolution MR images with excellent soft tissue contrast [1-2] with metabolic PET images while minimizing ionizing radiation exposure to the patients. Furthermore, advances in improved attenuation correction [3-7] and MR triggered motion correction [8-11] have led to improved image quality, making PET/MR a preferred imaging modality [12].

Once such clinical application where PET/MR is particularly advantageous and shows potential for innovation is the assessment of non-ischemic cardiac disease [13]. Cardiac PET [14-15] allows for the assessment of cardiac viability or perfusion using different tracers. With evolving advanced MR imaging sequences, anatomic and functional analysis of the heart and large vessels has manifested in the form of high-definition cine sequences providing dynamic visualization of the heart and vascular structures. First-pass imaging of contrast medium transit through the myocardium has also been shown to depict stress-induced alteration in myocardial blood flow, differentiating between normal and hypo-perfused myocardium [16]. The accuracy of PET for the measurement of unmatched regions of myocardial perfusion, biomarkers and myocardial viability has further contributed to the increasing scope of applications for PET/MR imaging.

Of the different cardiac applications of PET/MR, the detection of presence and extent of myocardial fibrosis is one of relevance in various cardiac diseases. Both the PET and MR modalities in such cases can not only quantify the fibrosis, but also offer insight into early detection and prognostication of such underlying conditions. The aim of this article is to review the existing technologies and clinical examples of PET/MR imaging in the evaluation of four main non-ischemic causes of myocardial fibrosis, namely non-ischemic cardiomyopathies, cardiac amyloidosis, myocarditis and heart failure. All cardiac PET/MR studies were performed on a United Imaging Healthcare's uPMR® 790 system (United Imaging Healthcare, Shanghai, China).

2. Technical review of PET/MR technology

2.1 PET radiotracers

While ^{82}Rb-RbCl, ^{13}N-NH_3.H_2O and ^{15}O-H_2O are the common radiotracers utilized in PET perfusion, there have been newer PET imaging agents being studied for various cardiac applications. Table 1 summarizes these novel cardiac PET imaging radiotracers, and their target disease processes.

Table 1. summary of novel PET radiotracers in evaluation of cardiac disease.

Target disease process	Cardiac PET radiotracers
Perfusion	^{13}N-NH_3, H_2O, ^{82}Rb, ^{15}O-H_2O, ^{18}F-flurpiridaz
Myocardial sympathetic nerve activity	^{11}C-hydroxyephedrine, ^{18}F-LMI1195
αvβ3 and αvβ5 integrins in angiogenesis or post myocardial infarction reperfusion	^{18}F-Fluciclatide
Cardiac amyloid	^{11}C-PIB, ^{18}F-florbetapir, ^{18}F-flutemetamol, ^{18}F-florbetaben
Fibrosis	^{68}Ga-FAPI, ^{18}F-FAPI
Atherosclerotic microcalcification	^{18}F-NaF
Tissue hypoxia	^{18}F-MISO, ^{18}F-HX4, ^{64}Cu-ATSM, ^{64}Cu-CTS
Angiogenesis	^{68}Ga-NOTA-RGD, ^{18}F-galacto-RGD
Macrophage-dependent inflammation	^{68}Ga-pentixafor, ^{64}Cu-DOTATATE, ^{68}Ga-DOTATATE, ^{89}Zr-DNP

2.2 CMR sequence technology

Table 2 summarizes the commonly used MRI sequences in the anatomic, functional, and biochemical characterization of myocardial tissue. As described in the applications below, these sequences provide information on early and late stages of various non-ischemic conditions [17].

Table 2. summary of commonly used sequences in the assessment of myocardial tissue and the relevant applications or findings.

Specific CMR sequence	Relevant application/finding
CINE T1W	Function, anatomical details, fat
Black Blood T2W	Anatomical details, edema
T1 mapping	Fibrotic areas (regional or diffuse), amyloidosis, fat
T2/T2* mapping	Edema, iron
ECV mapping	Fibrotic areas (regional or diffuse), amyloidosis
Late gadolinium enhancement	Fibrotic areas (regional fibrosis), viability

2.3 PET/MR cardiac image registration

The main challenge for cardiac PET in clinical practice is the compensation of physiologic motion, such as respiratory and cardiac motion, for which a few methods have been developed to overcome the problem [18-20] including a two-stage cardiac PET and LGE co-registration method (Figure 1) [21].

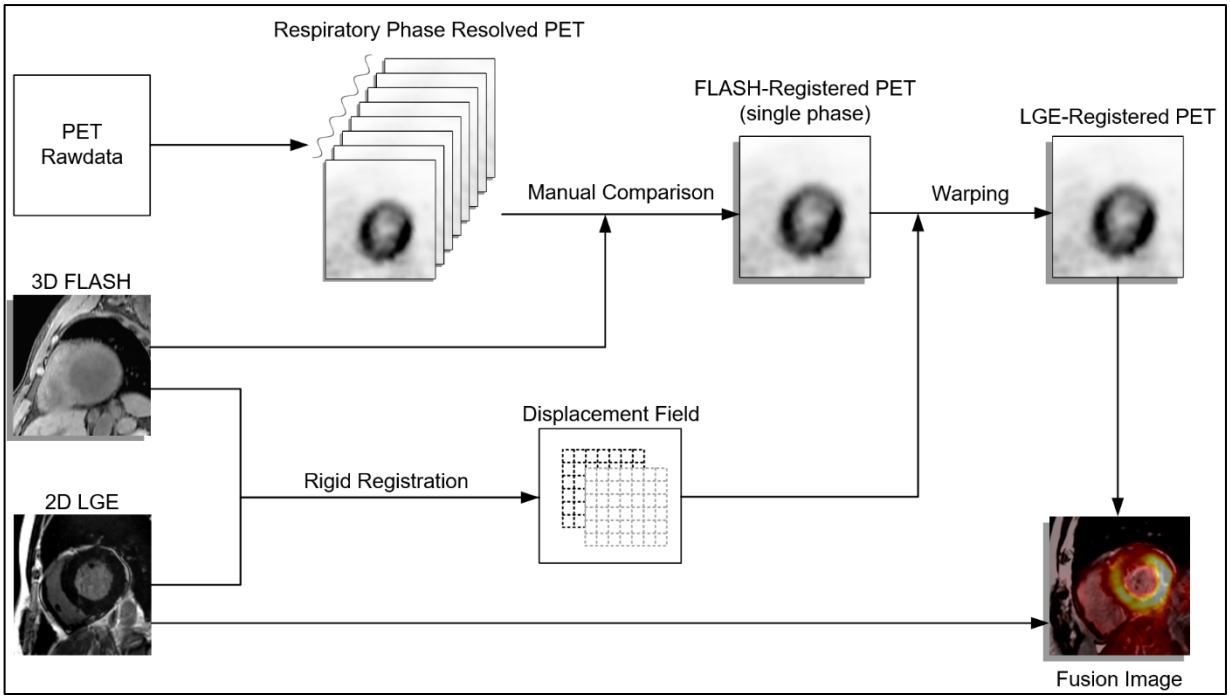

Figure 1. Two-stage cardiac PET and MR LGE co-registration method.

Figure 1 is an illustration of image co-registration of LGE and PET with two-stage registration. This comprises of four stages. The first is binning of list-mode PET data into eight respiratory bins based on respiratory signal. The second step is comparison of FLASH and respiratory phase resolved PET to choose one FLASH-registered phase. Thirdly, rigid registration is manually performed between 3D FLASH and 2D LGE and get the 3D displacement field. Finally, the displacement field is used to warp the images and generate LGE-registered PET.

3. Non-ischemic cardiomyopathies – hypertrophic and dilated cardiomyopathies

Non-ischemic cardiomyopathies are defined as diseases of the myocardium associated with mechanical or electrical dysfunction exhibiting inappropriate ventricular hypertrophy or dilatation and include dilated cardiomyopathy (DCM) and hypertrophic cardiomyopathy (HCM). Causes include primary and secondary causes, encompassing genetic and acquired factors. CMR remains the main diagnostic tool for distinguishing many of these diseases; however, for certain diseases, PET can add valuable information by characterizing metabolic activity in the myocardial region.

LGE sequence can detect focal myocardial fibrosis and provide significant risk stratification for sudden cardiac death, mortality, and heart failure hospitalization in patients with non-ischemic cardiomyopathy [22]. The combination of metabolic information from ^{18}F-fluoro-deoxy-glucose PET (^{18}F-FDG PET) and LGE can also provide additional evidence for the evaluation of myocardial viability and inflammation in non-ischemic cardiomyopathies.

Case Example

A 67-year-old male patient with known dilated cardiomyopathy (DCM) was evaluated for myocardial viability assessment. ^{18}F-FDG PET/MR was performed at an uptake time of 60 minutes. Figure 2 shows short axial LGE images (A, C) and LGE/PET fusion images (B, D) of two LGE-enhanced lesions.

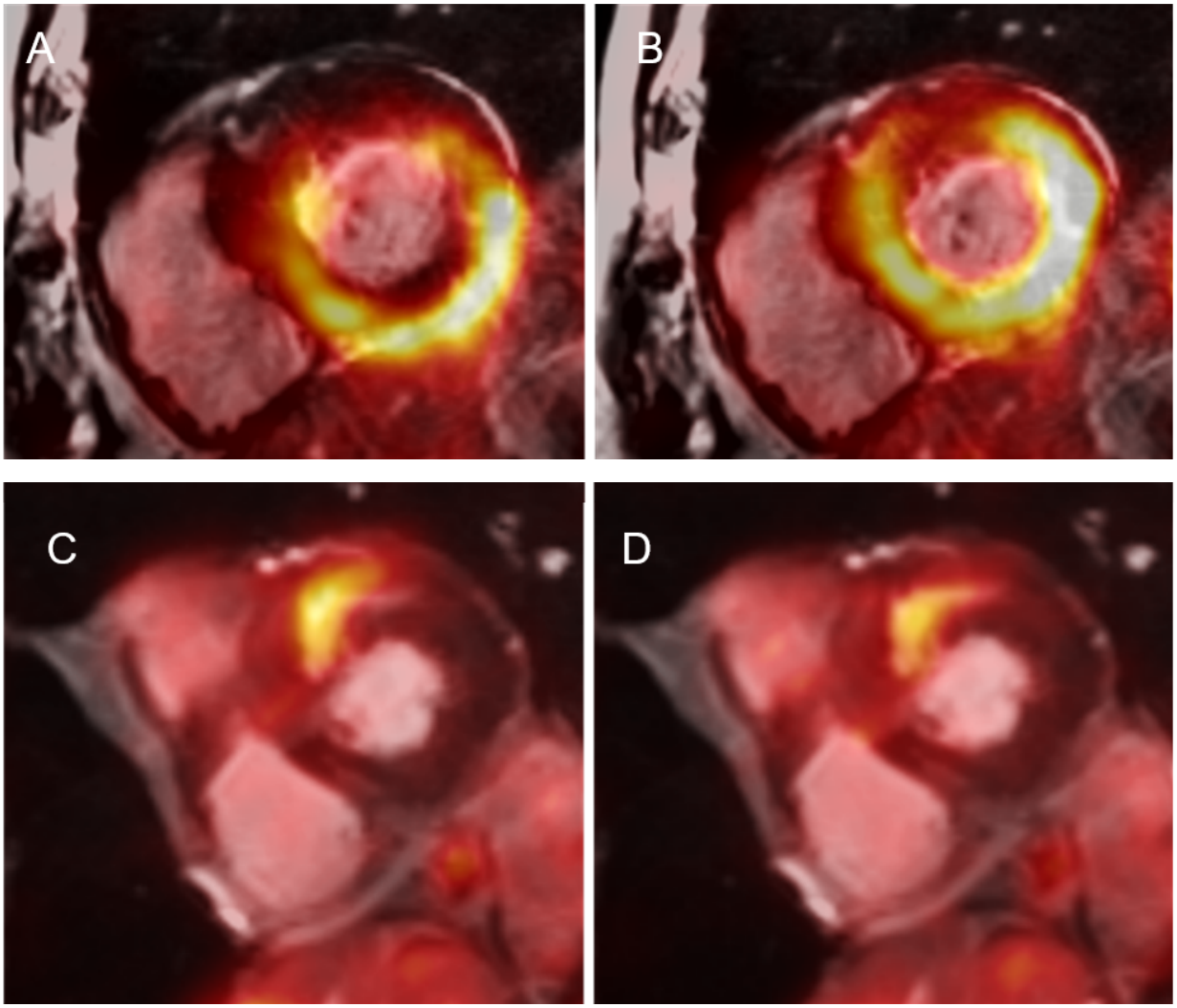

Figure 2. PET/MR images of a patient with dilated cardiomyopathy (DCM). Short axial LGE images (A, C) and LGE/PET fusion images (B, D) show two LGE-enhanced lesions.

4. Cardiac amyloidosis (Restrictive cardiomyopathy)

Cardiac amyloidosis is a myocardial condition characterized by extracellular amyloid infiltration throughout the heart and is the leading cause of morbidity and mortality in systemic amyloidosis. The two types of amyloid that commonly infiltrate the heart include acquired monoclonal immunoglobulin light chain amyloid (AL) and transthyretin-related (familial and wild-type/senile) amyloid (ATTR). Differentiation of the two types is important because they have different prognoses and are amenable to different management strategies.

Early cardiac amyloidosis is challenging to diagnose and may only present with the features of right-sided congestive heart failure in advanced disease. While endocardial biopsy is considered the gold standard for diagnosis of cardiac amyloidosis, it is not commonly used due to its high rate of complications. Other non-invasive diagnostic methods used include electrocardiography, echocardiography, CMR and nuclear medicine imaging.

Steady state free precession cine sequences in CMR are used to assess cardiac function and structure, while LGE imaging can diagnose cardiac amyloidosis. Although CMR is sensitive and specific for cardiac amyloidosis, CMR classically cannot differentiate the subtypes of cardiac amyloidosis and PET imaging is useful in this regard. However, recent studies have shown that AL frequently manifests as diffuse subendocardial LGE, while ATTR typically manifests as transmural LGE. MR parametric

mapping has also shown that the T1 value of ATTR patients was significantly higher than that of hypertrophic cardiomyopathy and normal controls, but not as high as that of AL patients, further helping in the characterization of cardiac amyloidosis.

Nuclear medicine imaging plays an important role in the diagnosis, classification, prognostic evaluation, and therapeutic response monitoring of myocardial amyloidosis [23-24]. Studies using ^{18}F-NaF PET imaging [25-26] have shown that the myocardial uptake in ATTR patients is higher than AL patients and control groups, and the myocardial radioactivity uptake was consistent with the extent of damaged myocardium as seen on MR LGE. Similar studies have shown differences in uptake using ^{18}F-florbetapir and ^{18}F-florbetaben imaging in both ATTR and AL patients [27-28]. Hence, an important benefit of combining PET with CMR is the combination of quantifiable parameters to potentially aid prognosis and track disease progression.

Case Example

A 65-year-old female with underlying history of amyloidosis presented with chest congestion and dyspnea. Echocardiography revealed pericardial effusion, pleural effusion, interventricular septum and left ventricular wall thickening. Gadolinium contrast enhanced CMR and dynamic cardiac PET imaging (Figure 3) was performed immediately after injection of ^{18}F-florbetapir (AV45). CMR imaging revealed LV hypertrophy and impaired systolic function (LVEF=22%). LGE imaging (B, short axis view; E, 4 chamber view) demonstrated transmural late enhancement in the left ventricle. Delayed whole body maximum intensity PET (A, 90min post-injection) demonstrated elevated AV45 uptake in heart (SUVmax=8.86), lung (SUVmax=2.69) and spleen (SUVmax=7.75), compared to moderate uptake in the liver (SUVmax=3.09) caused by hepatobiliary excretion of the drug.

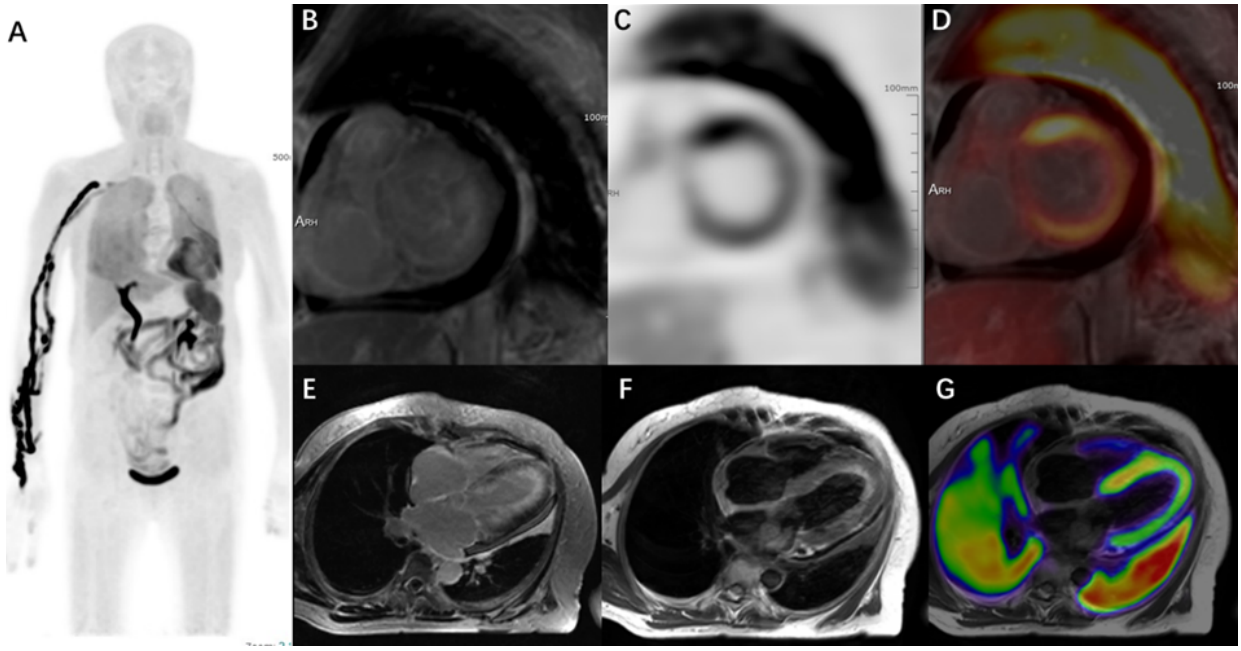

Figure 3. PET/MR images of a patient with cardiac amyloidosis.

5. Myocarditis

Myocarditis is an inflammatory disease of the myocardium that can be caused by various conditions including viral infections, autoimmune reactions, toxin exposure, drugs, and idiopathic factors [29].The condition has a predilection in young subjects, especially males [30]. Clinical symptoms are highly variable, making diagnosis challenging. In addition, investigations such as laboratory biomarkers (such as troponin, C-reactive protein), electrocardiography and echocardiography are nonspecific. Definite diagnosis relies on endomyocardial biopsy but this is not performed

frequently in practice due to its risk of complications.

Pathophysiological processes linked to myocardial inflammation, including myocardial hyperemia and edema in the early stages, and fibrosis or scarring in the later stages, as well as associated processes such as pericardial effusion and global or regional wall motion abnormalities, can be assessed using MR imaging [31]. The Lake Louise CMR criteria often used in assessment of myocarditis encompasses the three aspects of myocardial inflammation namely edema, hyperemia and necrosis and/or fibrosis. In addition to these, multiparametric T1 and T2 mapping can also be used for tissue characterization.

The use of ^{18}F-FDG PET [32] allows accurate assessment of the extent and grade of both active and healed inflammatory processes. FDG uptake in myocarditis could be focal, diffuse, or 'focal on diffuse' depending on the underlying disease [33]. Thus, ^{18}F-FDG PET/MR imaging has already been shown to be highly clinically relevant in patients with suspicion of myocarditis, with increasing evidence that ^{18}F-FDG PET/MR imaging can diagnose, grade, and monitor myocarditis [34-36], with a clinical sensitivity of 74% and a specificity of 97% [37]. Notably, it has also been shown that patients with biopsy-proven myocarditis have had abnormal uptake noted on ^{18}F-FDG PET imaging, while having no corresponding evidence of myocardial damage on MR imaging, allowing for early diagnosis of myocarditis. Performing FDG PET imaging after treatment could also show interval improvement or resolution of the abnormal FDG uptake, highlighting further potential application in monitoring treatment response [38].

Case Example

A 24-year-old male presented with signs and symptoms suggestive of myocarditis. Gadolinium contrast enhanced CMR and dynamic cardiac PET imaging starting immediately after injection of ^{18}F-FDG (Figure 4). CMR imaging showed normal anatomy of the atrioventricular chambers with normal left ventricular motion and function (LVEF 70%). Delayed enhancement imaging showed blurred patchy, slightly high signal and line-like high signal in the basal segment of the anterior and inferior lateral walls of the left ventricle, and no obvious abnormal enhancement was found in the remaining ventricular wall segments. Myocardial metabolic imaging revealed increased radioactive uptake in each segment of the left ventricle.

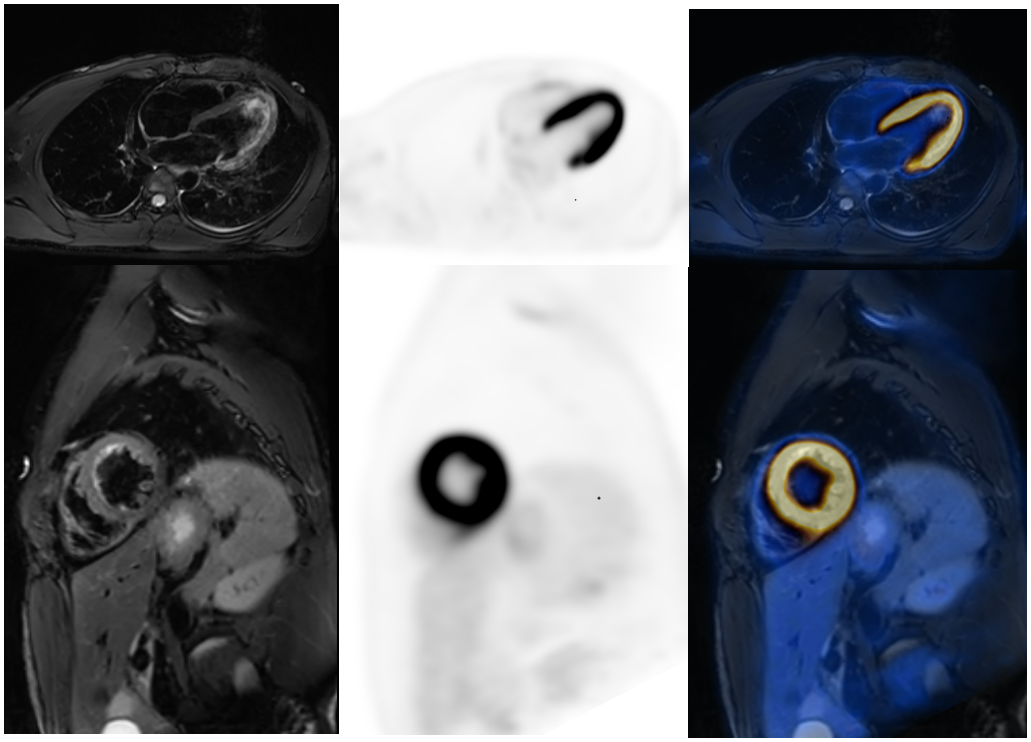

Figure 4. PET/MR images of a patient with myocarditis.

6. Heart Failure

Heart Failure is defined as a complex clinical syndrome resulting from any structural or functional cardiac condition that impairs the ability of the ventricle to fill or eject blood [39]. Several criteria have been proposed to diagnose heart failure such as the Framingham criteria [40]. Echocardiography is frequently used to provide information on the ventricular ejection fraction as well as the underlying cause of heart failure. Single-photon-emission computed tomography (SPECT) remains the most common imaging modality used for myocardial perfusion imaging in heart failure, but it has significant disadvantages such as limited resolution and involves the use of ionizing radiation. Due to these factors, there has been increasing use of myocardial perfusion imaging using PET to quantify myocardial blood flow using tracer kinetics, for which the sensitivity and specificity is thought to be approximately 90% [41-44]. It is also notable that a meta-analysis of single and multi-center studies confirmed the excellent sensitivity and specificity of CMR to quantify myocardial perfusion at rest and during stress [43-44][4]. There is report showing that MR perfusion imaging is compared to that of SPECT and showed significant agreement in results with PET perfusion [45-46][-46]. The combination of PET and MR imaging allows for direct comparison of myocardial blood flow under resting and stress conditions. The assessment of myocardial viability is a standard approach utilized in patients with advanced coronary disease or who are in early or advanced states of heart failure. Identification of glucose utilization in viable myocardium by PET is made possible by FDG uptake demonstrated in myocardial segments with decreased perfusion. Based on meta-analyses, ^{18}F-FDG PET predicts functional recovery after revascularization with a sensitivity of 92% and a specificity of 63% [47-48]. LGE also allows the identification of scarred myocardium as signal enhanced areas.

Case Example

Figure 5 shows an example of ^{68}Ga-FAPI and FDG PET imaging of a 77-year-old male with history of coronary artery disease, that presented with acute pulmonary embolism. Echocardiography showed severe pulmonary hypertension (pulmonary artery systolic blood pressure elevated at 99mm Hg), right atrioventricular enlargement, as well as decreased right ventricular motion and function, with normal left ventricular systolic function. Pulmonary angiography and balloon angioplasty was performed and revealed multiple filling defects in the bilateral pulmonary arteries with poor distal perfusion. Gadolinium contrast enhanced CMR and dynamic cardiac PET imaging starting immediately after injection of ^{68}Ga-FAPI was performed (Figure 5). Gadolinium contrast enhanced CMR and dynamic cardiac PET imaging starting immediately after injection of FDG was performed the following day. CMR showed right atrial and ventricular enlargement and hypertrophy as seen in the 4-chamber and short axis views. ^{68}Ga-FAPI PET/MR imaging showed diffusely increased FAPI uptake in the right atrial muscle wall and increased scattered patchy FAPI uptake in the right ventricular muscle wall. ^{18}F-FDG PET/MR fusion images demonstrated that radioactivity uptake in the right ventricle and atrium were increased, more so in the right ventricle.

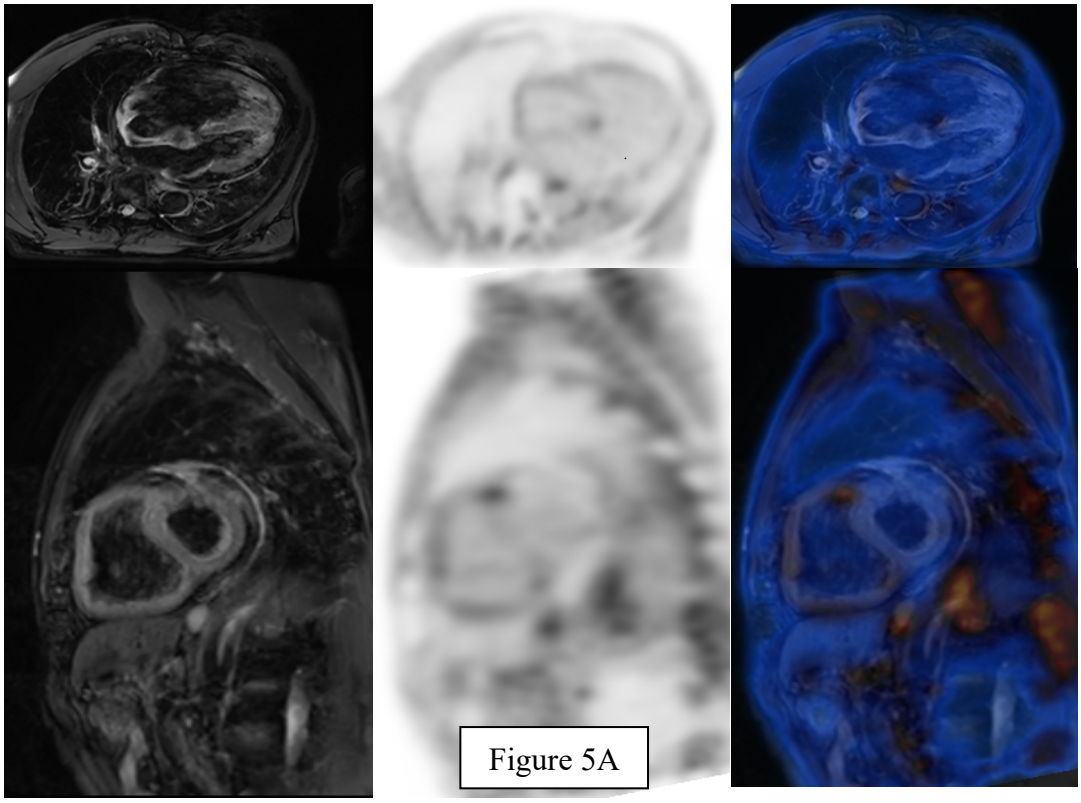

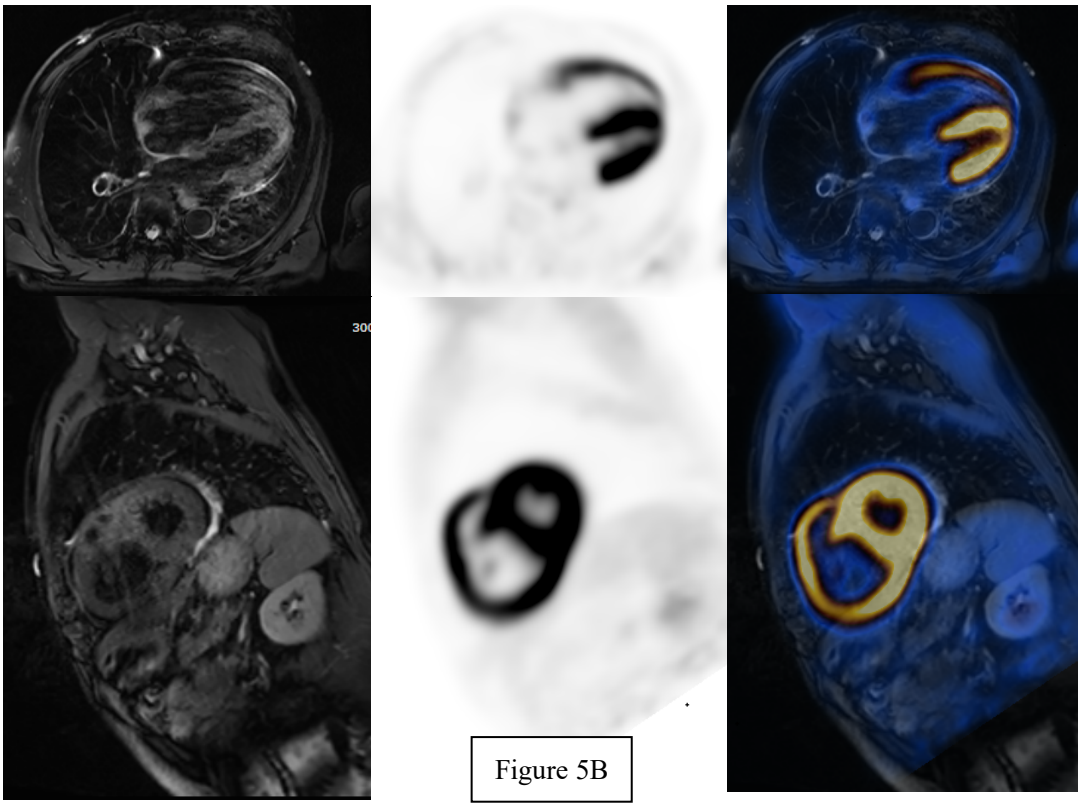

Figure 5. ^{68}Ga-FAPI and FDG PET/MR images of a patient with heart failure and extensive fibrosis.

7. Conclusion and Future Directions

Currently, there are three vendors providing PET/MR integrated scanners worldwide: Siemens Biograph mMR (2010), GE SIGNA (2013) and United Imaging Healthcare's **uPMR**® 790 (2017). The hybrid MR and PET imaging has demonstrated its clinical advantage in many cardiac applications and is increasing used in clinical routine imaging. Some disadvantages to this advancing technology exist, including the high cost of PET/MR exams and the complex technology requiring significant training in both PET and MR technology for technologists to run the scans. In addition, several cardiac devices including pacemakers, implantable cardioverter-defibrillators, and mechanical heart valves, as well as some coronary stents, are contraindications to PET/MR scans. However, with further improvements in PET/MR imaging technology and more studies evaluating the use of new imaging tracers, there is an exciting potential to harness the advantages of PET/MR in evaluating different cardiac diseases. Prospective single-center and multi-center study with large sample size are urgently needed to further explore the indications and new application area of integrated PET/MR.

8. Image/Figure Courtesy

All images are the courtesy of Shanghai East Hospital, Tongji University School of Medicine, Shanghai, China.

9. References

1. Fürst S, Grimm R, Hong I,et al. Motion correction strategies for integrated PET/MR. J Nucl Med. 2015;56:261–269.

2. Judenhofer MS, Wehrl HF, Newport DF, et al. Simultaneous PET-MRI: a new approach for functional and morphological. imaging. Nat Med. 2008;14:459–465.

3. A. P. Leynes et al., Hybrid ZTE/dixon MR-based attenuation correction for quantitative uptake estimation of pelvic lesions in PET/MRI, Med. Phys., vol. 44, no. 3, pp. 902–913, 2017.

4. G. Delso, D. Gillett, W. Bashari, T. Matys, I. Mendichovszky, and M. Gurnell, Clinical evaluation of C-11-met-avid pituitary lesions. using a ZTE-based AC method, IEEE Trans. Radiat. Plasma Med. Sci., vol. 3, no. 4, pp. 504–508, Jul. 2019.

5. P. Blanc-Durand et al., Attenuation correction using 3D deep convolutional neural network for brain 18F-FDG PET/MR: Comparison with Atlas, ZTE and CT based attenuation correction, PLoS ONE, vol. 14, Oct. 2019, Art. no. e0223141.

6. A. Rezaei, G. Schramm, S. M. A. Willekens, G. Delso, K. Van Laere, and J. A. Nuyts, Quantitative evaluation of joint activity and attenuation reconstruction in TOF PET/MR brain imaging, J. Nucl. Med., vol. 60, no. 1, pp. 1649–1655, 2019.

7. M. Cencini, M. Tosetti, and G. Buonincontri, An aristotelian view on MR-based attenuation correction (ARISTOMRAC): Combining the four elements, IEEE Trans. Radiat. Plasma Med. Sci., vol. 3, no. 4, pp. 491–497, Jul. 2019.

8. K. T. Chen et al., MR-assisted PET motion correction in simultaneous PET/MRI studies of dementia subjects, J. Magn. Reson. Imag., vol. 48, no. 5, pp. 1288–1296, 2018.

9. M. G. Spangler-Bickell et al., Rigid motion correction for brain PET/MR imaging using optical tracking, IEEE Trans. Radiat. Plasma Med. Sci., vol. 3, no. 4, pp. 498–503, Jul. 2019.

10. P. M. Robson et al., Correction of respiratory and cardiac motion in cardiac PET/MR using MR-based motion modeling, Phys. Med. Biol., vol. 63, no. 22, 2018, Art. no. 225011.

11. Smith R. L., Rahni, A. A. A. J. Jones, and K. Wells, A Kalman based approach with EM optimization for respiratory motion modeling in medical imaging, IEEE Trans. Radiat. Plasma Med. Sci., vol. 3, no. 4, pp. 410–420, Jul. 2019.

12. Ehman, E.C., Johnson, G.B.. Villanueva-Meyer, J.E., Cha, S.; Leynes, A.P.; Larson, P.E.Z.; Hope, T.A. PET/MRI: Where might it replace PET/CT? J. Magn. Reson. Imaging 2017, 46, 1247–1262.

13. Nazir MS, Ismail TF, Reyes E, Chiribiri A, Kaufmann PA, Plein S. Hybrid positron emission tomography-magnetic resonance of the heart: current state of the art and future applications. Eur Heart J Cardiovasc imaging. 2018;19:962–74.

14. Bengel FM, Higuchi T, Javadi MS, Lautamäki R. Cardiac positron emission tomography. J Am Coll Cardiol. 2009;54:1–15.

15. Schindler TH, Schelbert HR, Quercioli A, Dilsizian V. Cardiac PET imaging for the detection and monitoring of coronary artery disease and microvascular health. JACC Cardiovasc Imaging. 2010;3:623–640.

16. Schwitter J, Wacker CM, van Rossum AC, et al. MR-IMPACT: comparison of perfusion-cardiac magnetic resonance with single-photon emission computed tomography for the detection of coronary artery disease in a multicentre, multivendor, randomized trial. Eur Heart J. 2008;29:480–489.

17. Karamitsos TD, Arvanitaki A, Karvounis H, Neubauer S, Ferreira VM. Myocardial Tissue Characterization and Fibrosis by Imaging. JACC Cardiovasc Imaging. 2020 May;13(5):1221-1234.

18.Chander A, Brenner M, Lautamäki R, Voicu C, Merrill J, Be ngel FM. Comparison of measures of left ventricular function from electrocardiographically gated 82Rb PET with contrast-enhanced CT ventriculography: a hybrid PET/CT analysis. J Nucl Med. 2008;49:1643–1650.

19. Teräs M, Kokki T, Durand-Schaefer N, et al. Dual-gated cardiac PET: clinical feasibility study. Eur J Nucl Med Mol Imaging. 2010;37:505–516.

20. Kolbitsch C, Ahlman MA, Davies-Venn C, Evers R, Hansen M, Peressutti D, Marsden P, Kellman P, Bluemke DA, Schaeffter T. Cardiac and Respiratory Motion Correction for Simultaneous Cardiac PET/MR. J Nucl Med. 2017 May;58(5):846-852.

21. Zhang Z, Chen X, Wan Q, Wang H, Qi N, You Z, Yuan J, Hu L, Sun H, Wang Z, Hu C, Zhao J. A two-stage cardiac PET and late gadolinium enhancement MRI co-registration method for improved assessment of non-ischemic cardiomyopathies using integrated PET/MR. Eur J Nucl Med Mol Imaging. 2022 Jun;49(7):2199-2208.

22. Jagsi R, Moran JM, Kessler ML, Marsh RB, Balter JM, Pierce LJ. Respiratory motion of the heart and positional reproducibility under active breathing control. Int J Radiation Oncol Biol Phys. 2007;68:253–8.

23. Ren Jingyun, He Shan, Tian Zhuang, et al. Application progress of nuclear medicine imaging in the diagnosis of myocardial amyloidosis [J]. Chinese Journal of Nuclear Medicine and Molecular Imaging, 2019, 39(12): 759-762.

24. Ren JY, He S, Tian Z, et al. Application of nuclear medical imaging in the diagnosis of myocardial amyloidosis[J]. Chin J Nucl Med Mol Imaging, 2019 , 39(12): 759-762.

25. Morgenstern R, Yeh R, Castano A, et al. ^{18}Fluorine sodium fluoride positron emission tomography, a potential biomarker of transthyretin cardiac amyloidosis[J]. J Nucl Cardiol, 2018, 25(5): 1559-1567.

26. Trivieri MG, Dweck MR, Abgral R, et al. ^{18}F-Sodium fluoride PET/MR for the assessment of cardiac amyloidosis[J]. J Am Coll Cardiol, 2016, 68(24): 2712-2714.

27. Dorbala S, Vangala D, Semer J, et al. Imaging cardiac amyloidosis: a pilot study using ^{18} F-florbetapir positron emission tomography[J]. Eur J Nucl Med Mol Imaging, 2014, 41(9): 1652- 1662.

28. Baratto L, Park SY, Hatami N, et al. ^{18}F-florbetaben whole-body PET/MRI for evaluation of systemic amyloid deposition[J]. EJNMMI Res, 2018, 8(1): 66.

29. Caforio AL, Pankuweit S, Arbustini E, Basso C, Gimeno-Blanes J, Felix SB, et al. Current state of knowledge on aetiology, diagnosis, management, and therapy of myocarditis: a position statement of the European Society of CardiologyWorking Group on Myocardial and Pericardial Diseases. Eur Heart J. 2013;34:2636–48.

30. Caforio ALP, Malipiero G,Marcolongo R, Iliceto S.Myocarditis: a clinical overview. Curr Cardiol Rep. 2017;19:63–74.

31. Heusch P, Nensa F, Heusch G. Is MRI really the gold standard for the quantification of salvage from myocardial infarction? Circ Res 2015;117:222–4.

32. Erba PA, Sollini M, Lazzeri E, et al. FDG-PET in cardiac infections. Semin Nucl Med 2013;43:377–95.

33. Ozawa K, Funabashi N, DaimonM, Takaoka H, Takano H, Uehara M, et al. Determination of optimum periods between onset of suspected acute myocarditis and 18F-fluorodeoxyglucose positron emission tomography in the diagnosis of inflammatory left ventricular myocardium. Int J Cardiol. 2013;169:196–200.

34. Nensa F, Poeppel TD, Krings P, et al. Multiparametric assessment of myocarditis using simultaneous positron emission tomography/magnetic resonance imaging. Eur Heart J 2014;35:2173.

35. von Olshausen G, Hyafil F, Langwieser N, et al. Detection of acute inflammatory myocarditis in Epstein Barr virus infection using hybrid ^{18}F-fluorodeoxyglucose-positron emission tomography/magnetic resonance imaging. Circulation 2014;130:925–6.

36. Piriou N, Sassier J, Pallardy A, et al. Utility of cardiac FDG-PET imaging coupled to magnetic resonance for the management of an acutemyocarditis with non-informative endomyocardial biopsy. Eur Heart J Cardiovasc Imaging 2015;16:574.

37. Nensa F, Kloth J, Tezgah E, et al. Feasibility of FDGPET in myocarditis: comparison to CMR using integrated PET/MRI. J Nucl Cardiol 2018;25:785–94.

38. Moriwaki K, Dohi K, Omori T, Tanimura M, Sugiura E, Nakamori S, et al. A survival case of fulminant right-side dominant eosinophilic myocarditis. Int Heart J. 2017;58:459–62.

39. Jessup M, Abraham WT, Casey DE, Feldman AM, Francis GS, Ganiats TG, Konstam MA, Mancini DM, Rahko PS, Silver MA, Stevenson LW, Yancy CW. 2009 focused update: ACCF/AHA Guidelines for the Diagnosis and Management of Heart Failure in Adults: a report of the American College of Cardiology Foundation/American Heart Association Task Force on Practice Guidelines: developed in collaboration with the International Society for Heart and Lung Transplantation. Circulation. 2009; 119:1977–2016.

40. McKee PA, Castelli WP, McNamara PM, Kannel WB. The natural history of congestive heart failure: the Framingham study.N Engl J Med. 1971; 285:1441–1446.

41. Parker MW, Iskandar A, Limone B, Perugini A, Kim H, Jones C, Calamari B, Coleman CI, Heller GV. Diagnostic accuracy of cardiac positron emission tomography versus single photon emission computed tomography for coronary artery disease: a bivariate meta-analysis. Circ Cardiovasc Imaging. 2012;5:700–7.

42. Klocke FJ, Baird MG, Lorell BH, et al. ACC/AHA/ASNC guidelines for the clinical use of cardiac radionuclide imaging–executive summary: a report of the American College of Cardiology/ American Heart Association task force on practice guidelines (ACC/AHA/ASNC Committee to revise the 1995 guidelines for the clinical use of cardiac radionuclide imaging). J Am Coll Cardiol. 2003;42:1318–33.

43. Schwitter J, Nanz D, Kneifel S, Bertschinger K, Büchi M, Knüsel PR, Marincek B, Lüscher TF, von Schulthess GK. Assessment of myocardial perfusion in coronary artery disease by magnetic resonance: a comparison with positron emission tomography and coronary angiography. Circulation. 2001;103:2230–5.

44. Nandalur KR, Dwamena BA, Choudhri AF, Nandalur MR, Carlos RC. Diagnostic performance of stress cardiac magnetic resonance imaging in the detection of coronary artery disease: ameta-analysis. J Am Coll Cardiol. 2007;50:1343–53.

45. Greenwood JP, Maredia N, Younger JF, et al. Cardiovascular magnetic resonance and single-photon emission computed tomography for diagnosis of coronary heart disease (CE-MARC): a prospective trial. Lancet. 2012;379:453–60.

46. Morton G, Chiribiri A, Ishida M, et al. Quantification of absolute myocardial perfusion in patients with coronary artery disease: comparison between cardiovascular magnetic resonance and positron emission tomography. J Am Coll Cardiol. 2012;60:1546–55.

47. Tillisch J, Brunken R, Marshall R, Schwaiger M, Mandelkern M, Phelps M, Schelbert H. Reversibility of cardiac wall-motion abnormalities predicted by positron tomography. N Engl J Med. 1986;314:884–8.

48. Schinkel AFL, Poldermans D, Elhendy A, Bax JJ. Assessment of myocardial viability in patients with heart failure. J Nucl Med. 2007;48:1135–46.

Author Biography

Dr. Jun Zhao
Director of Nuclear Medicine
and Molecular Imaging
Shanghai East Hospital,
Tongji University
Shanghai, China

Dr. Jun Zhao is the director of nuclear medicine and molecular imaging at Shanghai East Hospital affiliated with Tongji University. Dr. Zhao is a pioneer in PET/CT and PET/MR imaging in China. Dr. Zhao is the executive editor for Journal of Chinese Nuclear Medicine and Molecular Imaging, International Radiology and Nuclear Medicine. Dr. Zhao also serves as the vice president for Shanghai Society of Nuclear Medicine and Molecular Imaging.

Mercy Radiology: our molecular imaging goals and journey

Remy Lim[a,*], BHB, MBChB
[a]Department of Radiology, Mercy Radiology, New Zealand

1. Background

Aotearoa New Zealand, an island nation in the middle of the Pacific Ocean, is split into two main land masses, with a collective land area equivalent to that of the state of Colorado. New Zealand's land mass, however, stretches in a north-south orientation, equivalent to the distance from Pennsylvania to Florida. The country is also sparsely populated relative to its land area, with a population of only 5 million and only 50% of the population residing in one of six major urban centres[1,2].

In total, there are only six PET/CT scanners in New Zealand, of which five are located in three major urban centres on the North Island, and one is a solitary PET/CT scanner on the South Island. The largest city in New Zealand, Auckland, in the upper North Island (population of 1.5 million), has three of the six PET/CT scanners[3].

At Mercy Radiology, a private radiology group with a long history of excellence in molecular imaging, we operate two of the three PET/CT scanners in Auckland. We are also proud to have the only New Zealand's PET/CT facilities with digital PET scanners: United Imaging's uMI® 550 and uMI® 780.

To understand our molecular imaging journey, it is useful to start with the New Zealand health landscape. Healthcare is delivered to New Zealanders in a two-tier system: the public health sector, which is funded by taxpayers providing universal health coverage, and the private sector.

Public health sector services include acute and elective inpatient care, outpatient, mental health and long-term care. Imaging needs are provided by in-hospital radiology departments and outpatient centres.

Total New Zealand government health spending as percentage of GDP is just under 10% in 2019 and is expected to have been increased in the last 2 years[4].

The private sector on the other hand, is made up of smaller outpatient specialists' offices, smaller private hospitals and private radiology providers. Private sector work is funded by private insurance companies, self-funding patients or the New Zealand government by way of outsourced public hospital work. Treatments and associated imaging related to accidents, usually conducted in the private sector, are covered by a no-fault Accident Compensation Scheme (ACC).

All six PET/CT scanners in Aotearoa New Zealand are currently operated by private radiology groups. The New Zealand Ministry of Health determined several years ago that rather than providing for a PET/CT facility in one of the many public hospitals in the country, patients treated in the public sector would be outsourced to private PET providers for their PET/CT scans. Currently, provided that patient's disease status meets one of the numerous approved national criteria for a funded PET/CT scan, patients would be able to access a fully funded PET/CT scanner.

Despite a clear pathway allowing patients to access a PET/CT scan, with 760 scans per million of population, OECD Health Statistics (2) suggests an overall underutilisation of PET/CT scanners in Aotearoa New Zealand. Although the numbers are likely to be at least twice that once privately funded patients are taken into account, it remains much lower than Aotearoa New Zealand's neighbour, Australia, which performs 4,500 scans annually per million of population.

*Mercy Radiology New Zealand has a research agreement with United Imaging Healthcare. Dr. Remy Lim is a principal investigator on a research grant funded by United Imaging Healthcare.
[1]https://en.wikipedia.org/wiki/List_of_New_Zealand_urban_areas_by_population
[2]https://en.wikipedia.org/wiki/New_Zealand
[3]https://www.stuff.co.nz/national/health/300667942/new-mobile-cancer-scan-unit-hitting-the-road-to-help-ease-barriers-waittimes
[4]https://data.worldbank.org/indicator/SH.XPD.CHEX.GD.ZS?locations=NZ
[5]https://humanhealth.iaea.org/HHW/DBStatistics/IMAGINE.html

Based on the IMAGINE database developed by the International Atomic Energy Agency (IAEA), the number of PET scanners in a high-income country such as New Zealand is expected to be 3.6 per million of population[5]. Based on this, New Zealand would be expected to have around 14 PET/CT scanners.

At Mercy Radiology we recognised that this underutilisation of PET/CT scanners is driven by two major constraints. First, being a sparsely populated country, there are geographical barriers to accessing a PET/CT facility. Rural New Zealanders are often expected to travel significant distances between their homes and the closest PET/CT facility. For instance, a patient who lives in the town of Gisborne, on the east coast of North Island will need travel 380km to access a PET/CT facility in Hamilton, a five-hour journey on the road. As a result of this geographical barrier, New Zealanders who live in the regions or remote areas are more likely to encounter obstacles to early detection of and treatment for their cancer.

Secondly, the collective capacity of the current fleet of PET/CT scanners scattered throughout the country is woefully inadequate to service the demand for PET/CT scans. An appointment for a PET/CT scan can be up to 10 to 15 business days wait time.

2. Mercy Radiology goals and journey

In 2019, Mercy Radiology set two goals to address the chronic underutilisation and inequality in access to PET/CT scans in New Zealand.

Our first goal is capacity expansion. Having operated a solitary PET/CT scanner for the last 12 years, it was apparent that we had reached the limit of what we were able to achieve with our preexisting centre.

Our second goal is to improve accessibility. This applies for not only our patients who live in the greater Auckland region but also patients who live in the rural areas of New Zealand.

So why have we set these lofty goals for ourselves?

Simply put, we believe New Zealanders deserve the best oncological imaging available when they are diagnosed with cancer so that they can be optimally managed to achieve the best possible health outcomes.

An additional PET/CT scanner at a sister site remote to our preexisting facility is a logical solution to expand our capacity and to derisk our reliance on a solitary PET/CT scanner. A pre-requisite for the additional PET/CT scanner is that it must deliver improved image quality in less time than our current 10-year-old scanner.

From the outset, our evaluation team was convinced that a digital PET camera with increased sensitivity and superior signal-to-noise ratio compared to an analog scanner would be capable of fulfilling these criteria and future proof the installed base.

A second facility would shorten the period patients would have to wait for their examination from 10 working days to three to five days. A digital PET camera coupled with a longer axial field of view would translate to fewer bed positions and therefore a shortened PET acquisition time. This would improve patient comfort and experience and increase overall patient throughput.

A potential turnaround time of less than 24 hours would be facilitated by Mercy Radiology's team of trained PET/CT readers. Ultimately, this would allow our clinicians and oncologists to have a complete picture of patients' disease status and manage accordingly.

Just as importantly, we wanted to work with a vendor who would be receptive to our specific needs. Local engineering support and excellent applications support fulfilled all the critical elements needed to achieve our objectives.

There are many vendors with digital PET/CT offerings and excellent service. How did we end up with two of United Imaging's uMI PET/CT scanners?

First, there was good alignment of our objectives with United Imaging's mission of providing greater access to PET/CT. United Imaging's digital PET solution included other positive physical attributes, such as superior axial field of view and air-cooled systems.

Secondly, United Imaging's unique Software Upgrades for Life™ program speaks to their desire to ensure new innovations are available to all of their installed base. The program ensures all new systems have the same software and core technology. New upgrades are cascaded to their existing installed base.

Third, United Imaging's All In Configurations™ program means transparent costing without the need to navigate

[5]https://humanhealth.iaea.org/HHW/DBStatistics/IMAGINE.html

through multiple options which would typically increase the price of the scanner substantially beyond the starting base price.

Ultimately, it was the digital PET camera's superior image quality, further enhanced and optimised by United Imaging's advanced PET AI algorithm in the form of uAI HYPER DLR and uAI HYPER DPR, which cemented our decision to proceed with United Imaging's digital PET/CT scanners.

In the midst of the pandemic in 2020, we commissioned our sister PET/CT site 25 minutes north of our current facility. This new PET/CT site caters to the 600,000 Aucklanders who reside north of the Auckland Harbour Bridge and over 200,000 other patients in the northern province of Northland.

Converting a preexisting building which previously housed medical consultation rooms and an operating theatre into a PET/CT facility with multiple uptake rooms and a hot lab with New Zealand's strict quarantine rules in 2020 was no easy feat. Coupled with all the logistical difficulties of COVID restrictions and border closure in NZ, this was a project destined to be hampered by delays and logistical challenges.

United Imaging demonstrated their commitment to the project by ensuring the PET/CT system arrived into the country on schedule. Overseas-based installation engineers and applications support personnel underwent mandatory 2-week quarantine to be available at critical times during the commissioning phase. Happily, the facility was successfully delivered on time and on budget, with the first patient scanned in the latter half of 2020.

In 2021, we turned our attention to our flagship site, where we had been operating an analog PET/CT scanner for the last 12 years. We had outgrown the facility due to increased patient numbers and the introduction of a theranostics service line in 2018. We took the opportunity to create a dedicated therapy suite that doubles as an additional uptake room, having anticipated a decreased scan time necessitating more uptake rooms.

As our flagship site, it was critical for us to have a high performing, reliable system to cater for greater patient throughput. Our evaluation team, which included our lead technologist, undertook due diligence and applied rigour in an open tender process before eventually settling on the uMI 780.

In the next 12 months, Mercy Radiology will work to further increase patient accessibility to PET/CT scans for our regional patients, by embarking on a project to deliver Australasia's first mobile PET/CT.

The custom designed trailer, incorporating a mobile uMI 550 unit on board once commissioned, will travel every day to service the regions in the North Island of New Zealand, obviating the need for regional patients to travel for up to six hours simply to have a PET/CT scan.

3. Mercy Radiology's experience with United Imaging

What has been our experience operating the uMI 550 and the uMI 780 so far?

First, we can attest to the field reliability of the scanners. Outside of scheduled down time for preventative maintenance, we have had a 100% uptime thus far with both scanners.

The United Imaging development team has been receptive to suggestions for workflow improvement. Our fruitful relationship with them has now evolved into a collaboration to develop advanced AI algorithm to enhance and optimise Prostate Specific Membrane Antigen (PSMA) PET images.

Secondly, in terms of image quality, our team has seen first-hand the major step up from analog to digital cameras and the progressive image improvement with successive iteration of United Imaging's AI algorithm. This is particularly striking when the same patient returns for their follow-up studies (see Figure 1-3) on the different platforms.

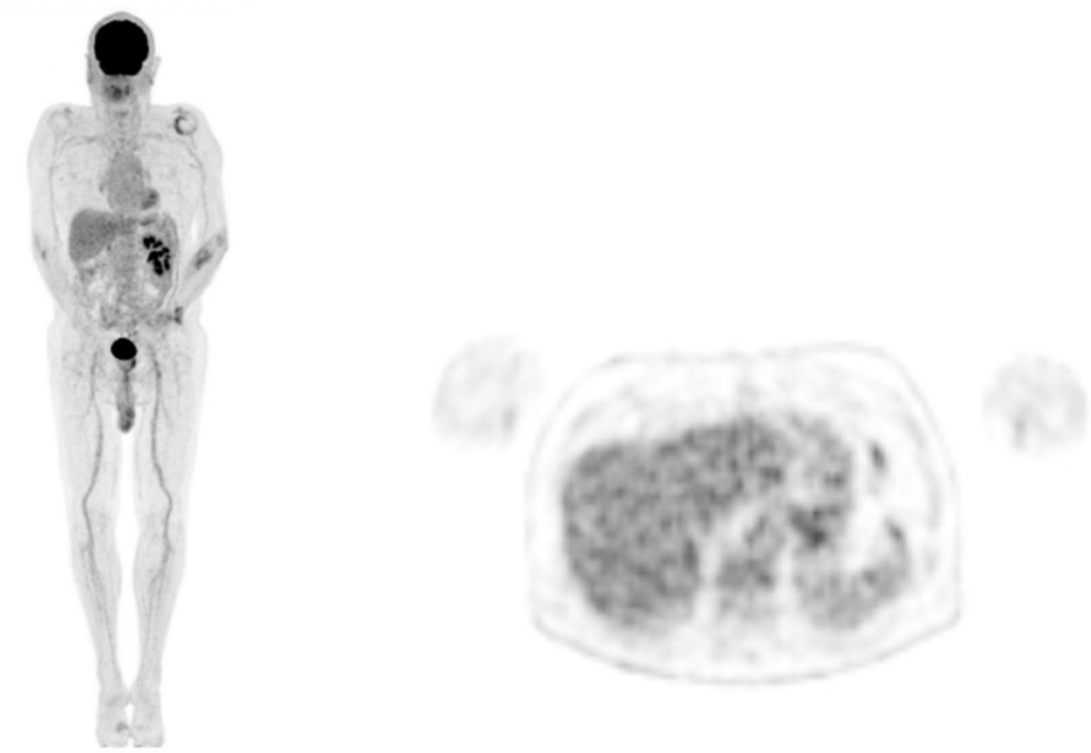

Figure 1. Whole body maximum intensity projection and axial image of a patient with metastatic renal cell carcinoma scanned on the now decommissioned analog PET/CT (injection dose: 242 MBq of ^{18}F-FDG, 60 min uptake time, scan time: 2 min/bed position).

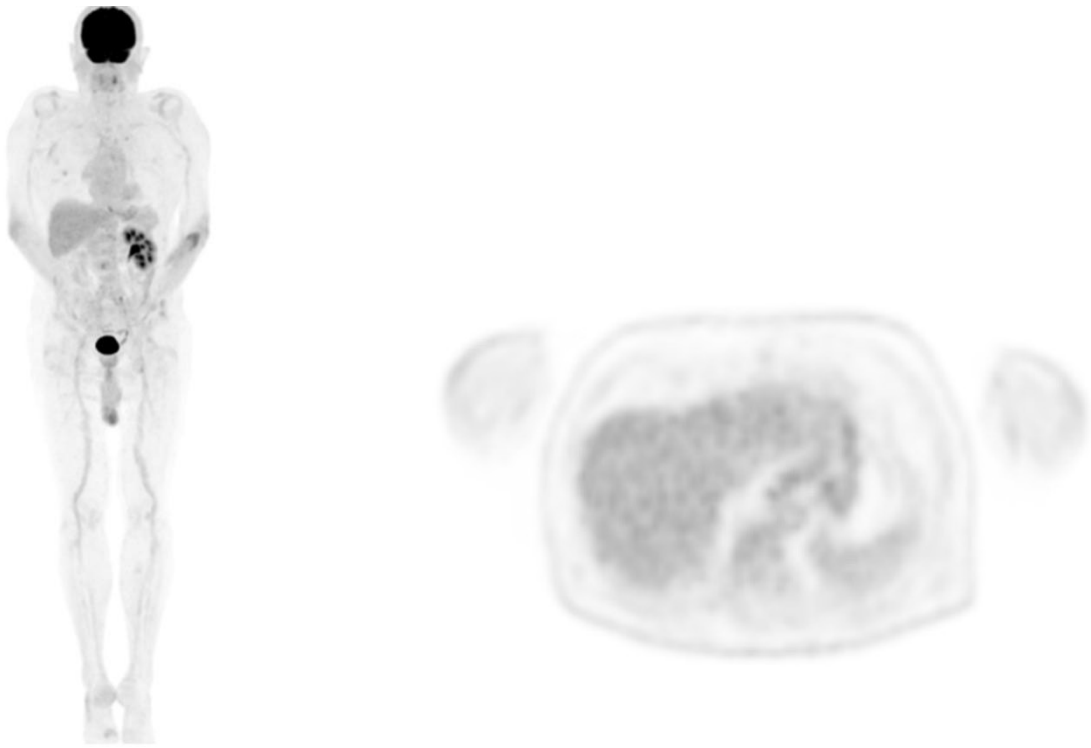

Figure 2. MIP and axial image of the same patient scanned on uMI 550 with HYPER DLR AI PET algorithm (injection dose: 239 MBq of ^{18}F-FDG, 60 min uptake time, scan time: 2 min/bed position).

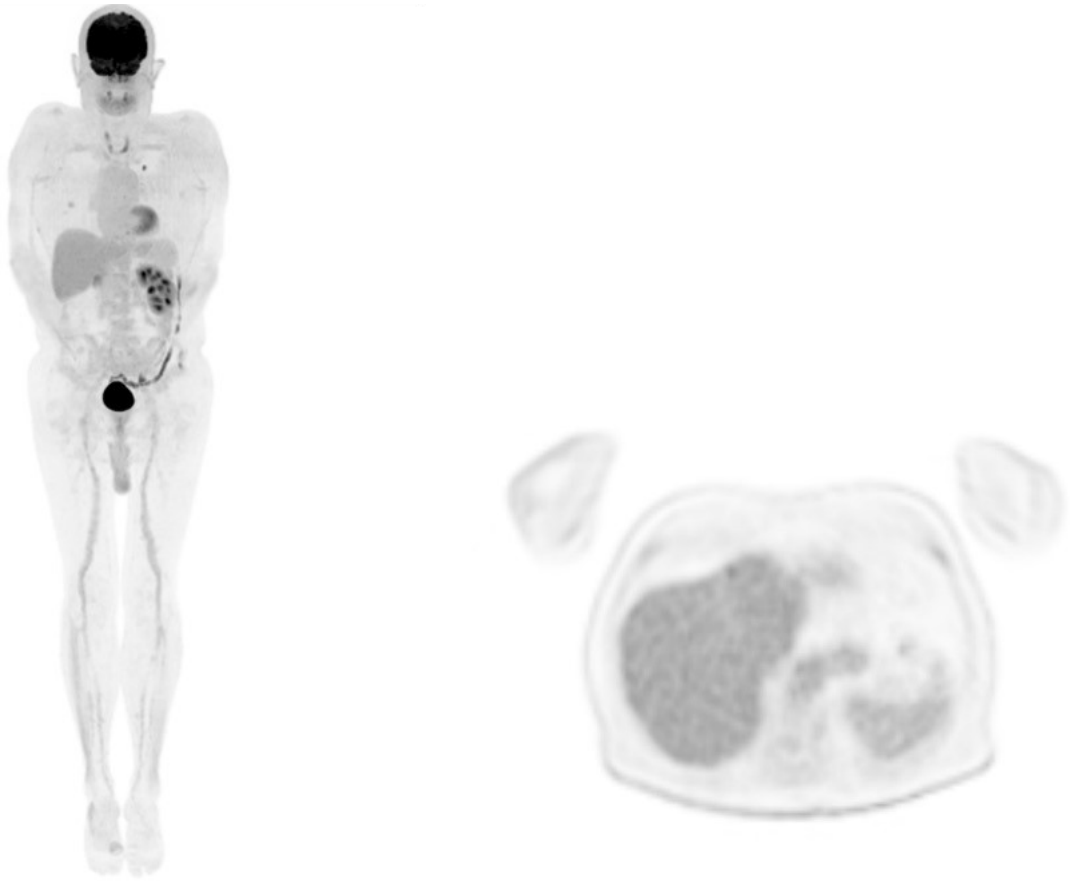

Figure 3. MIP and axial image of patient with metastatic renal cell carcinoma scanned on uMI 780 with latest generation HYPER DPR, AI PET algorithm (injection dose: 244 MBq of ^{18}F-FDG, 60 min uptake time, scan time: 2 min/bed position).

uAI HYPER DLR's algorithm is based on deep learning through artificial neural networks. The algorithm improves signal to noise ratio by up to 50%, allowing shorter acquisition time if required. It is also effective in reducing image noise in patients with high BMI.

uAI HYPER DPR builds on this, further enhancing the signal to noise ratio, accentuating lesion contrast and thus improving small lesion detectability. Compared with other possible AI algorithms, its unique advantage is that its networks were created using United Imaging's uEXPLORER® data. HYPER DPR claims a 32% improvement on noise reduction, 66% improvement on image contrast and overall 2.5 times improvement on SNR.

As a result, HYPER DLR and HYPER DPR have delivered images of consistently high signal-to-noise ratio. PET images with low levels of background noise and improved lesion conspicuity are now the expectation, even in patients with high BMI. In line with United Imaging's Software Upgrades for Life program, the uAI HYPER DPR algorithm has been cascaded into our two-year-old uMI 550.

Third, Mercy Radiology's in-house applications "superuser", trained in United Imaging's USA headquarters in Houston, Texas, now also serves as our applications support and provides support to other Australasian users. Our technologists have found United Imaging's platform to be user friendly and intuitive to operate. Combined with 30 cm axial field of view, the uMI 780 provides for an efficient workflow and has significantly increased our overall patient throughput.

Finally, we have expanded our capacity! PET acquisitions that previously required 25 minutes are now completed in 15 minutes or less on the new uMI 780, freeing up more appointment times and facilitating greater patient throughput.

With the uMI 550 and uMI 780, and a mobile uMI 550 in the pipeline, Mercy Radiology, in partnership with United

Imaging, is well on the way to achieving our twin goals of increasing capacity and improving PET/CT accessibility to the people of Aotearoa New Zealand.

4. Image/Figure Courtesy

All images are the courtesy of Mercy Radiology, Auckland, New Zealand.

Author Biography

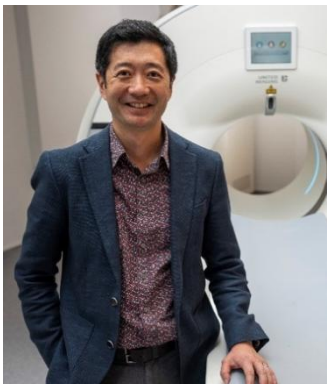

Dr. Remy Lim, BHB, MBChB (Auckland), FRANZCR, CMInstD
Medical Director, Mercy Radiology
Newmarket, Auckland, New Zealand

Remy Lim is a graduate of Auckland University School of Medicine and completed his Radiology training in Auckland and Hamilton. Following a two-year fellowship at Memorial Sloan Kettering Cancer Center in New York, Remy returned to NZ in 2011 to join Mercy Radiology and the public hospital. His subspecialty interest is in Oncology scans and Genitourinary scans, including the reporting of prostate MRI and PET/CT scans.

Remy introduced PSMA PET/CT scan to New Zealand in 2015, which fundamentally changed the way prostate cancer was imaged and treated in the country. In 2018, Remy administered the first dose of Lutetium PSMA in New Zealand in a pilot study. He has since treated over 200 men with advanced prostate cancer. Remy has been the Medical Director at Mercy Radiology for the last six years and is currently working on a couple of exciting projects that will hopefully change the way PET/CT imaging is delivered to the regional centres in North Island. He also has a part- time appointment at Auckland City Hospital where he is part of the Auckland region genitourinary multi-disciplinary team.

PASSION for CHANGE

If you have any questions about the magazine, or simply wish to reach out to us for any other reasons, you are welcomed to contact us at the following email address: uinnovation-global@united-imaging.com